

INVESTIGATION OF NEURODEGENERATIVE TAUOPATHIES USING
CAENORHABDITIS ELEGANS

By

Derek Vonarx

A THESIS

Submitted to
Michigan State University
in partial fulfillment of the requirements
for the degree of

Chemistry – Master of Science

2022

ABSTRACT

INVESTIGATION OF NEURODEGENERATIVE TAUOPATHIES USING *CAENORHABDITIS ELEGANS*

By

Derek Vonarx

Neurodegenerative tauopathies are a class of neurodegenerative disease characterized by the accumulation of tau protein into neurofibrillary tangles in the human brain. Alzheimer's disease (AD) is one such tauopathy. Until recently, the amyloid β hypothesis, suggesting that accumulation of amyloid β , was the leading hypothesis explaining cognitive decline in Alzheimer's disease patients. However, treatments that reduce amyloid β levels in the brain, such as aducanumab, have shown limited efficacy, and therefore, the role of tauopathy and the potential synergistic relationship of tau and amyloid β requires further study to understand the mechanism of cognitive decline in AD. One of the many difficulties of studying AD is that cognitive symptoms are not observed until late in life. Because of the late onset of symptoms, modelling AD in mammals is expensive and time consuming. To circumvent these issues, a nematode, *C. elegans*, model was developed because *C. elegans* have a short lifespan of three weeks, can be genetically modified to express human tau, and are inexpensive to maintain. A genetically modified *C. elegans* strain (*eat-4::GFP; aex-3::tau*) expressing both human tau in all neurons and green fluorescent protein in glutamatergic neurons was developed. It was found that the novel strain exhibits neurodegeneration that can be rescued by supplementation with the epoxide hydrolase inhibitor, 12-[[tricyclo[3.3.1.1^{3,7}]dec-1-ylamino]carbonyl]amino]-dodecanoic acid (AUDA), through an unknown mechanism. This novel strain serves as a useful model to study the mechanism of Alzheimer's disease cognitive decline as *C. elegans* have a relatively short lifespan that allows for extensive therapeutic and genetic screening.

ACKNOWLEDGEMENTS

I am so fortunate to be surrounded by a loving and supportive family. They have offered needed support and encouragement throughout my graduate career, especially my parents, John and Melanie, my brother, Kevin, and my sister, Julie. I am grateful for my friends and colleagues that took the time to read drafts, offer advice, and teach fundamental laboratory skills, especially Morteza, Devon, Ellie, Jennifer, Tommy, Olivia, and Alexis. I thank them all for their words of encouragement and support when I needed it most. I am also grateful for my advisor, Dr. Kin Sing Stephen Lee, and second reader, Dr. Jamie Alan, who taught me countless laboratory techniques and how to better communicate my science to the community. Lastly, I am thankful for my committee members, Dr. Babak Borhan and Dr. Liangliang Sun, for their advice on improving my thesis. I have learned so much about science and life working in this group of dedicated researchers. I am forever grateful.

TABLE OF CONTENTS

LIST OF TABLES	viii
LIST OF FIGURES	ix
KEY TO ABBREVIATIONS	xiii
CHAPTER ONE: INTRODUCTION TO ALZHEIMER'S DISEASE AND TAUOPATHY	1
1. INTRODUCTION	1
1.1. Alzheimer's Disease (AD)	1
1.1.1. Background and relevance	1
1.1.2. Tau and amyloid β as biomarkers and possible roles in AD neurodegeneration	2
1.1.3. Current treatments and medical interventions for AD	5
1.2. Tauopathy	6
1.2.1. The role of microtubule-associated protein tau in neurological disorders	6
1.2.2. The relevance of phosphorylated tau in AD	7
1.3. Potential neuronal cell death mechanisms in AD	11
1.3.1. Ferroptosis	11
1.3.2. Excitotoxicity	12
1.3.3. Possible links between ferroptosis and excitotoxicity	13
1.4. Lipid effects on neurodegeneration	14
1.4.1. Introduction to fatty acids	14
1.4.2. Role of ω -3 and ω -6 fatty acids in neurological disorders	15
1.4.3. Role of PUFA metabolism in neurological health	16
1.5. Epoxide hydrolase	18
1.5.1. Introduction to epoxide hydrolase	18
1.5.2. Increased 1,2-diol PUFA metabolites in AD patients	20
1.5.3. Soluble epoxide hydrolase inhibition in AD models	21
1.6. <i>Caenorhabditis elegans</i>	22
1.6.1. Introduction to <i>C. elegans</i>	22
1.6.2. Advantages of using <i>C. elegans</i> as an animal model	23
1.6.3. <i>C. elegans</i> as a model for AD	24
REFERENCES	27
CHAPTER TWO: INVESTIGATION OF NEURODEGENERATION IN GLUTAMATERGIC NEURONS USING <i>C. ELEGANS</i>	34
2. GLUTAMATERGIC NEURON SYSTEM	34
2.1. Introduction to glutamatergic neuron system	34
2.1.1. General identification and function of glutamatergic neurons	34
2.1.2. Alzheimer's Disease effects on glutamatergic neuron system	35
2.1.3. <i>C. elegans</i> glutamatergic neuron model strains	36

2.2. Experimental	37
2.2.1. Preparation of nematode growth media (NGM)	37
2.2.2. Preparation of bacterial food source (OP50)	37
2.2.3. Seeding NGM with bacteria	38
2.2.4. Transferring worms	38
2.2.5. Preparation of supplemented plates	39
2.2.6. Generation of novel strains through crossing	40
2.2.7. Generation of AD model with glutamatergic GFP (JKA71)	41
2.2.8. Age synchronization	42
2.2.9. Maintenance of age synchronized population	42
2.2.10. Glutamatergic neuron assay	43
2.2.11. Thrashing assay	44
2.2.12. Collecting and freezing worm samples for oxylipin and lipidomic analysis	45
2.2.13. Worm homogenization for oxylipin and lipidomic analysis	47
2.2.14. Solid phase extraction to isolate oxylipins from whole worm lysates	48
2.2.15. Isolation of PUFAs from whole worm lysates	50
2.2.16. Esterification of PUFAs for lipidomic analysis	51
2.2.17. Oxylipin analysis method using HPLC/MS/MS	52
2.2.18. Lipidomic analysis method using GC/MS	52
2.2.19. Synthesis of epoxyeicosatetraenoic acid (EEQ) regioisomeric mixture	53
2.2.20. Characterization of EEQ mixture by HPLC/MS/MS	54
2.3. Using GFP to assess neural health of glutamatergic neurons in <i>C. elegans</i>	56
2.3.1. Establishing the glutamatergic GFP model	56
2.3.2. Transgenic humanized tau <i>C. elegans</i> glutamatergic neuron assay	57
2.3.3. Glutamatergic neuron assay with epoxide hydrolase inhibitor, AUDA, treatment	58
2.3.4. Glutamatergic neuron assay with ω -3 fatty acid and ω -3 fatty acid metabolite supplements	60
2.3.5. Glutamatergic neuron assay with ferroptosis inhibitor, LIP-1, treatment	68
2.4. Assessing physical fitness using thrashing assay	70
2.4.1. Establishing the thrashing model in wildtype	70
2.4.2. Transgenic humanized <i>C. elegans</i> thrashing assay	72
2.4.3. Thrashing assay with epoxide hydrolase inhibitor, AUDA, treatment	73
2.4.4. Thrashing assay with ω -3 fatty acid and ω -3 fatty acid metabolite supplements	76
2.5. Assessing lipid and lipid metabolite profiles using mass spectrometry	80
2.5.1. Lipidomic profiling using GC/MS	80
2.5.2. Oxylipin profiling using HPLC/MS/MS	82
2.6. Discussion of the <i>eat-4::GFP</i> model	86
2.6.1. Neurological effects	86

2.6.2. Physical fitness effects	90
2.6.3. Experimental limitations	91
2.6.4. Future directions	92
REFERENCES	94
CHAPTER THREE: INVESTIGATION OF TAU FEEDING MODEL IN <i>C. ELEGANS</i>	98
3. TAU FEEDING MODEL	98
3.1. Introduction of PIMAX model	98
3.1.1. Using PIMAX to produce tau and hyperphosphorylated tau in <i>E. coli</i>	98
3.2. Experimental	100
3.2.1. Growing healthy bacteria stocks	100
3.2.2. Making IPTG and ampicillin palates	101
3.2.3. Serotonin (5-HT) assay	101
3.2.4. Cold tolerance assay	102
3.3. Thrashing assay results	102
3.3.1. <i>C. elegans</i> fed PIMAX DH5 α <i>E. coli</i> producing human tau	102
3.3.2. <i>C. elegans</i> fed PIMAX DH5 α <i>E. coli</i> producing human tau controlling for expression levels	104
3.4. Serotonin assay results	107
3.4.1. Introduction to the serotonin assay	107
3.4.2. Serotonin assay <i>C. elegans</i> fed PIMAX DH5 α <i>E. coli</i> producing human tau	108
3.5. Cold tolerance assay results	109
3.5.1. Introduction to the cold tolerance assay	109
3.5.2. Cold tolerance assay in <i>C. elegans</i> fed PIMAX DH5 α <i>E. coli</i> producing human tau	110
3.6. Discussion of the PIMAX feeding model	111
3.6.1. Physical fitness effects	111
3.6.2. Neurological effects	113
3.6.3. Model limitations	113
3.6.4. Future directions	113
REFERENCES	115
CHAPTER FOUR: INVESTIGATION OF ULTRASOUND AS TRAUMATIC BRAIN INJURY MODEL IN <i>C. ELEGANS</i>	117
4. ULTRASOUND EXPOSURE TBI MODEL	117
4.1. Introduction to traumatic brain injury (TBI)	117
4.1.1. General TBI relevance in humans and tauopathy	117
4.1.2. <i>C. elegans</i> tauopathy model	117
4.1.3. Ultrasound as a TBI model in <i>C. elegans</i>	118
4.2. Thrashing results after ultrasound exposure through 2.5 cm gap	118
4.2.1. Model description	118
4.2.2. Thrashing results	120
4.3. Thrashing results in solution	121

4.3.1. Model description	121
4.3.2. Optimization of exposure time results	122
4.3.3. Thrashing results in solution	124
4.4. Discussion of TBI ultrasound model	126
4.4.1. Physical fitness effects	126
4.4.2. Model limitations	126
4.4.3. Future directions	127
REFERENCES	129

LIST OF TABLES

Table 1: Deuterated standards used for oxylipin analysis.	48
Table 2: Solvent gradient for EEQ methyl ester separation.	53
Table 3: Solvent gradient for EEQ acid separation.	54

LIST OF FIGURES

Figure 1: Depiction of a typical healthy neuron with the key features labeled.	4
Figure 2: Depiction of tau and A β buildup in the neurons of AD patients.	4
Figure 3: Depiction of tau classification in primary protein structure.	7
Figure 4: Biosynthesis of PUFAs in mammals.	15
Figure 5: Arachidonic acid (AA) metabolism through typical CYP and EH activity.	18
Figure 6: Concentration of 1,2-diols derived from AA in <i>C. elegans</i> AD model.	26
Figure 7: Supplementing directly on the surface of the agar.	39
Figure 8: Supplementing plates in the agar.	40
Figure 9: Age synchronization process.	42
Figure 10: Age synchronization maintenance through filtration.	43
Figure 11: Neuron assay.	44
Figure 12: Thrashing assay.	44
Figure 13: Scoring thrashing of <i>C. elegans</i> .	45
Figure 14: Worm sample preparation for oxylipin and lipidomic analysis.	47
Figure 15: Worm homogenization for oxylipin and lipidomic analysis.	48
Figure 16: Solid phase extraction column preparation.	49
Figure 17: Loading the sample to the SPE column.	49
Figure 18: Elution of oxylipins from SPE column.	50
Figure 19: Synthesis of epoxyeicosatetraenoic acid (EEQ).	54
Figure 20: Characterization of 17,18-EEQ (EpETE) by HPLC/MS/MS.	55
Figure 21: Characterization of 14,15-EEQ (EpETE) by HPLC/MS/MS.	55
Figure 22: Characterization of 11,12-EEQ (EpETE) by HPLC/MS/MS.	55

Figure 23: Characterization of 8,9-EEQ (EpETE) by HPLC/MS/MS.	55
Figure 24: Characterization of 5,6-EEQ (EpETE) by HPLC/MS/MS.	56
Figure 25: GFP showing glutamatergic neuron somas in healthy <i>eat-4::GFP C. elegans</i> .	56
Figure 26: GFP in <i>eat-4::GFP; aex-3::tau C. elegans</i> .	57
Figure 27: Quantified glutamatergic neural health in <i>eat-4::GFP</i> (Control) and <i>eat-4::GFP; aex-3::tau</i> (Tau) worms.	58
Figure 28: Structure of AUDA.	59
Figure 29: Quantified glutamatergic neural health in <i>eat-4::GFP</i> (Control) and <i>eat-4::GFP; aex-3::tau</i> (Tau) treated with and without AUDA.	60
Figure 30: Quantified glutamatergic neural health in <i>eat-4::GFP</i> (Control) treated with EPA and EEQ.	61
Figure 31: Quantified glutamatergic neural health in <i>eat-4::GFP; aex-3::tau</i> (Tau) treated with EPA and EEQ.	62
Figure 32: Quantified glutamatergic neural health in <i>eat-4::GFP</i> (Control) and <i>eat-4::GFP; aex-3::tau</i> (Tau) treated with EPA and EEQ.	63
Figure 33: Quantified glutamatergic neural health in <i>eat-4::GFP</i> (Control) with cotreatment of EPA + AUDA and EEQ + AUDA.	64
Figure 34: Quantified glutamatergic neural health in <i>eat-4::GFP; aex-3::tau</i> (Tau) with cotreatment of EPA + AUDA and EEQ + AUDA.	65
Figure 35: Quantified glutamatergic neural health in <i>eat-4::GFP</i> (Control) and <i>eat-4::GFP; aex-3::tau</i> (Tau) with cotreatment of EPA + AUDA and EEQ + AUDA.	66
Figure 36: Quantified glutamatergic neural health in <i>eat-4::GFP; aex-3::tau</i> (Tau) treated with AUDA, EPA + AUDA, and EEQ + AUDA.	67
Figure 37: Structure of liproxstatin-1 (LIP-1).	68
Figure 38: Quantified glutamatergic neural health in <i>eat-4::GFP</i> (Control) treated with LIP-1.	69
Figure 39: Quantified glutamatergic neural health in <i>eat-4::GFP; aex-3::tau</i> (Tau) treated with LIP-1.	70

Figure 40: Quantified thrashing of N2 during the aging process.	71
Figure 41: Quantified thrashing of <i>eat-4::GFP</i> (Control) and <i>eat-4::GFP; aex-3::tau</i> (Tau).	73
Figure 42: Quantified thrashing of <i>eat-4::GFP</i> (Control) supplemented with AUDA.	74
Figure 43: Quantified thrashing of <i>eat-4::GFP</i> (Control) and <i>eat-4::GFP; aex-3::tau</i> (Tau) supplemented with AUDA.	75
Figure 44: Quantified thrashing of <i>eat-4::GFP</i> (Control) supplemented with EPA and EEQ.	76
Figure 45: Quantified thrashing of <i>eat-4::GFP; aex-3::tau</i> (Tau) supplemented with EPA and EEQ.	77
Figure 46: Quantified thrashing of <i>eat-4::GFP</i> (control) and <i>eat-4::GFP; aex-3::tau</i> (Tau) supplemented with EPA/AUDA and EEQ/AUDA.	79
Figure 47: Quantification of DGLA in <i>eat-4::GFP</i> (Control) and <i>eat-4::GFP; aex-3::tau</i> (Tau) using GC/MS.	81
Figure 48: Quantification of EPA in <i>eat-4::GFP</i> (Control) and <i>eat-4::GFP; aex-3::tau</i> (Tau) using GC/MS.	82
Figure 49: Oxylin quantification of EPA diol and epoxide metabolites.	83
Figure 50: Direct comparison of 14,15-EEQ and 17,18-EEQ concentrations in each treatment group.	84
Figure 51: Direct comparison of 14,15-DiHETE and 17,18-DiHETE concentrations in each treatment group.	85
Figure 52: PIMAX model producing free hyperphosphorylated tau in <i>E. coli</i> .	100
Figure 53: Serotonin assay.	101
Figure 54: Cold tolerance.	102
Figure 55: Quantified thrashing of N2 fed different PIMAX bacterial types.	103
Figure 56: Quantified thrashing of N2 fed different PIMAX bacterial types controlling for expression levels.	105
Figure 57: Quantified thrashing of N2 fed different PIMAX and control bacterial types.	106

Figure 58: Quantified healthy N2 worms after 10-minute 5-HT exposure.	109
Figure 59: Quantified alive N2 worms after exposure to 4°C.	111
Figure 60: Ultrasound exposure model through a 2.5 cm space.	119
Figure 61: Quantified thrashing of N2 and <i>aex-3::tau</i> (Tau) with and without exposure to ultrasound.	120
Figure 62: Ultrasound exposure directly in the buffer solution.	122
Figure 63: Quantified thrashing of N2 and <i>aex-3::tau</i> (Tau) exposed to varying duration of ultrasound.	123
Figure 64: Quantified thrashing of N2 and <i>aex-3::tau</i> (Tau) with and without exposure to 3 seconds of ultrasound.	125

KEY TO ABBREVIATIONS

3R	three repeating units
4R	four repeating units
5-HT	5-hydroxytryptamine
AA	arachidonic acid
AD	Alzheimer's disease
ADA	adrenic acid
ALA	α -linoleic acid
ANOVA	analysis of variance
APP	amyloid precursor protein
AUDA	12-[[[(tricyclo[3.3.1.1.3,7]dec-1-ylamino)carbonyl]amino]-dodecanoic acid
A β	amyloid beta
BHT	butylated hydroxytoluene
CAA	cerebral amyloid angiopathy
CEEH	<i>C. elegans</i> epoxide hydrolase
CNS	central nervous system
COX	cyclooxygenase
CSF	cerebrospinal fluid
CUDA	12-[(cyclohexylcarbonyl)amino]dodecanoic acid
CYP	cytochrome P450
DGLA	dihomo- γ -linolenic acid
DHA	docosahexaenoic acid
DHET	dihydroxyeicosatetraenoic

DI	deionized
DiHETE	dihydroxyeicotetraenoic acid
DiHETrE	dihydroxyeicosatrienoic acid
DiHOME	dihydroxyoctadecenoic acid
DNA	deoxyribonucleic acid
DPA3	docosapentaenoic acid (ω -3)
DPA6	docosapentaenoic acid (ω -6)
ECF	extracellular fluid
EDTA	ethylenediamine tetraacetic acid
EEG	electroencephalogram
EEQ	epoxyeicosatetraenoic acid
EET	epoxyeicosatetraenoic acid,
EH	epoxide hydrolase
EH4	epoxide hydrolase 4
EI	electron ionization
ELOVL	elongase of very long chain fatty acids
ep	epoxy
EPA	eicosapentaenoic acid
EPA-ME	eicosapentaenoic acid methyl ester
ETA	eicosatrienoic acid
FADS 1	fatty acid desaturase 1
FADS2	fatty acid desaturase 2
FAME	fatty acid methyl esters

FDA	food and drug administration
g	gram
GC	gas chromatography
GFP	green fluorescent protein
GLA	γ -linolenic acid
GPX4	glutathione peroxidase 4
GSK-3 β	glycogen synthase kinase 3 β
hAPP	human amyloid precursor protein
HED-EM	high energy diode-electron multiplier
HETE	hydroxyeicosatetraenoic acid
HPLC	high-performance liquid chromatography
iGluRs	glutamatergic ligand-gated ionotropic receptors
IPTG	isopropyl β -D-1-thiogalactopyranoside
L	liter
L1	larval stage 1
L2	larval stage 2
L3	larval stage 3
L4	larval stage 4
LA	linoleic acid
LB	Luria broth
LIP-1	lipoxstatin-1
LOX	lipoxygenase
M	molar

MAPT	microtubule-associated protein tau
MBD	microtubule binding domain
mCPBA	meta-chloroperoxybenzoic acid
mEH	microsomal epoxide hydrolase
mg	milligram
mL	milliliter
mm	millimeter
MRM	multiple reaction monitoring
MS	mass spectrometry
NFT	neurofibrillary tangles
NGM	nematode growth media
nm	nanometer
nM	nanomolar
NMDA	N-methyl-D-aspartate
NMDAR	N-methyl-D-aspartate receptor
NORT	novel object recognition test
OD ₆₀₀	optical density at 600 nm
PBS	phosphate-buffered saline
PET	positron emission tomography
PHF	paired helical filaments
PIMAX	protein interaction module-assisted function X
PKN	protein kinase N
PUFA	polyunsaturated fatty acid

RFP	red florescent protein
ROS	reactive oxygen species
SAW	surface acoustic wave
sEH	soluble epoxide hydrolase
sEHi	soluble epoxide hydrolase inhibitor
SEM	standard error
SP	serine-proline
SPE	solid phase extraction
STA	stearidonic acid
TBI	traumatic brain injury
TEV	tobacco etch virus
THA	tetracosahexaenoic acid
TLC	thin layer chromatography
TP	threonine-proline
TPA3	tetracosapentenoic acid (ω -3)
TPA6	tetracosapentenoic acid (ω -6)
TPP	triphenylphosphine
TTA	tetracosatetraenoic acid
UPLC	ultra-performance liquid chromatography
VGLuT	vesicular glutamate transporter
Δ 4	delta-4 desaturase
Δ 5	delta-5 desaturase
Δ 6	delta-6 desaturase

μL	microliter
μm	micrometer
μM	micromolar
ω	omega naming convention for fatty acids

CHAPTER ONE:

INTRODUCTION TO ALZHEIMER'S DISEASE AND TAUOPATHY

1. INTRODUCTION

1.1. Alzheimer's Disease (AD)

1.1.1. Background and relevance

Alzheimer's disease (AD) is the most common type of dementia, accounting for 60-80 % of all dementia cases, and its prevalence has increased in recent years¹. The increase in cases can be attributed to the aging population in the US and around the world because of significant medical advances, leading to an increase in the global lifespan. The global life expectancy is expected to increase, especially in developed countries. However, the aging population is becoming more susceptible to diseases like AD because these types of diseases selectively affect the elderly population. Therefore, the number of people suffering from AD is likely to increase. AD can be defined as a slowly progressive neurodegenerative disease that affects memory where patients lose the ability to meaningfully interact with their environment. Early symptoms include difficulty or inability to remember recent events, as well as apathy and depression. As the disease progresses, the patient's health further deteriorates leading to more debilitating symptoms like disorientation, confusion, behavioral changes, difficulty swallowing, impaired judgement, and difficulty walking^{1,2}. The progression ultimately leads to a requirement of constant caregiving and can lead to disease complications such as blood clots and infections causing death. Additionally, recent statistical analyses suggest that routine mortality statistics of AD and related dementia may underestimate the mortality by a factor of 2.7³. Underestimation of mortality suggests that the disease may be more prevalent than it appears. A diagnosis of AD is crippling to the patient and family members as current treatments options are unable to provide a cure.

AD is not only debilitating and deadly, but also extremely costly. On average, the annual direct cost of care for a patient suffering from AD is \$27,126⁴. In the United States, the total annual cost for direct AD care was approximately \$200 billion^{1,4}. The projected cost of care for AD will increase to \$1.1 trillion by 2050¹. To keep costs down, it is extremely common for family members or close friends to attempt to serve as caregivers for individuals suffering from AD. Due to the demands required of the caregivers, nearly two-third report high levels of stress, and one-third report symptoms of depression¹. The emotional turmoil of the caregivers increases the cost of healthcare for the caregivers and generally interferes with their quality of life. In addition, the stress and depression of caregivers provides another obstacle for the AD patients to receive the care they require. AD is a devastating and deadly disease that requires further research to understand the underlying mechanism(s), which may lead to development of more effective therapies.

1.1.2. Tau and amyloid β as biomarkers and possible roles in AD neurodegeneration

The pathology of AD can be described macroscopically and microscopically. Macroscopically, widespread atrophy of the brain and amyloid buildup in arterial walls of the brain, termed cerebral amyloid angiopathy (CAA), is observed⁵. Synaptic damage in the neocortex and limbic system, causing memory impairment, are usually observed during the early stages of AD. The mechanism behind these changes involves mitochondrial damage, oxidative stress, and disruption of physiological axonal transport⁵. Microscopically, there are two main molecular markers of AD, amyloid beta ($A\beta$) and tau. $A\beta$ is a peptide generated by the amyloidogenic pathway. Amyloid precursor protein (APP) is a transmembrane protein that is cleaved by α - or β - secretases, which generates large, secreted fragments, $sAPP\alpha$ and $sAPP\beta$, and $A\beta$ ⁶. Physiological $A\beta$ may have neurotrophic properties⁶. Additionally, recent evidence suggests

that A β acts as an antioxidant to protect from metal-induced oxidative damage⁶. However, in AD pathology, excess pathological concentrations of A β cause neurotoxicity and cell death⁶. The excess A β is deposited extracellularly in the form of senile plaques^{6,7}.

Tau is a microtubule-associated protein encoded in humans by the microtubule-associated protein (MAPT) gene. Under physiological conditions, tau is localized primarily in the axons as a soluble and natively unfolded protein. Tau primarily functions to polymerize tubulins and stabilize microtubules^{8,9}. However, in AD pathology, tau is post-translationally modified, which causes tau to lose the ability to bind microtubules. Unable to interact with its physiological partner, tau aggregates together to form neurofibrillary tangles (NFTs). It is hypothesized that NFTs lead to disruption in axonal transport, preventing key communication with organelles such as mitochondria, which are essential for healthy synaptic function^{10, 11}.

A β and eventually A β plaques primarily accumulate extracellularly at or near the synapse. Tau aggregation, in the form of NFTs, primarily occurs intracellularly. Physiological neurons and some key features are illustrated in Figure 1, and location of pathological biomarkers of AD, A β and tau, are illustrated in Figure 2. Accumulation of A β and tau at synaptic sites can contribute to the synaptic loss. Specifically, accumulation of A β and tau eventually lead to the loss of dendritic spines and axonal dystrophy, which causes neuronal cell loss^{10,11,12,17}. AD patients experience severe cognitive decline after severe neuronal cell loss. Another pathological marker of AD is neuroinflammation in affected brain regions, suggested to be caused by pathological recruitment of microglia and astrocytes. Neuroinflammation is a defense mechanism that initially protects the brain by removing diverse pathogens. Therefore, the inflammatory response has beneficial effects by promoting tissue repair and removing cellular debris. However, sustained inflammatory responses are detrimental and inhibit

regeneration. Persistent inflammatory responses involve excessive release of inflammatory mediators, such as cytokines, and can lead to neuronal cell death¹².

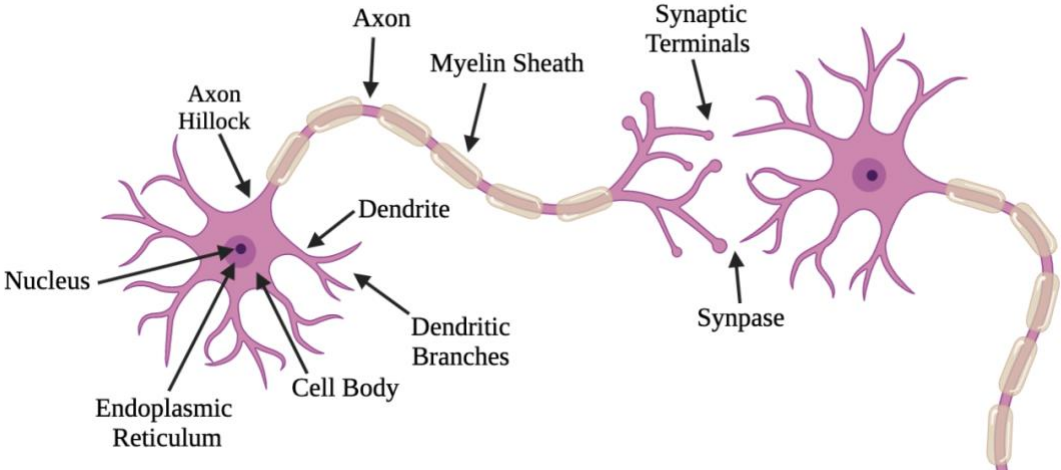


Figure 1: Depiction of a typical healthy neuron with the key features labeled.

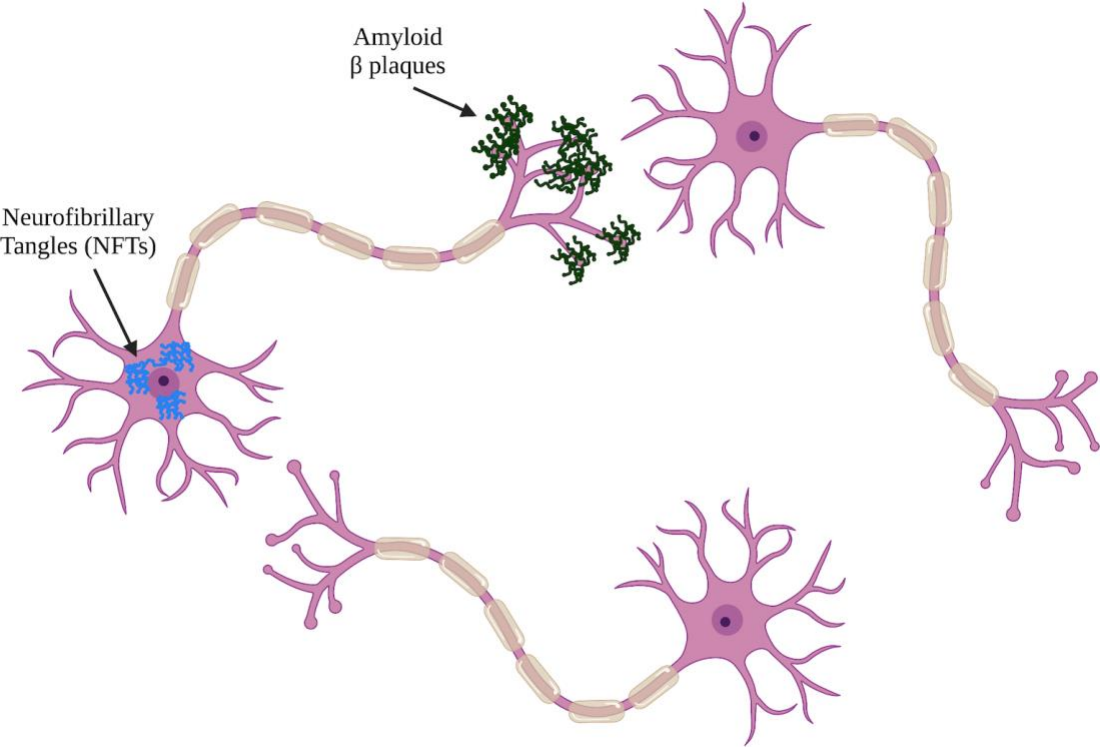


Figure 2: Depiction of tau and Aβ buildup in the neurons of AD patients^{5,6}.

1.1.3. Current treatments and medical interventions for AD

The US Food and Drug Administration (FDA) has approved at least five drugs that slow the progression of the AD by 6 to 12 months depending on the individual¹³. However, no treatments are currently available that delay the onset or cure an individual from the disease. Because the current treatment options are insufficient, there is a large research effort to identify drugs that can slow or even stop the disease progression. Most of the research has focused on A β as the primary drug target because the amyloid hypothesis suggests that A β accumulation leads to neurodegeneration. The most recent FDA approved drug is aducanumab, (Aduhelm), which has been shown to reduce total levels of A β in the brain¹⁴. Aducanumab is an anti-A β antibody that has demonstrated A β reduction in the brain observed and quantified by florbetapir positron emission tomography (PET) imaging in a dose- and time-dependent fashion. The PET images showed a mean PET standard uptake value ratio of A β reduced from 1.44 to 1.16 after 53 weeks of 10 mg/kg of aducanumab¹⁵. Therefore, the reduced uptake suggests less A β in the brain. However, it remains unclear how effective this treatment will be for slowing the progression of the disease and reducing symptoms^{15,16}. Other treatment options are cholinesterase inhibitors, such as galantamine, rivastigmine, and donepezil, and N-methyl-D-aspartate (NMDA) antagonists, such as memantine, which have been used to reduce some cognitive and behavioral symptoms with moderate success¹³. Despite the moderate success observed, currently available cholinesterase inhibitors and NMDA antagonists do not stop the disease progression¹³. Due to the inconclusive efficacy of treating A β only, much of the current research has shifted focus on the microtubule associated protein tau, and its possible interactions with A β in AD pathology.

1.2. Tauopathy

1.2.1. The role of microtubule-associated protein tau in neurological disorders

Tau is a microtubule-associated protein encoded in humans by the microtubule-associated protein (MAPT) gene. The major tau protein in the human brain is encoded by 11 exons. In the adult human brain, tau exists in six isoforms composed of 352-441 residues. The different composition arises from alternative splicing of exon 2, exons 2 and 3, or exon 10. Tau isoforms are classified by the number of microtubule binding regions located in the C-terminus. In humans, there are two categories namely, three-repeat (3R) tau and four-repeat (4R) tau¹⁸. Additionally, tau is classified by the number of inserts at the N-terminal namely, exons 2 and 3. There are three such conditions: zero, one, or two inserts of 29 amino acids. Therefore, the largest tau protein is 4R2N, which implies four microtubule binding repeats and 2 inserts of 29 amino acids at the N-terminus. A general depiction of the classification of tau in the primary protein structure is shown in Figure 3. Under physiological conditions, tau is localized primarily in the axons as a soluble and natively unfolded protein. The primary physiological function of tau is to polymerize tubulins and stabilize microtubules^{8,9}. However, in AD pathology, tau undergoes posttranslational modifications, which causes tau to lose the ability to bind microtubules. Tau that has undergone posttranslational modifications is unable to interact with its normal physiological partners, and the aberrant tau proteins aggregate together to form neurofibrillary tangles (NFTs), which contribute to AD progression.

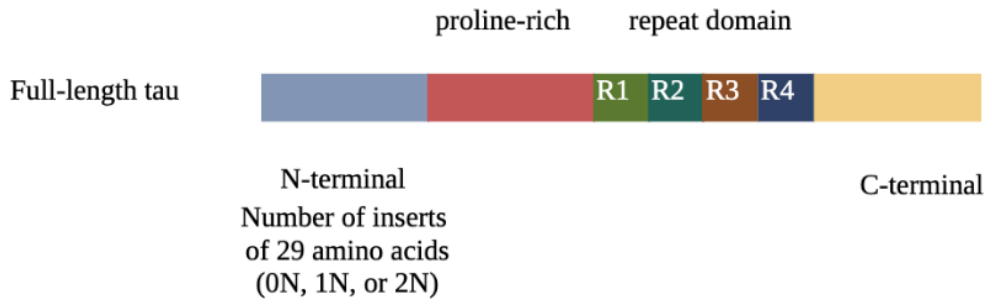


Figure 3: Depiction of tau classification in primary protein structure¹⁸.

1.2.2. The relevance of phosphorylated tau in AD

Tau is regulated post-translationally by a variety of mechanisms. Post-translational phosphorylation likely plays an important role in AD pathology, and therefore, it will be the primary post-translational modification discussed herein. Under physiological conditions, tau can bind outside of microtubules influencing the structure and function of the microtubules. The N-terminal region of tau can associate with the plasma membrane of neuronal cells in a membrane-associated complex. In this complex, tau plays an important role in regulating the spacing between microtubules. Tau's ability to bind microtubules depends on the microtubule binding domain (MBD) on adjacent regions¹⁸. The repeat binding sequences may directly bind microtubules¹⁸. Phosphorylation of specific amino acids in the microtubule binding domain renders the protein unable to bind microtubules and regulates microtubule structure and function. Tau is phosphorylated by a variety of kinases in both physiological and pathological conditions. The longest tau isoform contains a total of 79 potential serine and threonine phosphorylation sites. Approximately 30 of these sites have evidence of phosphorylation in physiological tau²². The phosphorylation events lead to dissociation of tau from the microtubules and causes aggregation of tau in neuronal cell bodies and neurites, ultimately forming NFTs^{18,19,20,21}.

Phosphorylation of tau is mediated by several different kinases including serine/threonine kinases like protein kinase N (PKN). Activation of PKN causes tau phosphorylation and disrupts the organization of microtubules^{18,22,23}. The amount of phosphorylation is regulated throughout human development. Specifically, fetal tau in the embryonic central nervous system (CNS) is more highly phosphorylated than tau found in the adult CNS²³. Hyperphosphorylation of fetal tau may be necessary to regulate microtubule structure and function during development²³. Phosphorylation decreases with age because of an observed increased phosphatase activity. Phosphatases are responsible for removing a phosphate group from a phosphorylated protein. Specifically, two phosphatases, PP2A and PP2B, are present in higher concentrations in adult brain tissues compared to embryonic CNS tissues^{22,24}. The increased phosphatase concentration in adult brain tissues contributes to the observed difference in phosphorylated tau levels between the embryonic and healthy adult CNS. However, in AD pathology, the observed phosphatase activity is decreased, likely leading to an increase in phosphorylated tau forming aggregated tau^{18,22}. Phosphorylated tau levels are regulated by both kinase and phosphatase activity, both enzyme classes are likely dysregulated in AD, which contributes to the buildup of phosphorylated tau¹⁸.

Tauopathy in AD is thought to function primarily through the effects that neurofibrillary tangles have on neuron health. Neurofibrillary tangles are abnormal filaments of hyperphosphorylated tau protein that in some stages can be twisted around each other to form paired helical filaments (PHFs)^{1,25}. The PHFs primarily accumulate in the neuron cell body, which cause a loss of cytoskeletal microtubules and tubulin-associated proteins. The hyperphosphorylated tau protein is the major constituent of NFTs in AD patient's brain. The morphological changes of tau can be characterized into three stages during AD progression: (1)

the pre-tangle phase, where phosphorylated tau proteins are accumulated in the dendritic compartment of the neuron without formation of PHFs, (2) the mature NFTs, where there is filament aggregation of the tau protein with displacement of the nucleus to the periphery of the soma, and (3) the extracellular tangles, where neuronal loss is observed most likely due to large amounts of filamentous tau^{1,25}. Additionally, recent literature suggests that NFT accumulation has associated negative effects on neurotransmitter systems such as the glutamatergic system that impairs synaptic plasticity and long-term potentiation^{20,25,26}. The role of tau in AD pathology remains poorly understood, but understanding the role of tau and its phosphorylated state in AD is critical to the development of more effective treatments.

Tau microtubule binding may regulate axonal transport, which is the process of motor proteins actively navigating microtubules that carry diverse cargo from one end of the axon to another. Tau interferes with the binding of motor proteins to microtubules, and there is a gradient of tau along the axon with the highest concentration closest to the synapse^{18,22}. Therefore, tau may facilitate the detachment of motor proteins near presynaptic terminals, which increases axonal transport efficiency. Because phosphorylation regulates tau binding of microtubules, the mechanism of cognitive decline, as it relates to tau hyperphosphorylation, may be disruption of axonal transport, which leads to neuronal cellular dysfunction.

To investigate the role of tauopathy in AD, several *in vivo* and *in vitro* models have been developed. One model generated includes tau-deficient mice with no functional tau producing alleles²⁸. To assess the effects of the tau deficiency, tau-deficient mice were crossed with hAPPJ9 mice, which is a human amyloid precursor protein (hAPP) transgenic mouse. The hAPP model is an established AD model with distinct loss of cognition phenotypes observed in Morris water maze^{28,29}. Researchers found that the tau-deficient hAPP crossed mice showed significant

recovery of latency time, as measured by the duration to escape, and path length, as measured by the distance covered to escape. Therefore, total reduction of tau seems to reduce some of the cognitive deficits in the mice observed in the Morris water maze results²⁸. However, the mechanism causing the improved cognitive function is not well understood, but the detrimental effects of hyperphosphorylated tau are more severe than insufficient tau levels, which seems to explain the observed improvement of cognitive function in the tau-deficient hAPP mice. Another model includes a transgenic approach used to express human tau in fruit flies, *Drosophila melanogaster*³⁰. The lifespan of the transgenic flies was significantly reduced when compared to wildtype control³⁰. However, the mechanism of the decreased lifespan was unclear. Follow up studies investigated the role of tau phosphorylation on the decreased lifespan. Specifically, phosphorylation at the serine-proline (SP) and threonine-proline (TP) sites were investigated in a follow up study using *D. melanogaster*. To investigate the role of SP and TP phosphorylation in the AD phenotypes associated with the transgenic model, SP and TP sites were specifically mutated to alanine using site-directed mutagenesis³¹. Blocking all 14 SP/TP sites of human tau in *D. melanogaster* markedly inhibited tau-induced neurodegeneration observed by a significant decrease in the “rough eye” phenotype, which is the buildup of tau in the retina of the flies³¹. Additionally, blocking phosphorylation at specific, but not all, SP and TP sites did not significantly reduce the “rough eye” phenotype³¹. Therefore, it is unlikely that one or a select few phosphorylation sites are responsible for pathological accumulation of phosphorylated tau. Additionally, replacing all SP/TP sites with glutamate, a phosphomimetic, generated a more severe “rough eye” phenotype compared to human wildtype tau³¹. Therefore, the *Drosophila* AD model established the importance of tau phosphorylation in the observed AD phenotypes. The regulation of tau through phosphorylation seems to be a critical component of AD pathology.

1.3. Potential neuronal cell death mechanisms in AD

1.3.1. Ferroptosis

Cell death is a common phenomenon in many neurological disorders including Alzheimer's Disease³². However, the mechanism of triggering neuronal cell death in AD remains elusive. One possible mechanism responsible for neuronal cell death in AD is ferroptosis³². Ferroptosis is an iron-dependent, lipid peroxidation-driven, non-apoptotic programmed cell death³³. The hallmarks of AD pathology are consistent with characteristics of ferroptosis namely, excess iron accumulation, elevated lipid peroxides, elevated reactive oxygen species (ROS), reduced glutathione, and reduced glutathione peroxidase 4 (GPX4) levels^{33,35}. This evidence suggests that ferroptosis may be responsible for neuronal cell death in AD. Additionally, specific ferroptosis inhibitors, such as liproxstatin (LIP-1), can relieve some of the cognitive decline in AD mammalian animal models³⁴. Therefore, the field is now focusing on ferroptosis as the primary cell death mechanism in AD pathology. However, direct evidence suggesting a link between AD neuronal cell death and ferroptosis remain understudied.

In the CNS, iron is an essential element for ferroptosis and is involved in many biological processes, such as oxygen transportation, myelin production, and neurotransmitter synthesis^{32, 35}. The two primary biomarkers of AD pathology are the presence of A β plaques and NFT. Iron has been shown to be selectively accumulated in A β plaques and NFTs³⁶. Iron accumulation has been linked to an acceleration of cognitive decline in AD patients³⁷. Additionally, age-related iron accumulation contributes to tissue damage and pathological AD symptoms³⁸. Therefore, iron accumulation seems to be a common pathological feature, which supports ferroptosis as a possible cell death mechanism in AD.

1.3.2. Excitotoxicity

Another potential cell death mechanism in AD is excitotoxicity. In excitotoxicity, nerve cells suffer damage or death when the levels of excitatory neurotransmitters exceed physiological concentrations, which results in the excessive stimulation of neurotransmitter receptors³⁹. Excess neurotransmitter receptor stimulation can lead to an influx of metal ions, such as Ca^{2+} , into the cell⁴⁰. The additional metal ions activate several enzymes including phospholipases, endonucleases, and proteases, which damage cellular structures. The damage to cellular structures ultimately leads to cell death⁴⁰.

Glutamate is one of the major excitatory neurotransmitters in the mammalian central nervous system⁴¹. Glutamate excitotoxicity is triggered by overactivation of glutamate receptors, which leads to an influx of Na^+ and Ca^{2+} through the plasma membrane⁴⁰. The influx of ions disrupts cellular structure leading to cell death. Therefore, tight regulation of glutamate and glutamate receptors is necessary for physiological function.

Glutamate excitotoxicity may contribute to neuronal cell death mechanisms in AD pathology^{43,44}. Specifically, overactivation of a ligand-gated ionotropic glutamate receptor, N-methyl-D-aspartate (NMDA) receptor, leads to the glutamate excitotoxicity^{43,44}. Overactivation of the NMDA receptor leads to Ca^{2+} influx into the cell, which causes cell death. Overactivation of the NMDA receptor is caused by two main factors namely, glutamate availability and modulation of NMDA receptor function. In AD patients, decreased vesicular glutamate transporter (VGluT) were reported⁴⁵. VGluTs are responsible for transporting glutamate to presynaptic vesicles. Additionally, $\text{A}\beta$ peptides in neuronal cell culture impair glutamate reuptake mechanisms, which increases extracellular glutamate⁴⁶. In addition, AD patients have increased concentrations of glutamate in the cerebrospinal fluid (CSF)⁴⁷, which supports the

suggested increased glutamate availability. Lastly, A β peptides cause elevated NMDA receptor-mediated synaptic currents, which suggests an increase in activation of the NMDA receptor⁴⁸. Therefore, AD pathology seems to increase overall glutamate supply and function of the NMDA receptor, which contributes to neurodegeneration.

1.3.3. Possible links between ferroptosis and excitotoxicity

Glutamate and glutamine are important regulators of ferroptosis^{49,50}. High extracellular concentrations of glutamate can induce ferroptosis⁵⁰, which may contribute to the observed cell death in AD. In other words, both glutamate excitotoxicity and ferroptosis may contribute to the cell death observed in AD through excess glutamate. Additionally, tau function and lack thereof has been linked to both ferroptosis and excitotoxicity. Functional failure of tau contributes to iron-mediated neurotoxicity in ischemia animal models⁵². In AD, tau becomes non-functional after hyperphosphorylation. Therefore, non-functional tau may contribute to ferroptosis-induced neurotoxicity in AD as it does in ischemia. Furthermore, tau has been linked to excitotoxicity in mouse models. Tau reduction decreased the frequency and duration of electroencephalogram (EEG) seizure activity and hyperexcitability of pyramidal neurons, and increased survival in an excitotoxicity mouse model⁵³. Therefore, it is possible that tau is involved directly or indirectly in the mechanism of excitotoxicity. Another link between the two mechanisms of cell death is polyunsaturated fatty acids and their metabolites. During ferroptosis, PUFAs are peroxidized to lipid peroxides, which have been used to characterize ferroptosis⁵¹. Therefore, PUFA lipid peroxides are intimately linked to the ferroptosis cell death mechanism. Additionally, it has been shown in mammalian animal models that supplementation with ω -3 PUFAs may inhibit NMDA receptor activity⁵⁴. Therefore, glutamate excitotoxicity may be mitigated by manipulation of PUFA and PUFA metabolite concentrations. Ferroptosis and glutamate excitotoxicity are

responsible for some of the observed neuronal cell death in AD, and the cell death may be attenuated by manipulation of PUFA concentration.

1.4. Lipid effects on neurodegeneration

1.4.1. Introduction to fatty acids

The current literature suggests that polyunsaturated fatty acid (PUFA) metabolism plays an important role in age-associated neurodegenerative (ND) diseases like AD⁵⁵. PUFAs are long-chain fatty acids comprised of at least two carbon-carbon double bonds that play important roles in several physiological processes⁵⁵. PUFAs are characterized by the ω naming system, which refers to the position the double bond furthest from the carboxylic acid group appears from the methyl end of the PUFA. For example, ω -3 PUFAs contain the most terminal double bond, three carbons from the methyl end. The critical steps in PUFA biosynthesis are elongation and desaturation. Elongation is catalyzed by enzymes called elongases, and desaturation is catalyzed by desaturases. Some invertebrates can convert monounsaturated ω -9 oleic acid into various ω -3 and ω -6 PUFAs^{55,56}. Therefore, these organisms do not require dietary sources of ω -3 and ω -6 PUFAs. Vertebrates also express many desaturase and elongase enzymes. However, they do not possess ω -3 desaturases, and therefore, cannot endogenously synthesize PUFAs from oleic acid, which implies mammals must get ω -3 PUFAs from dietary sources. Despite the lack of ω -3 desaturases, vertebrates can convert linoleic acid (LA), an ω -6 PUFA, and α -linoleic acid (ALA), an ω -3 PUFA, into other ω -6 and ω -3 PUFAs, respectively^{55,57}. Therefore, in mammals, dietary consumption of LA and ALA is sufficient as the body can convert these precursors to the remaining ω -6 and ω -3 PUFAs. The current consensus of biosynthesis of ω -6 and ω -3 PUFAs from LA and ALA is illustrated in Figure 4.

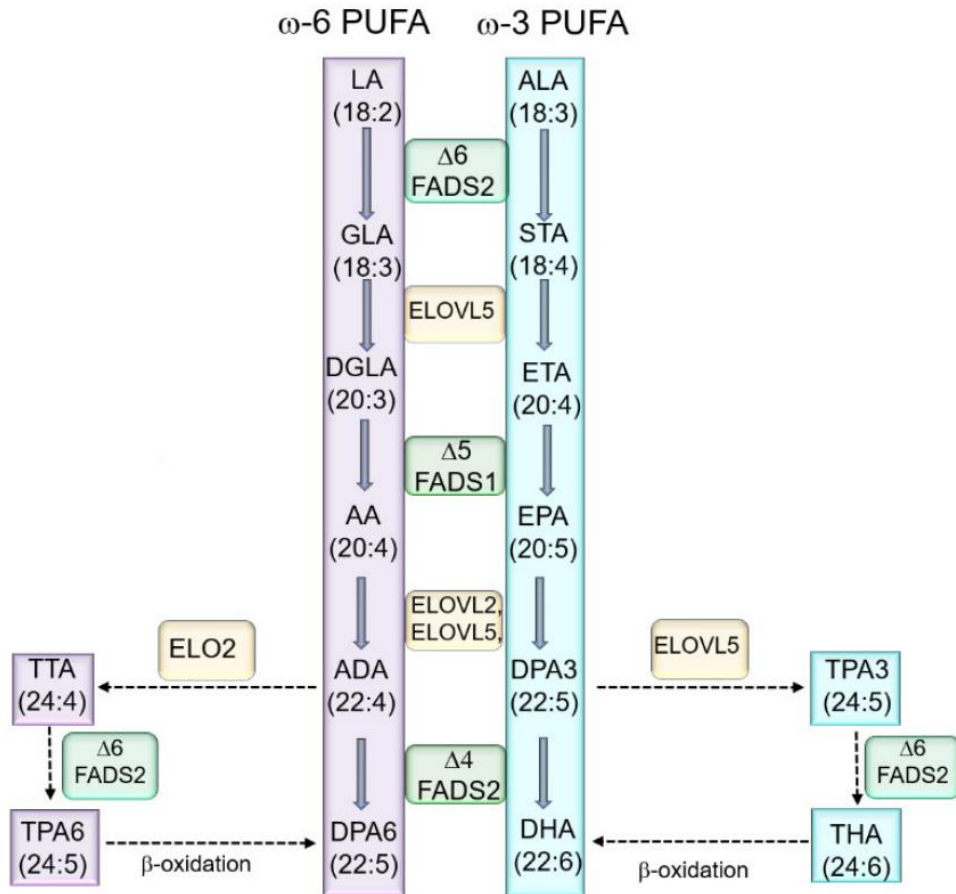


Figure 4: Biosynthesis of PUFAs in mammals⁵⁵. AA: arachidonic acid, ADA: adrenic acid, ALA: α -linolenic Acid, $\Delta 4$: delta-4 desaturase, $\Delta 5$: delta-5 desaturase, $\Delta 6$: delta-6 desaturase, DGLA: dihomo- γ -linolenic acid, DPA3: docosapentaenoic acid (ω -3), DPA6: docosapentaenoic acid (ω -6), DHA: docosahexaenoic acid, ELOVL: elongase of very long chain fatty acids, EPA: eicosapentaenoic acid, ETA: eicosatrienoic acid, FADS 1: fatty acid desaturase 1, FADS2: fatty acid desaturase 2, GLA: γ -linolenic acid, LA: linoleic acid, PUFA: polyunsaturated fatty acid, THA: tetracosahexaenoic acid, TPA3: tetracosapentenoic acid (ω -3), TPA6: tetracosapentenoic acid (ω -6), TTA: tetracosatetraenoic acid, STA: stearidonic acid

1.4.2. Role of ω -3 and ω -6 fatty acids in neurological disorders

There are two major classes of PUFAs namely, omega-3 (ω -3) and omega-6 (ω -6).

Mammals do not possess the biomolecular machinery to endogenously synthesize ω -3 PUFAs, as illustrated in Figure 4⁵⁵. Therefore, mammals must consume ω -3 PUFAs in their diet. It is likely that PUFAs play an important role in neural functions because they are found in abundance in neural tissues. Specifically, arachidonic acid (AA), an ω -6 PUFA, and

docosahexaenoic acid (DHA), an ω -3 PUFA, are the two most abundant PUFAs in the mammalian nervous system. These two PUFAs make up approximately 35% of the lipid content in brain tissue⁵⁵. There is evidence suggesting that dietary PUFA intake is beneficial for neurodevelopment and limits the effects of neurodegeneration⁵⁸. A dramatic decrease in brain PUFA content was observed in rodent models fed an ω -3 PUFA deficient diet. The decreased brain PUFA content was accompanied by a decrease in the number of dopaminergic neurons found in the substantia nigra^{55,59}. Manipulation of the PUFA composition of cell membranes has been shown to alter the function of a variety of neurotransmitter receptors. Endogenous levels of PUFAs significantly affects the downstream PUFA metabolites *in vivo*^{55,60}. Therefore, downstream metabolites may be involved in the mechanism of action of ω -3 and ω -6 PUFAs in neuronal function.

1.4.3. Role of PUFA metabolism in neurological health

PUFAs are primarily metabolized in three oxidative pathways: (1) lipoxygenase (LOX), (2) cyclooxygenase (COX), and (3) cytochrome P450 (CYP). The products of these reactions are different oxidized lipid mediators called oxylipins⁵⁵. In general, ω -6 PUFA oxylipins tend to be proinflammatory, and ω -3 PUFA oxylipins tend to be anti-inflammatory or pro-resolving. DHA oxylipins seem to prevent age-associated memory decline and protect the brain from cellular injury^{55,60}. The described role of DHA metabolites on neurological health suggests that oxylipins might play an important role in neuronal function, and therefore, studying oxylipin involvement in AD may provide another avenue to gain insight into the disease.

Major products of CYP450 metabolism of PUFAs are epoxy PUFAs (ep-PUFAs) and hydroxy PUFAs. The final metabolic products depend entirely on the specific CYP450 enzyme and the type of PUFA substrate. There are many CYP isoforms with differing levels of regio-

and stereoselectivity. The epoxide functional group is a three-membered ring containing two carbons and one oxygen with unfavorable highly strained bond angles and a polarized carbon-oxygen bond, which lends itself to nucleophilic attack. This reactivity causes a wide range of biological and pathological effects. Specifically, styrene epoxide derivatives are susceptible to nucleophilic attack by exocyclic amine groups of nucleotides, which cause DNA adducts and mutations^{55,61}. As ep-PUFAs share the structural feature of an epoxide, it is possible that similar effects can occur with ep-PUFAs. However, there is extensive evidence suggesting that certain ep-PUFAs act as secondary messengers in the initiation of different physiological pathways. Specifically, AA oxylipins have been shown to have neuroprotective properties⁶². CYP metabolism of AA is summarized in Figure 5. The role of ep-AA suggests that ep-PUFAs may have several physiological effects, both beneficial and detrimental likely determined by the parent PUFA. Additionally, epoxide hydrolases (EHs) hydrolyze both endogenous and exogenous epoxides producing the 1,2-diol as shown in Figure 5. The beneficial effects of ep-PUFAs appear to be limited when they are converted to their corresponding 1,2-diols by epoxide hydrolase^{62,63}. Due to the neuroprotective properties of ep-PUFAs and subsequent metabolism to deleterious diol compounds by EH, it may be useful to investigate the involvement of ep-PUFAs and EH in AD.

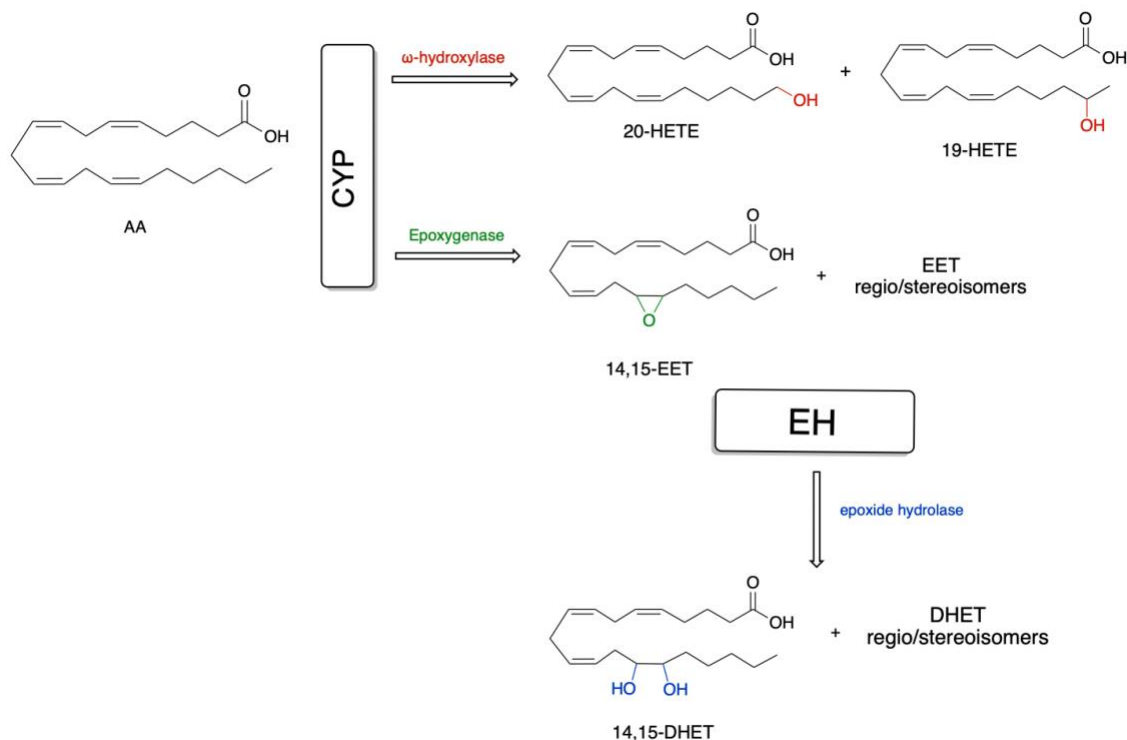


Figure 5: Arachidonic acid (AA) metabolism through typical CYP and EH activity^{55,65}. AA: arachidonic acid, CYP: Cytochrome P450 DHET: dihydroxyeicosatetraenoic acid, EET: epoxyeicosatetraenoic acid, EH: epoxide hydrolase HETE: hydroxyeicosatetraenoic acid

1.5. Epoxide hydrolase

1.5.1. Introduction to epoxide hydrolase

The major function of EH is to hydrolyze xenobiotic epoxides and ep-PUFAs. All EHs capable of metabolizing ep-PUFA to the corresponding diol contain an aspartate residue in the active site that appears to be necessary for successful hydrolysis. The catalytic activity of EH can be described in three enzymatic steps. First, the epoxide enters the L-shaped hydrophobic tunnel with the nucleophilic aspartate in the center. This enzyme-substrate complex is stabilized intermolecularly through hydrogen bonding between two tyrosine amino acids and the epoxide group of the substrate. Next, aspartate functions as an activated nucleophile and attacks the epoxide forming an ester intermediate. The third step is base activated hydrolysis of the ester

group forming the 1,2-diol and reforming the aspartate⁶⁶. This described mechanism is likely conserved in all functional EHs.

Microsomal epoxide hydrolase (mEH) was the first identified mammalian EH. It is encoded by the *EPHX1* gene and contains 455 amino acids in its primary structure. This membrane-bound enzyme is found attached to the surface of the endoplasmic reticulum (ER) or the plasma membrane by its N-terminal anchor⁶⁷. Another identified mammalian EH is soluble epoxide hydrolase (sEH). Humans sEH, encoded by *EPHX2*, is a 62 kDa homodimeric enzyme found in the cytosol and peroxisomes. The C-terminus is responsible for the epoxide hydrolase activity, and the N-terminus is responsible for the phosphatase activity. sEH enzymes are widely found in different tissues in the human body. Their expression as well as activity can be altered by sex, tissue, and age^{55,68}. Another identified mammalian epoxide hydrolase is EH4. EH4 is a 42 kDa protein encoded by the *EPHX4* gene. EH4 is more highly expressed in the brain than other tissues⁶². Higher expression of EH4 in the brain compared to other tissues suggests that it may play a more active role in the brain. However, all EHs identified in humans are expressed in brain tissues, and therefore, all EHs could possibly play a role in the relative ep-PUFA and 1,2-diol concentrations in the CNS.

In the brain, mEH is highly expressed in epithelial cells. Additionally, lower concentrations of mEH are found in a variety of neuronal cells including cerebellar granule cells, striatal neurons, hippocampal pyramidal neurons, and central amygdala neurons⁶⁹. Furthermore, elevated mEH expression occurs in the hippocampus of AD patients⁷⁰. The hippocampus is one of the primary regions affected by AD pathology. Therefore, mEH may be important in the pathological effects observed in this part of the brain of AD patients.

Soluble epoxide hydrolase (sEH) is expressed in different regions of the brain and in several cell types including astrocytes, endothelial cells, and neural cell bodies⁷¹. Additionally, sEH is involved in regulating pathways related to axonal growth in neurons and neural development, mainly through sEH catalyzed hydrolysis of ep-PUFAs⁷². Due to the neuronal effects of sEH, sEH can be another useful target to gain insight into AD pathology and/or be targeted for therapeutic benefits.

1.5.2. Increased 1,2-diol PUFA metabolites in AD patients

The primary product of EH activity are dihydroxy-PUFAs, which have increased polarity compared to ep-PUFAs. Therefore, they generally reside in the extracellular fluid (ECF) compartment and are generally considered to have little to no biological activity⁷³. However, several recent studies have suggested that dihydroxy-PUFAs play an important physiological role. For example, dihydroxy-PUFAs are present in human urine and plasma, and these levels correspond to various disease states⁷³. Therefore, dihydroxy-PUFAs may be directly or indirectly involved in various disease states, and/or dihydroxy-PUFAs may be useful biomarkers⁷³. Specifically, glucuronic acid conjugates, dihydroxy-9Z-octadecenoic acid (DiHOME), were found in the urine of children with peroxisomal disorders⁷⁴. Additionally, blood serum analyses of AD patients showed a significant increase (20%) of all four dihydroxyeicosatrienoic acid (DHET) species compared to healthy individuals⁷⁵. Further investigation of the molecular involvement of dihydroxy-PUFAs may be useful in developing potential therapeutics for neurodegenerative diseases and/or validating biomarkers for diseases like AD.

The brain has a high capacity to make ep-PUFAs from their parent PUFAs using CYP enzymes⁵⁵. In neuronal cells, ep-PUFAs are rapidly degraded by EHs, primarily by sEH^{55,76}. The major elimination pathway of ep-PUFAs is their hydrolysis to 1,2-diols. Additionally, recent

literature suggests that brain oxylipin levels may correlate to the amount of ingested dietary lipid content. Supplementation with ω -3 PUFAs (EPA and DHA) increases the level of EPA- and DHA-derived CYP metabolites and decreases ω -6 fatty acid, AA-derived, CYP metabolites in rat brains⁷⁷. The observed metabolite concentration change suggests that brain ep-PUFA concentrations are closely related to the concentrations of ω -3 and ω -6 fatty acids consumed in the diet. Additionally, ω -3 rich diets (EPA and DHA) reduced ep-PUFA levels and decreased ratio of epoxy to dihydroxy-PUFAs, which suggests increased sEH activity and/or increased sEH expression^{55,78}. Therefore, the ep-PUFA concentrations in the CNS are largely controlled by dietary sources and intake in mammals.

AD patients have increased expression levels of EH in specific regions of the brain, such as the hippocampus. A recent study investigated whether higher expression of EH in AD patients corresponds to higher diol concentrations in the serum. To test if higher expression of EH corresponds to higher diol concentration, serum was collected from 126 elderly individuals. Of these patients, 62 were considered cognitively healthy and 64 were diagnosed with AD. The oxylipin concentrations were analyzed using UPLC-MS/MS. The AD patients had higher levels of all four dihydroxyeicosatrienoic acid (DiHETrE) species: 14,15-DiHETrE (18% higher), 11,12-DiHETrE (18% higher), 8,9-DiHETrE (23% higher), and 5,6-DiHETrE (15% higher)⁷⁵. These data suggest that the EH expression levels do correlate to the increased 1,2-diol concentration in AD patients. Therefore, further investigation into the role of 1,2-diol species in AD patients may be useful in further understanding the pathology of the disease.

1.5.3. Soluble epoxide hydrolase inhibition in AD models

sEH function has been closely linked to neuroinflammation, likely caused by oxidative stress from reactive oxygen species (ROS), in neurological disorders, such as AD. Several nonsteroidal

anti-inflammatory drugs and antioxidant therapies have failed in clinical trials⁷⁹. Therefore, expanding the scope of novel targets may be the next logical step in therapy development. Recent literature suggests that brain-penetrant sEH inhibitors (sEHi) may stabilize EETs in the brain^{80,81}. Stabilizing EETs could lead to a cascade of events that reduce reactive oxygen species (ROS) and diminish neuroinflammation^{80,81}. The reduction in neuroinflammation may protect neurons from degeneration and ultimately lead to positive outcomes for AD patients. Three brain penetrant sEHs have been investigated in detail namely, TPPU, AS-2586114, and UB-EV-52. To demonstrate that the compounds had the desired effect of sEH inhibition, the levels of regulatory lipid mediators were measured in the cortex of treated and control mice. After treatment, the levels of proinflammatory lipid mediators, such as cytokines, were reduced in the treated mice, and concentrations of anti-inflammatory ep-fatty acids are found to be higher in all treated groups⁸⁰. Additionally, soluble epoxide hydrolase inhibition provoked a reduction in hyperphosphorylated tau concentration. Therefore, sEH inhibition may protect against the negative effects of hyperphosphorylated tau. Furthermore, treatment with all three sEH inhibitors drastically increased the discrimination index (DI) in a novel object recognition test (NORT)⁸⁰. In both models, a separate group of mice were also treated with donepezil, which is a treatment option for mild cases of AD. Interestingly, in all cases, the sEH inhibitors reduced cognitive decline better than donepezil. Therefore, sEH inhibition can be another useful avenue to investigate AD pathology and could also be used as new therapy.

1.6. *Caenorhabditis elegans*

1.6.1. Introduction to *C. elegans*

To investigate tauopathy in AD and other neurological disorders, the model organism *C. elegans* was selected. *C. elegans* are a free-living, non-parasitic nematode that was first

introduced as a model organism by Sydney Brenner in 1963. It is a small (~1 mm), transparent roundworm, with a short life cycle of ~3 weeks⁸². Additionally, the *C. elegans* genome has been published for over 20 years, and techniques like direct microinjection allow for production of transgenic worms that can model human disease, such as AD. Furthermore, the *C. elegans* genome shares 41% sequence homology with humans, with sequence similarity of 59%⁸³, and many signaling pathways are conserved between *C. elegans* and humans⁸⁴. Therefore, *C. elegans* serve as a suitable animal model to investigate specific diseases in which important biological features of that disease are conserved in *C. elegans* and humans.

C. elegans are self-fertilizing hermaphrodites with a 3-4 day reproductive cycle, and an average lifespan of 18-20 days when maintained at 20°C⁸⁵. After hatching, *C. elegans* can develop directly through four larval stages (L1-L4) or proceed to the dauer stage after L2, instead of L3. The dauer stage is a developmentally stunted stage with the ability to survive adverse conditions. Dauer should be avoided when actively conducting experiments with *C. elegans*. Worms will go into dauer when they experience adverse conditions, such as extreme temperature or lack of food. However, once the adverse conditions subside, *C. elegans* can recover and continue normal development where they exit dauer and re-enter the cycle at the L4 stage⁸⁵. Researchers must consider reproductive and developmental issues when actively performing the experiments, such as contamination of an age synchronized population with progeny. Despite the additional considerations that must be made, *C. elegans* are an incredibly useful model to study specific diseases, including AD.

1.6.2. Advantages of using *C. elegans* as an animal model

There are several advantages to using *C. elegans* as a model organism for human disease. First, *C. elegans* share significant sequence homology, ~41%, and sequence similarity, ~59%,

with humans^{83,84}. Therefore, it is likely that *C. elegans* possess homologs to much of the biological machinery involved in human disease. Additionally, the entire genome of *C. elegans* is published⁸². *C. elegans* are genetic malleable, and the *C. elegans* genome can be modified to express proteins of interest in human diseased states. Moreover, *C. elegans* consume non-pathogenic *E. coli.*, and the maintenance cost is extremely low. Furthermore, *C. elegans* are a transparent nematode, which enables imaging live animals with fluorescent microscopy. Researchers can genetically engineer *C. elegans* to express a fluorescent marker in specific cells to track cellular function. The tracking can be done throughout the lifespan of the worm as *C. elegans* are transparent. Therefore, no surgical intervention is necessary to study the fluorescence. Lastly, *C. elegans* have a short lifespan of ~3 weeks. Therefore, complete studies with multiple trials can be performed relatively quickly. The advantages of *C. elegans* enable large scale and relatively quick studies of complicated human diseased states. However, all models have some limitations. As *C. elegans* are nematodes and not mammals, the translatability of observed effects can always be brought into question. Therefore, the most effective way to use *C. elegans* is to perform large scale screening that cannot practically be performed in mammalian studies to narrow the research focus for more complicated mammalian models.

1.6.3. *C. elegans* as a model for AD

Accumulation of intracellular neurofibrillary tangles is a hallmark of AD. The primary molecular component of these tangles is the microtubule associated protein tau. A transgenic *C. elegans* strain has been developed that contains the molecular machinery to produce human tau *in vivo*. The first such model was based on the overexpression of human 4R1N tau pan-neuronally through the *Paex-3* promoter^{86,87}. The mutant worms show reduced survival, accumulate detergent-insoluble tau, and undergoes late-onset neurodegeneration. The human tau

expressing *C. elegans* provides a model to study AD, which can be further genetically modified through crossing to investigate specific molecular mechanisms of AD pathogenesis.

Tau is regulated post-translationally by a host of enzymes. One of particular interest in AD is phosphorylation. There are approximately 45 protein kinases that have been shown to phosphorylate tau^{22,88}. Kinases are highly conserved through evolution, and more than 65% of the human kinases have clear homologs with *C. elegans*^{86,87}. Therefore, human tau expressed in *C. elegans* neurons is expected to become phosphorylated by *C. elegans* kinases, which can further increase the neurodegeneration seen in the transgenic worm. Furthermore, *C. elegans* express two epoxide hydrolases that have high sequence homology with mammalian EH4⁵⁵. The homologs also contain the aspartate catalytic triad that is thought to be crucial for function. Lastly, recent unpublished data from the Lee lab analyzing the oxylipin profile of *C. elegans* AD model, containing both transgenic addition of human tau and human A β , shows an increase in AA derived 1,2-diols summarized in Figure 6. This increase in diol concentration was also observed in AD patient blood serum. PUFA and PUFA metabolite concentration have been linked to two primary methods of cell death suggested in AD pathology, namely ferroptosis and excitotoxicity^{89,90,91}. Therefore, *C. elegans* provide a useful model to study both tau phosphorylation and epoxide hydrolase activity in AD pathology as related to ferroptosis and excitotoxicity.

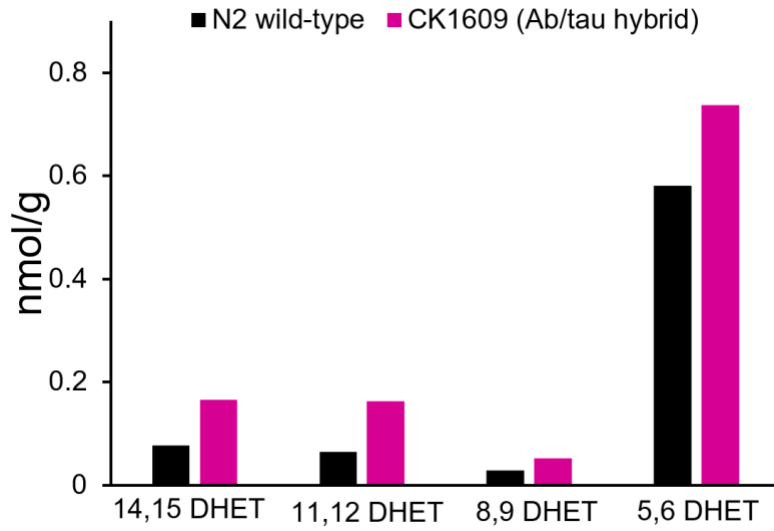


Figure 6: Concentration of 1,2-diols derived from AA in *C. elegans* AD model. DHET: dihydroxyeicosatrienoic acid

REFERENCES

REFERENCES

- (1) 2021 Alzheimer's Disease Facts and Figures. *Alzheimers. Dement.* **2021**, *17* (3), 327–406.
- (2) Bature, F.; Guinn, B.-A.; Pang, D.; Pappas, *BMJ Open* **2017**, *7* (8).
- (3) Stokes, A. C.; Weiss, J.; Lundberg, D. J.; Xie, W.; Kim, J. K.; Preston, S. H.; Crimmins, E. M. *JAMA Neurol.* **2020**, *77* (12), 1543–1550.
- (4) Wong, W. *Am. J. Manag. Care* **2020**, *26* (8), S177–S183.
- (5) Chen, X.-Q.; Mobley, W. C. *Front. Neurosci.* **2019**, *13*, 659.
- (6) Crdenas-Aguayo, M. del C.; del C. Crdenas-Aguayo, M.; del C. Silva-Lucero, M.; Cortes-Ortiz, M.; Jimnez-Ramos, B.; Gmez-Virgilio, L.; Ramrez-Rodrguez, G.; Vera- Arroyo, E.; Fiorentino-Prez, R.; Garca, U.; Luna-Muoz, J.; Meraz Ros, M. A. *Neurochemistry*. 2014.
- (7) Breijyeh, Z.; Karaman, R. *Molecules* **2020**, *25* (24).
- (8) Tarutani, A.; Miyata, H.; Nonaka, T.; Hasegawa, K.; Yoshida, M.; Saito, Y.; Murayama, S.; Robinson, A. C.; Mann, D. M. A.; Tomita, T.; Hasegawa, M. *Brain* **2021**, *144* (8), 2333–2348.
- (9) Orr, M. E.; Sullivan, A. C.; Frost, B. *Trends Pharmacol. Sci.* **2017**, *38* (7), 637–648.
- (10) Salvadores, N.; Gerónimo-Olvera, C.; Court, F. A. *Front. Aging Neurosci.* **2020**, *12*, 581767.
- (11) Kwon, H. S.; Koh, S.-H. *Transl. Neurodegener.* **2020**, *9* (1), 42.
- (12) Heneka, M. T.; Carson, M. J.; El Khoury, J.; Landreth, G. E.; Brosseron, F.; Feinstein, D. L.; Jacobs, A. H.; Wyss-Coray, T.; Vitorica, J.; Ransohoff, R. M.; Herrup, K.; Frautschy, S. A.; Finsen, B.; Brown, G. C.; Verkhratsky, A.; Yamanaka, K.; Koistinaho, J.; Latz, E.; Halle, A.; Petzold, G. C.; Town, T.; Morgan, D.; Shinohara, M. L.; Perry, V. H.; Holmes, C.; Bazan, N. G.; Brooks, D. J.; Hunot, S.; Joseph, B.; Deigendesch, N.; Garaschuk, O.; Boddeke, E.; Dinarello, C. A.; Breitner, J. C.; Cole, G. M.; Golenbock, D. T.; Kummer, M. P. *Lancet Neurol.* **2015**, *14* (4), 388–405.
- (13) Yiannopoulou, K. G.; Papageorgiou, S. G. *J. Cent. Nerv. Syst. Dis.* **2020**, *12*, 1-12.
- (14) Sevigny, J.; Chiao, P.; Bussière, T.; Weinreb, P. H.; Williams, L.; Maier, M.; Dunstan, R.; Salloway, S.; Chen, T.; Ling, Y.; O’Gorman, J.; Qian, F.; Arastu, M.; Li, M.; Chollate, S.; Brennan, M. S.; Quintero-Monzon, O.; Scannevin, R. H.; Arnold, H. M.; Engber, T.; Rhodes, K.; Ferrero, J.; Hang, Y.; Mikulskis, A.; Grimm, J.; Hock, C.; Nitsch, R. M.; Sandrock, A. *Nature* **2016**, *537* (7618), 50–56.

- (15) Aisen, P.; Lemere, C.; Atri, A.; Sabbagh, M.; Salloway, S. *Alzheimers. Res. Ther.* **2021**, *13* (1), 98.
- (16) How is Alzheimer's disease treated? <https://www.nia.nih.gov/health/how-alzheimers-disease-treated> (accessed 2022 -03 -12).
- (17) Pereira, J. B.; Janelidze, S.; Ossenkoppele, R.; Kivitsberg, H.; Brinkmalm, A.; Mattsson-Carlsson, N.; Stomrud, E.; Smith, R.; Zetterberg, H.; Blennow, K.; Hansson, O. *Brain* **2021**, *144* (1), 310–324.
- (18) Morris, M.; Maeda, S.; Vessel, K.; Mucke, L. *Neuron* **2011**, *70* (3), 410–426.
- (19) Miao, J.; Shi, R.; Li, L.; Chen, F.; Zhou, Y.; Tung, Y. C.; Hu, W.; Gong, C.-X.; Iqbal, K.; Liu, F. *Front. Aging Neurosci.* **2019**, *11*, 34.
- (20) Conway, M. E. *Biogerontology* **2020**, *21* (3), 257–274.
- (21) Musi, N.; Valentine, J. M.; Sickora, K. R.; Baeuerle, E.; Thompson, C. S.; Shen, Q.; Orr, M. E. *Aging Cell* **2018**, *17* (6), e12840.
- (22) Noble, W.; Hanger, D. P.; Miller, C. C. J.; Lovestone, S. *Front. Neurol.* **2013**, *4*, 83.
- (23) Neddens, J.; Temmel, M.; Flunkert, S.; Kerschbaumer, B.; Hoeller, C.; Loeffler, T.; Niederkofler, V.; Daum, G.; Attems, J.; Hutter-Paier, B. *Acta Neuropathol Commun* **2018**, *6* (1), 52.
- (24) Kenessey, A.; Yen, S. H. *Brain Res.* **1993**, *629* (1), 40–46.
- (25) Santa-Maria, I.; Varghese, M.; Ksiazak-Reding, H.; Dzhun, A.; Wang, J.; Pasinetti, G. M. *J. Biol. Chem.* **2012**, *287* (24), 20522–20533.
- (26) Rajmohan, R.; Reddy, P. H. *J. Alzheimers. Dis.* **2017**, *57* (4), 975–999.
- (27) Kaletta, T.; Hengartner, M. O. *Nat. Rev. Drug Discov.* **2006**, *5* (5), 387–398.
- (28) Roberson, E. D.; Halabisky, B.; Yoo, J. W.; Yao, J.; Chin, J.; Yan, F.; Wu, T.; Hamto, P.; Devidze, N.; Yu, G.-Q.; Palop, J. J.; Noebels, J. L.; Mucke, L. *J. Neurosci.* **2011**, *31* (2), 700–711.
- (29) Hall, A. M.; Roberson, E. D. *Brain Res. Bull.* **2012**, *88* (1), 3–12.
- (30) Wittmann, C. W.; Wszolek, M. F.; Shulman, J. M.; Salvaterra, P. M.; Lewis, J.; Hutton, M.; Feany, M. B. *Science* **2001**, *293* (5530), 711–714.
- (31) Steinhilb, M. L.; Dias-Santagata, D.; Fulga, T. A.; Felch, D. L.; Feany, M. B. *Mol. Biol. Cell* **2007**, *18* (12), 5060–5068.

- (32) Chen, K.; Jiang, X.; Wu, M.; Cao, X.; Bao, W.; Zhu, L.-Q.. *Front Cell Dev Biol* **2021**, *9*, 704298.
- (33) Dixon, S. J. *Immunol. Rev.* **2017**, *277* (1), 150–157.
- (34) Majerníková, N. 'a; den Dunnen, W. F. A.; Dolga, A. M. *Front. Aging Neurosci.* **2021**, *13*, 745046.
- (35) Ward, R. J.; Zucca, F. A.; Duyn, J. H.; Crichton, R. R.; Zecca, L.. *Lancet Neurol.* **2014**, *13* (10), 1045–1060.
- (36) Tao, Y.; Wang, Y.; Rogers, J. T.; Wang, F. *J. Alzheimers. Dis.* **2014**, *42* (2), 679–690.
- (37) Ayton, S.; Wang, Y.; Diouf, I.; Schneider, J. A.; Brockman, J.; Morris, M. C.; Bush, A. I.. *Mol. Psychiatry* **2020**, *25* (11), 2932–2941.
- (38) Raven, E. P.; Lu, P. H.; Tishler, T. A.; Heydari, P.; Bartzokis, G. *J. Alzheimers. Dis.* **2013**, *37* (1), 127–136.
- (39) Jaiswal, M. K.; Zech, W.-D.; Goos, M.; Leutbecher, C.; Ferri, A.; Zippelius, A.; Carrì, M. T.; Nau, R.; Keller, B. U. *BMC Neurosci.* **2009**, *10*, 64.
- (40) Manev, H.; Favaron, M.; Guidotti, A.; Costa, E. *Mol. Pharmacol.* **1989**, *36* (1), 106–112.
- (41) Meldrum, B. S. *J. Nutr.* **2000**, *130* (4S Suppl), 1007S – 15S.
- (42) Dysken, M. W.; Guarino, P. D.; Vertrees, J. E.; Asthana, S.; Sano, M.; Llorente, M.; Pallaki, M.; Love, S.; Schellenberg, G. D.; McCarten, J. R.; Malphurs, J.; Prieto, S.; Chen, P.; Loreck, D. J.; Carney, S.; Trapp, G.; Bakshi, R. S.; Mintzer, J. E.; Heidebrink, J. L.; Vidal-Cardona, A.; Arroyo, L. M.; Cruz, A. R.; Kowall, N. W.; Chopra, M. P.; Craft, S.; Thielke, S.; Turvey, C. L.; Woodman, C.; Monnell, K. A.; Gordon, K.; Tomaska, J.; Vatassery, G. *Alzheimers. Dement.* **2014**, *10* (1), 36–44.
- (43) Liu, J.; Chang, L.; Song, Y.; Li, H.; Wu, Y. *Front. Neurosci.* **2019**, *13*, 43.
- (44) Wang, R.; Reddy, P. H. *J. Alzheimers. Dis.* **2017**, *57* (4), 1041–1048.
- (45) Kirvell, S. L.; Esiri, M.; Francis, P. T. *J. Neurochem.* **2006**, *98* (3), 939–950.
- (46) Fernández-Tomé, P.; Brera, B.; Arévalo, M.-A.; de Ceballos, M. L. *Neurobiol. Dis.* **2004**, *15* (3), 580–589.
- (47) Madeira, C.; Vargas-Lopes, C.; Brandão, C. O.; Reis, T.; Laks, J.; Panizzutti, R.; Ferreira, S. T. *Front. Psychiatry* **2018**, *9*, 561.

- (48) Kawamoto, E. M.; Lepsch, L. B.; Boaventura, M. F. C.; Munhoz, C. D.; Lima, L. S.; Yshii, L. M.; Avellar, M. C. W.; Curi, R.; Mattson, M. P.; Scavone, C. *J. Neurosci. Res.* **2008**, *86* (4), 845–860.
- (49) Stockwell, B. R.; Friedmann Angeli, J. P.; Bayir, H.; Bush, A. I.; Conrad, M.; Dixon, S. J.; Fulda, S.; Gascón, S.; Hatzios, S. K.; Kagan, V. E.; Noel, K.; Jiang, X.; Linkermann, A.; Murphy, M. E.; Overholtzer, M.; Oyagi, A.; Pagnussat, G. C.; Park, J.; Ran, Q.; Rosenfeld, C. S.; Salnikow, K.; Tang, D.; Torti, F. M.; Torti, S. V.; Toyokuni, S.; Woerpel, K. A.; Zhang, D. D. *Cell* **2017**, *171* (2), 273–285.
- (50) Dixon, S. J.; Lemberg, K. M.; Lamprecht, M. R.; Skouta, R.; Zaitsev, E. M.; Gleason, C. E.; Patel, D. N.; Bauer, A. J.; Cantley, A. M.; Yang, W. S.; Morrison, B., 3rd; Stockwell, B. R. *Cell* **2012**, *149* (5), 1060–1072.
- (51) Lee, J.-Y.; Kim, W. K.; Bae, K.-H.; Lee, S. C.; Lee, E.-W. *Biology* **2021**, *10* (3).
- (52) Tuo, Q.-Z.; Lei, P.; Jackman, K. A.; Li, X.-L.; Xiong, H.; Li, X.-L.; Liuyang, Z.-Y.; Roisman, L.; Zhang, S.-T.; Ayton, S.; Wang, Q.; Crouch, P. J.; Ganio, K.; Wang, X.-C.; Pei, L.; Adlard, P. A.; Lu, Y.-M.; Cappai, R.; Wang, J.-Z.; Liu, R.; Bush, A. I. *Mol. Psychiatry* **2017**, *22* (11), 1520–1530.
- (53) Holth, J. K.; Bomben, V. C.; Reed, J. G.; Inoue, T.; Younkin, L.; Younkin, S. G.; Pautler, R. G.; Botas, J.; Noebels, J. L. *J. Neurosci.* **2013**, *33* (4), 1651–1659.
- (54) Zhang, E.; Kim, J.-J.; Shin, N.; Yin, Y.; Nan, Y.; Xu, Y.; Hong, J.; Hsu, T. M.; Chung, W.; Ko, Y.; Lee, W.; Lim, K.; Kim, D. W.; Lee, S. Y. *J. Med. Food* **2017**, *20* (6), 535–541.
- (55) Sarparast, M.; Dattmore, D.; Alan, J.; Lee, K. S. S. *Nutrients* **2020**, *12* (11).
- (56) Mokoena, N. Z.; Sebolai, O. M.; Albertyn, J.; Pohl, C. H. *Prostaglandins Other Lipid Mediat.* **2020**, *148*, 106426.
- (57) Monroig, Ó.; Tocher, D. R.; Navarro, J. C. *Mar. Drugs* **2013**, *11* (10), 3998–4018.
- (58) Wall, R.; Ross, R. P.; Fitzgerald, G. F.; Stanton, C. *Nutr. Rev.* **2010**, *68* (5), 280–289.
- (59) Cardoso, H. D.; dos Santos Junior, E. F.; de Santana, D. F.; Gonçalves-Pimentel, C.; Angelim, M. K.; Isaac, A. R.; Lagranha, C. J.; Guedes, R. C. A.; Beltrão, E. I.; Morya, E.; Rodrigues, M. C. A.; Andrade-da-Costa, B. L. da S. *Biochim. Biophys. Acta* **2014**, *1840* (6), 1902–1912.
- (60) Bazinet, R. P.; Layé, S. *Nat. Rev. Neurosci.* **2014**, *15* (12), 771–785.
- (61) Moore, M. M.; Pottenger, L. H.; House-Knight, T. *Environ. Mol. Mutagen.* **2019**, *60* (7), 624–663.

- (62) Decker, M.; Arand, M.; Cronin, A. *Arch. Toxicol.* **2009**, *83* (4), 297–318.
- (63) Bishop-Bailey, D.; Thomson, S.; Askari, A.; Faulkner, A.; Wheeler-Jones, C. *Annu. Rev. Nutr.* **2014**, *34*, 261–279.
- (64) Harris, T. R.; Aronov, P. A.; Jones, P. D.; Tanaka, H.; Arand, M.; Hammock, B. D. *Arch. Biochem. Biophys.* **2008**, *472* (2), 139–149.
- (65) Kroetz, D. L.; Zeldin, D. C. *Curr. Opin. Lipidol.* **2002**, *13* (3), 273–283.
- (66) Morisseau, C.; Hammock, B. D. *Annu. Rev. Pharmacol. Toxicol.* **2005**, *45*, 311–333.
- (67) Holler, R.; Arand, M.; Mecky, A.; Oesch, F.; Friedberg, T. *Biochem. Biophys. Res. Commun.* **1997**, *236* (3), 754–759.
- (68) Harris, T. R.; Hammock, B. D. *Gene* **2013**, *526* (2), 61–74.
- (69) Marowsky, A.; Burgener, J.; Falck, J. R.; Fritschy, J.-M.; Arand, M. *Neuroscience* **2009**, *163* (2), 646–661.
- (70) Liu, M.; Sun, A.; Shin, E.-J.; Liu, X.; Kim, S.-G.; Runyons, C. R.; Markesbery, W.; Kim, H.-C.; Bing, G. *Eur. J. Neurosci.* **2006**, *23* (8), 2027–2034.
- (71) Sura, P.; Sura, R.; Enayetallah, A. E.; Grant, D. F. *J. Histochem. Cytochem.* **2008**, *56* (6), 551–559.
- (72) Abdu, E.; Bruun, D. A.; Yang, D.; Yang, J.; Inceoglu, B.; Hammock, B. D.; Alkayed, N. J.; Lein, P. J. *J. Neurochem.* **2011**, *117* (4), 632–642.
- (73) Spector, A. A.; Kim, H.-Y. *Biochim. Biophys. Acta* **2015**, *1851* (4), 356–365.
- (74) Gabbs, M.; Leng, S.; Devassy, J. G.; Monirujjaman, M.; Aukema, H. M. *Adv. Nutr.* **2015**, *6* (5), 513–540.
- (75) Morris, J. K.; Piccolo, B. D.; John, C. S.; Green, Z. D.; Thyfault, J. P.; Adams, S. H. *Metabolites* **2019**, *9* (9).
- (76) Wagner, K.; Inceoglu, B.; Hammock, B. D. *Prostaglandins Other Lipid Mediat.* **2011**, *96* (1-4), 76–83.
- (77) Ostermann, A. I.; Waindok, P.; Schmidt, M. J.; Chiu, C.-Y.; Smyl, C.; Rohwer, N.; Weylandt, K.-H.; Schebb, N. H. *PLoS One* **2017**, *12* (9).
- (78) Hashimoto, M.; Katakura, M.; Tanabe, Y.; Al Mamun, A.; Inoue, T.; Hossain, S.; Arita, M.; Shido, O. *Biochim. Biophys. Acta* **2015**, *1851* (2), 203–209.

- (79) Rivers-Auty, J.; Mather, A. E.; Peters, R.; Lawrence, C. B.; Brough, D. *Brain Commun* **2020**, *2* (2), fcaa109.
- (80) Griñán-Ferré, C.; Codony, S.; Pujol, E.; Yang, J.; Leiva, R.; Escolano, C.; Puigoriol-Illamola, D.; Companys-Aleman, J.; Corpas, R.; Sanfeliu, C.; Pérez, B.; Loza, M. I.; Brea, J.; Morisseau, C.; Hammock, B. D.; Vázquez, S.; Pallàs, M.; Galdeano, *Neurotherapeutics* **2020**, *17*, 1825–1835.
- (81) Ghosh, A.; Comerota, M. M.; Wan, D.; Chen, F.; Propson, N. E.; Hwang, S. H.; Hammock, B. D.; Zheng, H. *Sci. Transl. Med.* **2020**, *12* (573).
- (82) Riddle, D. L.; Blumenthal, T.; Meyer, B. J.; Priess, J. R. *Cold Spring Harbor Laboratory Press*, **1997**.
- (83) Alexander, A. G.; Marfil, V.; Li, C. *Front. Genet.* **2014**, *5*, 279.
- (84) Lai, C. H.; Chou, C. Y.; Ch'ang, L. Y.; Liu, C. S.; Lin, W.. *Genome Res.* **2000**, *10* (5), 703–713.
- (85) Zhang, S.; Li, F.; Zhou, T.; Wang, G.; Li, Z. *Front. Endocrinol.* **2020**, *11*, 554994.
- (86) Pir, G. J.; Choudhary, B.; Mandelkow, E. *FASEB J.* **2017**, *31* (12), 5137–5148.
- (87) Kraemer, B. C.; Zhang, B.; Leverenz, J. B.; Thomas, J. H.; Trojanowski, J. Q.; Schellenberg, G. D. *Proc. Natl. Acad. Sci. U. S. A.* **2003**, *100* (17), 9980–9985.
- (88) Dolan, P. J.; Johnson, G. V. W. *Curr. Opin. Drug Discov. Devel.* **2010**, *13* (5), 595–603.
- (89) Brandt, R.; Gergou, A.; Wacker, I.; Fath, T.; Hutter, H. A. *Neurobiol. Aging* **2009**, *30* (1), 22–33.
- (90) Bao, W.-D.; Pang, P.; Zhou, X.-T.; Hu, F.; Xiong, W.; Chen, K.; Wang, J.; Wang, F.; Xie, D.; Hu, Y.-Z.; Han, Z.-T.; Zhang, H.-H.; Wang, W.-X.; Nelson, P. T.; Chen, J.-G.; Lu, Y.; Man, H.-Y.; Liu, D.; Zhu, L.-Q. *Cell Death Differ.* **2021**, *28* (5), 1548–1562.
- (91) Babaei, P. *Eur. J. Pharmacol.* **2021**, *908*, 174310.

CHAPTER TWO:
INVESTIGATION OF NEURODEGENERATION IN GLUTAMATERGIC NEURONS
USING *C. ELEGANS*

2. GLUTAMATERGIC NEURON SYSTEM

2.1. Introduction to glutamatergic neuron system

2.1.1. General identification and function of glutamatergic neuron system

Glutamate is one of the major excitatory neurotransmitters in the nervous system.

Glutamate is an amino acid and neurotransmitter, and therefore, it has many normal physiological functions. Consequently, disruption of the physiological function of glutamate has profound effects both in disease and injury¹.

Glutamate concentrations in the extracellular space of humans are low (~25 μM) and tightly controlled by several mechanisms at the synapse^{1,2,3}. Perturbations to the regulatory system can lead to release of excessive glutamate, which can cause excitotoxicity and cell death. Disruptions of the regulatory system have been linked to impaired spatial learning and reduced sensitivity to reward^{1,4,5}. Therefore, the endogenous level of glutamate is tightly regulated to maintain health of the organism.

Glutamatergic neurons can be identified through detection of mRNA encoding vesicular glutamate transporters (VGluTs), which transport glutamate into synaptic vesicles at presynaptic terminals⁶. Three isoforms of the vesicular glutamate transporter are known and present in the CNS namely, VGluT1, VGluT2, and VGluT3⁶. As VGluTs are responsible for the transport of glutamate into synaptic vesicles, VGluTs are also tightly regulated⁷. Any disruption in the tight regulation of VGluTs can lead to increased glutamate at the synapse, which causes excitotoxicity and eventually cell death⁸. A plethora of neurological disorders can cause dysregulation of

VGluTs leading to uncontrolled glutamate concentrations leading to cell death⁹. Additionally, the glutamatergic system has a host of ligand-gated ionotropic receptors (iGluRs) who play fundamental roles in synaptic plasticity, which is an underlying mechanism of learning and memory¹⁰. Due to the important roles of the iGluRs in glutamate neurotransmission, disruption of the normal signaling can also lead to excitotoxicity and eventually cell death. Therefore, regulation of iGluRs is implicated in a range of neurological disorders including AD.

2.1.2. Alzheimer's Disease effects on glutamatergic neuron system

Many neurological disorders, including AD, share a final common deadly pathway known as excitotoxicity⁹. Recent literature suggests that excitotoxicity may be one of the primary mechanisms of cell death in patients with AD patients^{10,11}. There is significant evidence suggesting that the glutamatergic neuron system becomes degenerated as AD progresses. For example, the concentrations of VGluT1 and VGluT2 were quantified in the prefrontal and dorsolateral cortex of healthy and AD patients using specific antisera¹². The results showed a dramatic decrease in VGluT1 and VGluT2 concentrations in AD patients postmortem. These results suggest that VGluT1 and VGluT2 cannot regulate the concentration of glutamate at the synapse as efficiently, which can lead to excitotoxicity of the glutamatergic neurons¹². Furthermore, activation of extrasynaptic iGluR N-methyl-d-aspartate receptor (NMDAR) promotes cell death¹⁰. Therefore, glutamate receptor involvement can also contribute to the cell death of glutamatergic neurons observed in AD. Most likely neurodegeneration of the glutamatergic neurons observed in AD is caused by some combination of dysregulation of VGluTs, iGluRs like NMDAR, and possibly other receptors.

Ferroptosis is another possible mechanism of neuronal cell death in AD¹³. Ferroptosis is an iron-dependent lipid peroxidation-driven cell death mechanism¹⁴. AD pathological hallmarks

are consistent with characteristics of ferroptosis namely, excess iron accumulation, elevated lipid peroxides, elevated reactive oxygen species (ROS), reduced glutathione, and reduced glutathione peroxidase 4 (GPX4) levels¹⁵. Additionally, specific ferroptosis inhibitors, such as liproxstatin-1, can relieve some of the cognitive decline in AD mammalian animal models¹⁵. Therefore, ferroptosis may be contributing to the cell death mechanism observed in AD pathology.

2.1.3. *C. elegans* glutamatergic neuron model strains

EAT-4 is the only homologue of human VGluT identified in *C. elegans*. As glutamatergic neurons are identified by the presence of VGluT, the EAT-4 homologue has been studied in detail to understand the glutamatergic neuron system in *C. elegans*¹⁷. To investigate the glutamatergic neuron system in *C. elegans*, the *eat-4* gene, which encodes for the EAT-4 protein, was tagged with a GFP reporter¹⁷. Therefore, all neurons with the EAT-4 protein, namely glutamatergic neurons, will fluoresce. The reporter was identified in 78 of the 302 neurons of the adult hermaphrodite. Therefore, approximately 25% of the neurons in a *C. elegans* hermaphrodite are glutamatergic. The reporter study establishes an excellent baseline understanding of the glutamatergic neuron system in *C. elegans* that can be used for further investigation of neurological disorders like AD.

As previously described, AD is linked to two key proteins, tau and A β . To generate an AD *C. elegans* model, human 4R1N tau was inserted into wildtype *C. elegans* using the *Paex-3* promoter by direct microinjection¹⁸. The *aex-3::tau(4R1N)* transgenic *C. elegans* line displayed significant phenotypes including decreased thrashing and decreased cholinergic neuronal transmission¹⁸. Therefore, tau significantly affects the worm healthspan observed in both thrashing (movement) and neuron function phenotypes. To further investigate the role of the glutamatergic neuron system in AD, a cross between the tau transgene and the *eat-4::GFP*

reporter gene can be generated through traditional *C. elegans* genetic crossing. The progeny provides a method to directly observe the effects of tau insertion on the glutamatergic neurons through fluorescence microscopy.

2.2. Experimental

2.2.1. Preparation of nematode growth media (NGM)

C. elegans were maintained on nematode growth media (NGM) poured into petri dishes using a standard protocol. All work herein uses large petri dishes with a diameter (100 mm) from ThermoFisher unless otherwise denoted. NGM was prepared by mixing 3 g of NaCl, 15 g of agar, and 2.5 g of tryptone. The solid mixture was dissolved in 975 mL of DI H₂O. The solution was then autoclaved for 1 hour and cooled to 55°C before pouring. Then, 25 mL of 1 M KH₂PO₄/K₂HPO₄ buffer was added to the NGM solution to control pH to approximately 7. After addition of buffer, 1 mL of 5 mg/mL cholesterol in ethanol, 1 mL of 1 M CaCl₂, and 1 mL of 1 M MgSO₄ were added to the NGM solution. Approximately 15 mL of the final NGM mixture was added to each plate¹⁹.

2.2.2. Preparation of bacterial food source (OP50)

A liquid media of Luria broth (LB) was prepared in a 1 L bottle mixing 10 g Bacto-tryptone, 5 g Bacto-yeast, 5 g sodium chloride, and DI water to a total solution volume of 1 L. Approximately 1 mL of starter stock OP50 *E. coli.*, obtained from *Caenorhabditis* Genetics Center (CGC), was transferred to the LB and allowed to grow overnight in an incubator at 37°C. After the overnight culture was grown, several 1 mL samples were removed and optical density at 600 nm (OD₆₀₀) was measured. Desirable bacterial stocks have an OD₆₀₀ of 0.4-0.6²⁰. All studies presented herein used bacterial stocks within this OD₆₀₀ range.

2.2.3. Seeding NGM with bacteria

Approximately 40 mL of bacterial culture with an OD₆₀₀ of 0.4-0.6 were aliquoted from the culture to a 50 mL centrifuge tube using sterile technique. Then, 100-150 µL of the solution was placed on each NGM plate and spread using a glass rod. Care was taken to ensure that the bacteria lawn was confined to the center of the NGM plate as the worms have a propensity to crawl up the sides of the petri plate if the bacteria is too close to the edge. Plates seeded with bacteria were left to dry overnight at room temperature. The dry, seeded NGM plates were then placed into an airtight box and stored at 4°C for future use. Seeded plates remain usable for approximately 2 weeks¹⁹.

2.2.4. Transferring worms

C. elegans constantly produce progeny throughout the early stages of adulthood. An unattended plate will become overrun with worms of various ages. Therefore, worm stocks need to be consistently transferred to freshly seeded NGM plates to avoid overpopulation and eventual lack of food²¹. In this research, two methods were used, chunking and picking. Chunking was performed with a sterile spatula. The sterile spatula was used to remove a piece of the agar, referred to as a chunk, and moved to a freshly seeded plate. The chunk contains many worms that will generate new progeny. The progeny was assessed for health through qualitative healthspan assays of crawling and locomotion before using this population for a quantitative assay. The second method used for transferring worms was individually picking worms with a worm pick. Worm picks were made by mounting a 1-inch piece of 32-gauge platinum wire into the tip of a Pasteur pipet. Platinum was used because of its high thermal conductivity. Therefore, it can be easily sterilized with a flame and cooled quickly to room temperature between each worm transfer. The end of the platinum wire of each pick was flattened with pliers to prevent

damaging the worm's cuticle and piercing the agar on each plate²². Approximately 50-100 μL of s-basal solution was placed on the seeded NGM plate in an area free of bacteria. S-basal was prepared by mixing 5.85 g of sodium chloride, 50 mL of a 1 M $\text{KH}_2\text{PO}_4/\text{K}_2\text{HPO}_4$, 1 mL of a 5 mg/mL cholesterol in ethanol solution, and DI water to 1 L total solution volume. The s-basal solution was sterilized by autoclaving before use¹⁹. Picked worms are transferred to the s-basal on the freshly seeded plate for an easier transfer. All worms are maintained in incubators at 20°C unless otherwise denoted.

2.2.5. Preparation of supplemented plates

Throughout this research, the effects of different supplements were tested. Two methods were used to prepare supplemented plates. First, supplements dissolved in ethanol at desired concentration were added directly to the surface of the agar plate and spread using a sterilized glass rod. OP50 bacteria was placed on top of this supplement and spread as quickly as possible to prevent oxidation of the compound/supplement²⁴. The process of supplementation is illustrated in Figure 7.

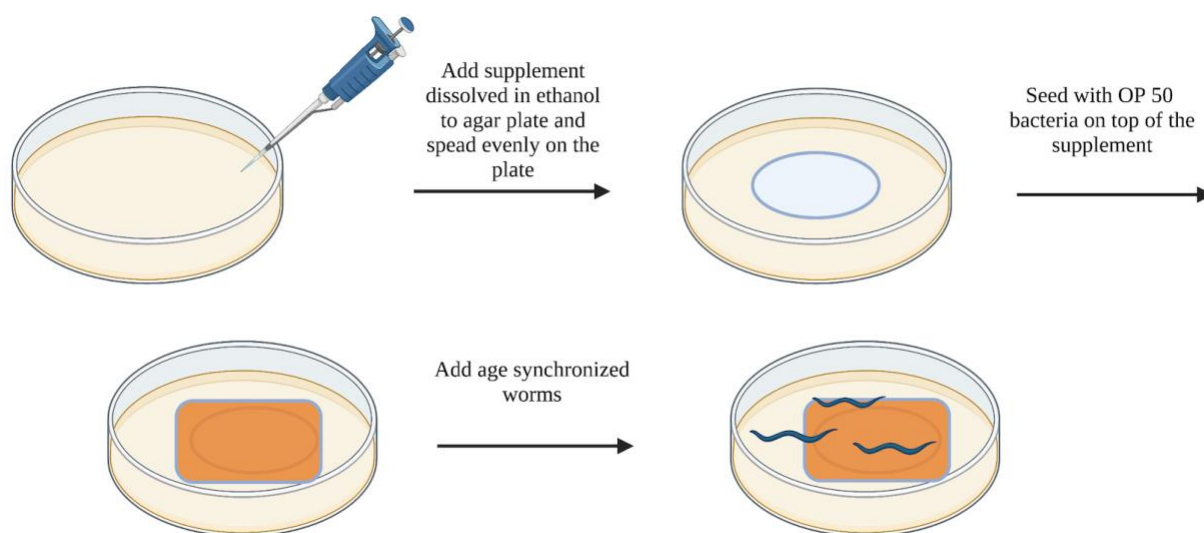


Figure 7: Supplementing directly on the surface of the agar.

Additionally, supplements were added to the agar solution before plates were poured. During the NGM preparation process, supplements were added to the agar solution after autoclaving and cooling to 55°C. Therefore, the supplement was directly inside of the agar that the worms were grown on²⁴. This process is illustrated in Figure 8. These methods were often used in tandem to provide multiple supplements used at the same time, and the methods were optimized for each supplement.

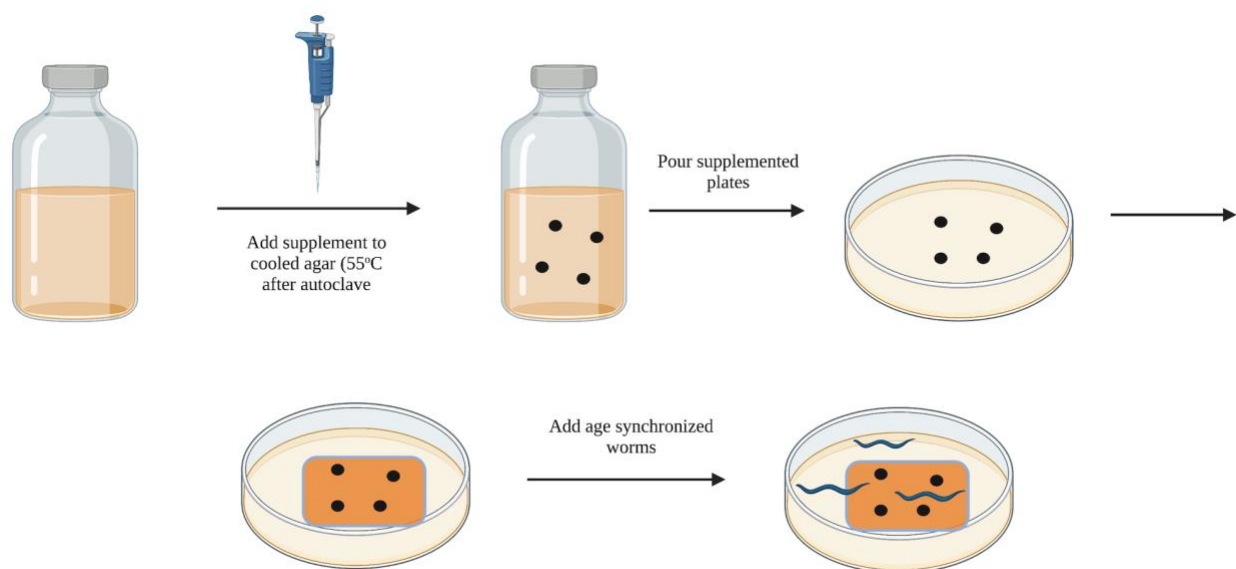


Figure 8: Supplementing plates in the agar.

2.2.6. Generation of novel strains through crossing

Five larval stage 4 (L4) N2 males were collected and transferred to a freshly seeded NGM plate. Additionally, five L4 hermaphrodites with desired trait #1 were placed on the same plate. In this research, all desired traits were detected with green fluorescent protein (GFP) and/or red fluorescent protein (RFP). The mixed N2 male and trait #1 hermaphrodite population were allotted sufficient time to produce progeny, which is approximately 1-2 days¹⁸. Next, five larval stage 4 (L4) male of new progeny (P₁#1) were collected and transferred to a freshly seeded NGM plate. Then, five L4 hermaphrodites with desired trait #2 were placed on the same plate

and allotted sufficient time to produce new progeny, which is approximately 1-2 days. Then, five larval stage 4 (L4) hermaphrodite of new progeny (F₁#1:: #2) that has the GFP/RFP markers of both trait #1 and trait #2 were collected and transferred to five freshly seeded NGM plate (1 larva/plate) and let to produce new progeny. Homozygous populations were identified by isolating the plates with all progeny expressing both traits (GFP/RFP). Only the homozygous populations were picked for generating larger population stocks. The progeny containing both desired traits are then crossed two to three more times with wildtype N2 to ensure that outcrossing has taken place. Outcrossing ensures that all progeny with the desired trait are homozygotes, and therefore, the outcrossed population will only produce progeny with the desired traits until single nucleotide polymorphisms affect the region of DNA responsible for the trait^{18,25}.

2.2.7. Generation of AD model with glutamatergic GFP (JKA71)

To produce the novel strain, JKA71, *eat-4::GFP; aex-3::tau*, N2 males were crossed with OH11152 [*eat-4::GFP; ttx-3::DsRed*] to produce GFP and RFP/+ males. Refer to section 2.2.6. for more details about crossing. These GFP and RFP/+ males were crossed with CK1441 [*Paex-3::tau(4RIN); Pmyo-2::DsRed*] hermaphrodites. The progeny expressing two specific traits namely, *myo-2::DsRed* labeled pharynx and *eat-4::GFP* neurons in the head, were isolated and transferred to a freshly seeded plate. The red pharynx serves as a biomarker that the tau insertion has been expressed. It is difficult to detect the *ttx-3::DsRed* neurons as the neurons often overlap with the pharynx. The progeny expressing both desired traits, *myo-2::DsRed* labeled pharynx and *eat-4::GFP* neurons, were left to produce progeny for 2-3 days. The homozygote was left to self-fertilize and produce progeny for 2 generations¹⁸. If after the second generation all progeny contain both traits, the cross was successful in producing homozygotes. The homozygous

progeny was used as a stock for all phenotypic assays using the *eat-4::GFP; aex-4::tau* strain (JKA71).

2.2.8. Age synchronization

To produce an age synchronized population, 100 healthy adult worms, typically day 1 to day 4 unless specifically mentioned, were moved to a freshly seeded plate. Healthy adult worms lay approximately 50-200 eggs per day²⁶. The adult worms were given sufficient time, approximately 12-24 hours, to lay eggs. Once the plate contained the desired number of eggs and L1 stage worms, which varies depending on the assay to be performed, the healthy adult worms (egg layers) were removed from the plate. Afterwards, the plate was covered in hundreds of eggs that are within a few hours of identical age. The plate full of eggs and L1 was used as the age synchronized population. The age synchronization process is illustrated in Figure 9.

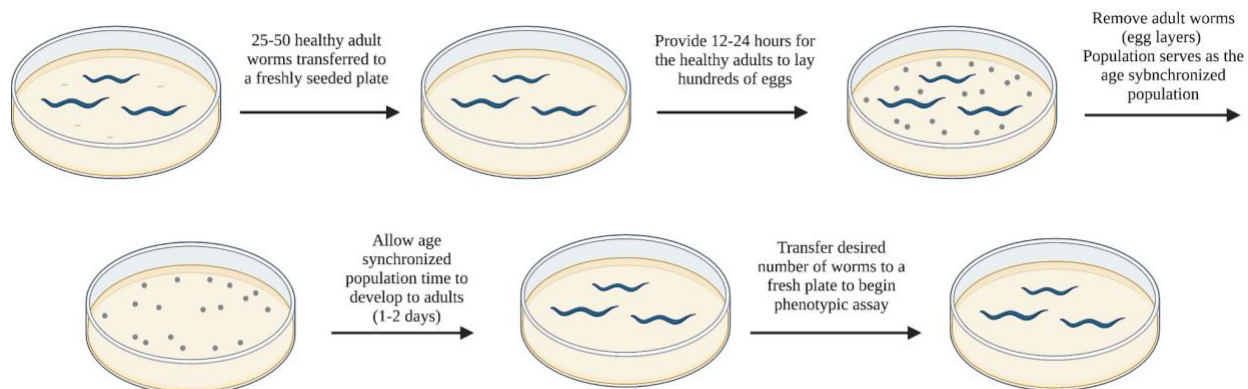


Figure 9: Age synchronization process.

2.2.9. Maintenance of age synchronized population

Once the worms were age synchronized, they were allotted sufficient time to develop to adulthood through the larval stages (L1, L2, L3, L4, adults). The age synchronized population of adult worms will begin producing progeny, and the progeny will contaminate the age synchronized population. After the progeny develops to the adult stage, it becomes difficult if not impossible to distinguish the adult progeny from the initial age synchronized population.

Therefore, it is important to constantly separate the progeny from the age synchronized population. Every day the age synchronized population was filtered through a 40 μm cell strainer placed on top of a 50 mL centrifuge tube. The adult worms are approximately 1 mm in length and 80-100 μm in diameter²⁷. Therefore, the adult worms will not pass through the cell strainer and are caught on the surface. The eggs and the larval stage have a diameter smaller than 40 μm ²⁸. The progeny was collected in the filtrate and removed. The adult worms were removed from the surface of the cell strainer and placed on a freshly seeded NGM plate. The filtration process was repeated every day during early adulthood of the age synchronized population to avoid any contamination from the progeny. Maintenance of the age synchronized population is described in Figure 10.

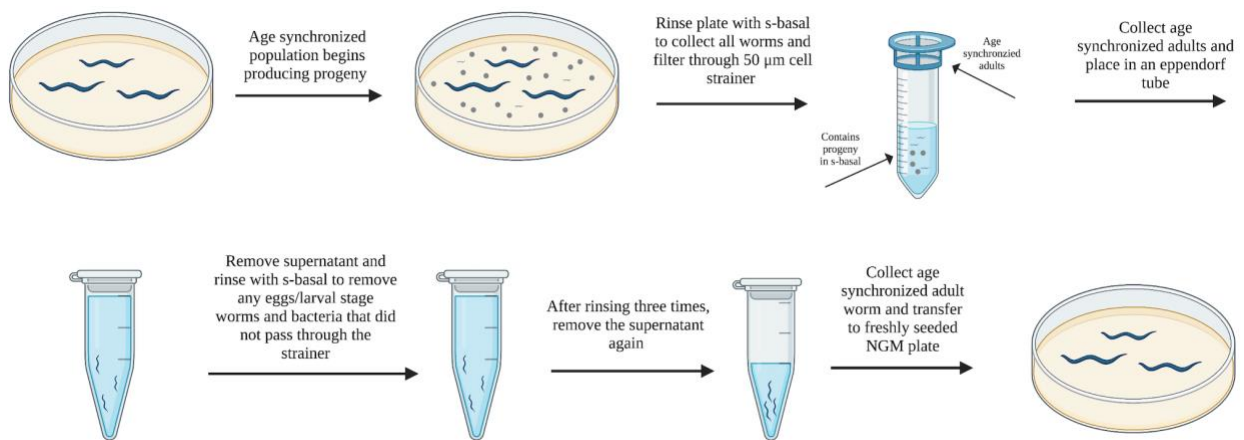


Figure 10: Age synchronization maintenance through filtration.

2.2.10. Glutamatergic neuron assay

A 1% agarose solution was prepared in 200 mL of DI water. Sufficient sodium azide was added to generate a 2 mM NaN_3 solution mixed in the 1% agarose solution. Approximately 200-400 μL agarose/sodium azide solution was placed on a microcopy slide. Another slide was placed on top of agarose/sodium azide droplet to generate a smooth pad that the worms can be placed. Once the agar pad is sufficiently dry, the second slide was removed. Then, 10 μL of 5

mM sodium azide was placed on top of the pad, and approximately 20 worms were placed into the droplet of sodium azide, which functioned to paralyze the worms for imaging. The worms were observed until all were fully paralyzed. Lastly, a microscopy slide cover was placed on top of the paralyzed worms when the sodium azide solution had near completely evaporated. The microscopy slide containing the paralyzed worms was then placed under a Nikon Ti-2 inverted microscope for analysis of neuronal GFP in the paralyzed worms²⁹. The neuron assay process is illustrated in Figure 11.

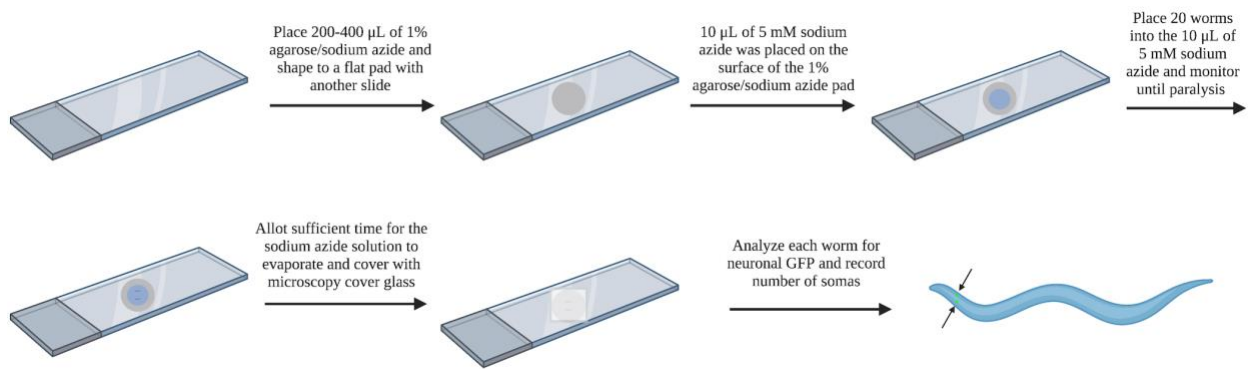


Figure 11: Neuron assay.

2.2.11. Thrashing assay

For thrashing assays, 20 age synchronized worms of a desired age, (day 1, day 4, etc.) were transferred by a worm pick to 10 μL of s-basal on a NGM only plate at room temperature. The worms were allotted 30 seconds to move or “thrash”. After the 30 seconds, the worms’ movement or “thrashing” was recorded using a camera. The thrashing assay process is illustrated in Figure 12.

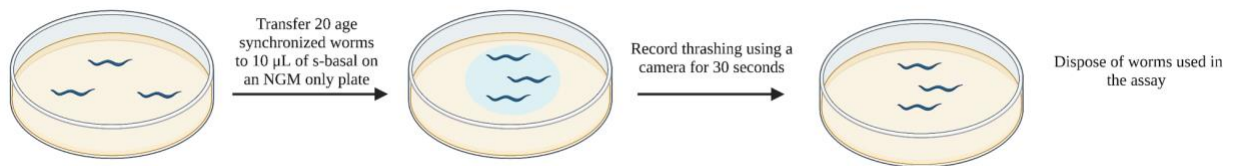


Figure 12: Thrashing assay.

One “thrash” was recorded when a complete sinusoidal motion was completed. Therefore, “thrashes” were only counted when the worms head and body moved from their starting position to the other side of a vertical axis and back to the starting position³⁰. The scoring process is illustrated in Figure 13.

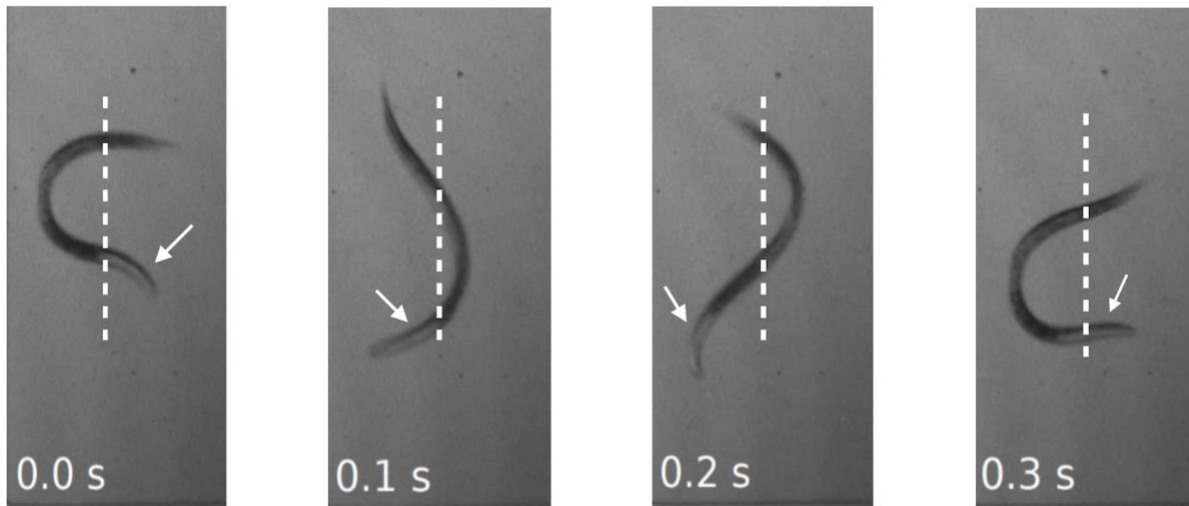


Figure 13: Scoring thrashing of *C. elegans*³⁰.

2.2.12. Collecting and freezing worm samples for oxylipin and lipidomic analysis

Oxylipins are a class of bioactive lipid metabolites derived from PUFAs via cyclooxygenase (COX), lipoxygenase (LOX), and cytochrome P450 enzymatic pathways. To investigate the oxylipin profile in *C. elegans*, we collected 5 mg of worms per trial to ensure that the whole worm lysates contain a sufficient concentration of oxylipins for detection. A sufficiently sized population of worms was generated by growing a population on 7 large plates, (100 mm diameter) per trial, with approximately 300-400 worms. Therefore, to generate 5 mg of whole worm lysates, we prepared approximately 2000-3000 worms. The age synchronized population of worms were generated and maintained using the filtration method illustrated and described in section 2.2.8 and 2.2.9. When a population of worms was ready for isolation and collection, the entire population was transferred and filtered using s-basal and a 40 μ M cell

strainer. The worms that collected on the surface of the cell strainer were transferred using a Pasteur pipet to an Eppendorf vial. The worms were rinsed with s-basal and centrifuged. The supernatant was collected and discarded. The worms were then washed four more times to ensure that all bacteria and supplemented PUFA was removed. After the bacteria and supplement was removed, the Eppendorf vials containing each worm sample were transferred to a benchtop centrifuge. The vials were centrifuged for 10 minutes at 10,000 rpm at 4°C. The supernatant was removed using 100 µL and 10 µL pipets. A 20 µL pipet with a long tip was pushed to the bottom of the vial to remove liquid between the worms. Lastly, standard filter paper was cut into sharp triangles that were small enough to fit into the Eppendorf vials. One filter paper triangle was placed into each vial and left for 5 minutes to remove any remaining liquid within the worm sample. Additional filter paper was added until the paper remained dry after placement in the vial for 5 minutes. After all the liquid was removed, the worm samples were flash frozen using liquid nitrogen and stored in the -80°C freezer. The collection of worms for oxylipin and lipidomic analysis is illustrated in Figure 14.

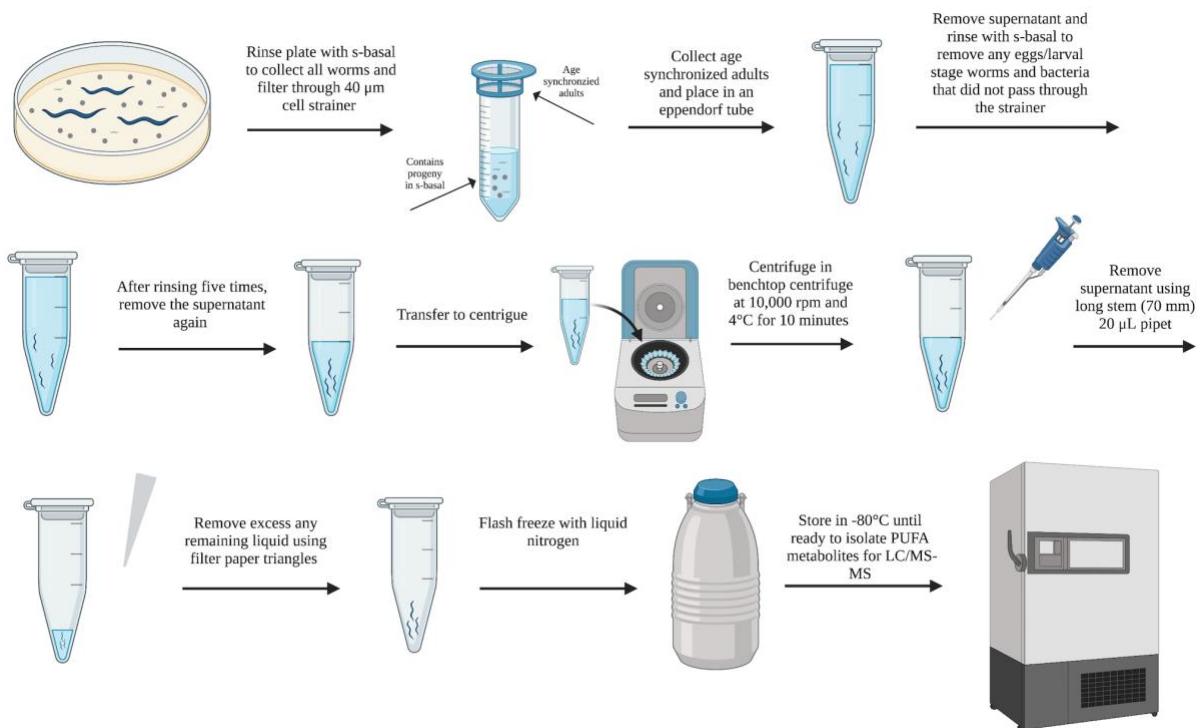


Figure 14: Worm sample preparation for oxylipin and lipidomic analysis.

2.2.13. Worm homogenization for oxylipin and lipidomic analysis

Eppendorf vials containing dry worm samples were removed from -80°C storage. The worm samples were flash frozen using liquid nitrogen once more, and the solid worm mass was broken loose using a 0.7 mm needle. The solid worm mass was transferred to the homogenizer vial and mass was recorded. Three homogenization beads were added to each homogenizer vial. Additionally, 100 μL phosphate-buffered saline (PBS), 10 μL of internal standard, consisting of 10 deuterated oxylipins, and 10 μL of antioxidants, consisting of ethylenediamine tetraacetic acid (EDTA), butylated hydroxytoluene (BHT), and triphenylphosphine (TPP) were added to each homogenizer vial. The details of the deuterated oxylipin standards are shown in Table 1. Each homogenizer vial containing the worm samples were flash frozen using liquid nitrogen and then homogenized for five 30 second cycles at 5 M/s using an omni bead ruptor 24 homogenizer. After homogenization, an additional 900 μL of PBS was added to the homogenized sample. The

sample was centrifuged using a benchtop centrifuge at 10,000 rpm for 5 minutes. The supernatant was collected and transferred to a new Eppendorf for solid phase extraction. The process of homogenization is illustrated in Figure 15.

Oxylipin standard name	Oxylipin standard abbreviation
6-keto prostaglandin F _{1α} -d4	6-keto-PGF _{1α} -d4
5(S)-hydroxyeicosatetraenoic-d8 acid	5(S)-HETE-d8
8,9-epoxyeicosatrienoic-d11 acid	8,9-EET-d11
Arachidonic-d8 acid	AA-d8
15(S)-hydroxyeicosatetraenoic-d8 acid	15(S)-HETE-d8
Prostaglandin B ₂ -d4	PGB ₂ -d4
8,9-dihydroxyeicosatrienoic-d11 acid	8,9-DiHETrE-d11
9(S)-hydroxyoctadecadienoic-d4 acid	9(S)-HODE-d4
Leukotriene B ₄ -d4	LTB ₄ -d4
Prostaglandin E ₂ -d9	PGE ₂ -d9

Table 1: Deuterated standards used for oxylipin analysis.

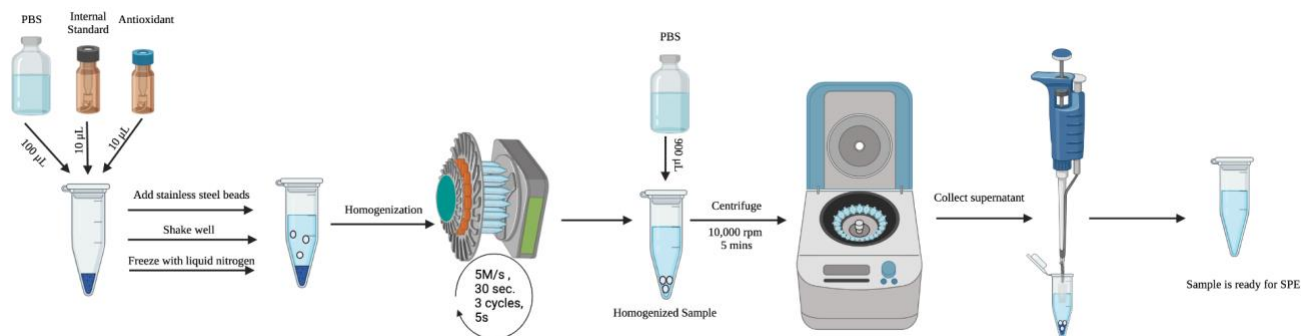


Figure 15: Worm homogenization for oxylipin and lipidomic analysis.

2.2.14. Solid phase extraction to isolate oxylipins from the whole worm lysate

To isolate oxylipins from the whole worm lysates, solid phase extraction (SPE) was used. We used a polar stationary phase to trap extremely polar biological material such as sugars. The oxylipins that we are isolating are significantly less polar in comparison. To begin, the SPE column was prepared by sequential washing with 2 mL ethyl acetate, two washes with 2 mL methanol, and then washing with 2 mL of 95:5 (v/v) mixture of water and methanol containing 0.1% acetic acid. The column was not allowed to completely dry during preparation. The process of SPE column preparation is illustrated in Figure 16.

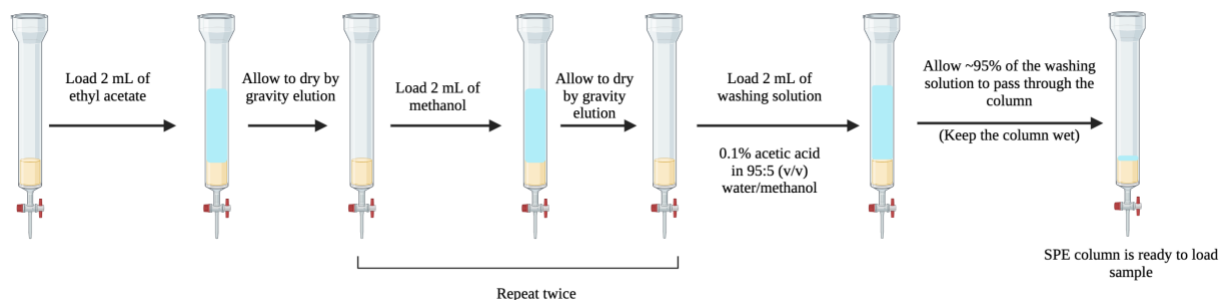


Figure 16: Solid phase extraction column preparation.

After the SPE column was prepared, the Eppendorf vials containing the prepared samples after homogenization were loaded onto the SPE column. The sample was washed by gravity with no added pressure. After the column was loaded with the sample from gravity, 1.5 mL of the washing solution, 95:5 (v/v) mixture of water and ethanol with 0.1% acetic acid, was added to the column. The column was dried by gravity until all liquid was undetectable by eye. Next, the column was thoroughly dried with vacuum pump for 20 minutes. After thorough drying, the column was ready for elution. The process of loading the sample to the SPE column is illustrated in Figure 17.

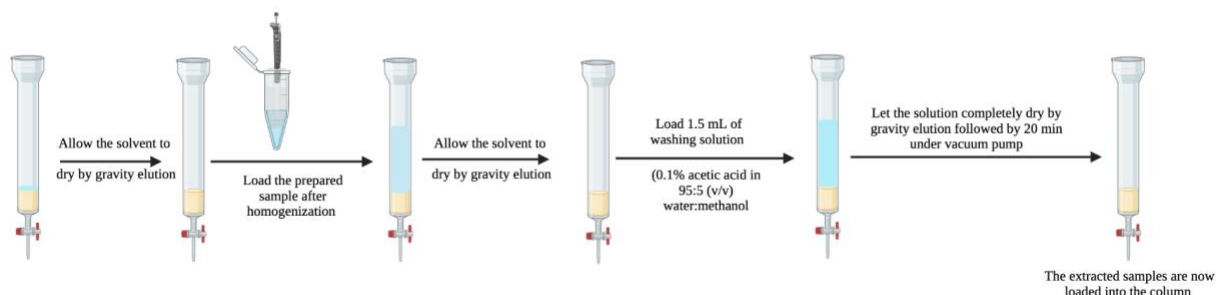


Figure 17: Loading the sample to the SPE column.

After the column was loaded with the sample and completely dried, 0.5 mL of methanol was added to begin the elution step. Eluted compounds were collected to an Eppendorf vial containing 6 μL of 30% glycerol in methanol, which serves as a trap solution. The column was allowed to gravity elute until the column appeared dry. A 5 mL syringe was filed with air and placed on the top of the SPE column to gently push the remaining solvent out of the column with

air. Once the column was completely dry, 1 mL of ethyl acetate was added to the column. The solvent was allowed to gravity elute until the column appeared dry. The remaining solvent was again removed using a 5 mL syringe gently pushing air through the column. The process of eluting is illustrated in Figure 18.

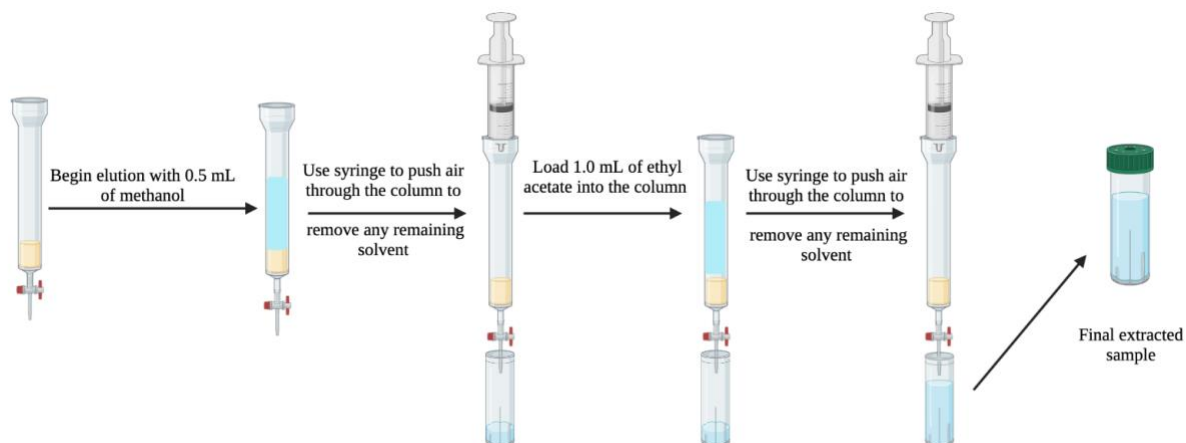


Figure 18: Elution of oxylipins from SPE column.

Upon completion of SPE, the final extracted sample was dried using a speed-vac until the trap solution was all that remained. The residues were reconstituted with 100 μ L of 75% methanol/water containing 10 nM of internal standard, 12-[(cyclohexylcarbamoyl)amino]dodecanoic acid (CUDA). The samples were then mixed on a vortex for five minutes and filtered with a 0.45 μ m filter. Lastly, the samples were transferred to auto-sampler vials with salinized inserts, purged with argon gas, and stored at -80°C until injection.

2.2.15. Isolation of PUFAs from whole worm lysates

Whole worm samples for lipidomic analysis were prepared as described in sections 2.2.13. Next, 20 mL of the lipid extraction solvent, consisting of 50:50 (v/v) methanol and chloroform containing 0.1% butylated hydroxytoluene (BHT), was prepared. The worms were flash frozen using liquid nitrogen before transferring to a 2 mL cryogenic vials by a 0.7 mm

needle as described in section 2.2.14. After the worms were transferred to the cryogenic vial, 0.1 mL of the lipid extraction solvent and 2-3 homogenization beads were added to each cryogenic vial. Each homogenizer vial containing the worm samples were flash frozen using liquid nitrogen and then homogenized for five 30 second cycles at 5 M/s using an omni bead ruptor 24 homogenizer. The whole worm lysates were transferred to a borosilicate glass tube using an additional 0.4 mL of cold methanol and 1 mL of cold chloroform. Lastly, 5 μ L of internal standard, nonadecanoic acid, was added to each sample. Each vial was mixed using a vortex for two minutes each. The samples were then sonicated using a benchtop sonicator bath for 15 mins on ice. After sonication, 0.5 mL of washing buffer, consisting of 0.2 M phosphoric acid and 1 M potassium chloride, and mixed using a vortex for five minutes. Each sample was incubated on ice for 10 minutes. The samples were then centrifuged for 10 minutes at 1,000 rpm in benchtop centrifuge. The bottom, chloroform, layer was collected into a 1 dram vial. The samples were then dried using a rotary evaporator. Lastly, each sample was purged with argon and stored in the -80°C until the esterification step.

2.2.16. Esterification of PUFA for lipidomic analysis

The dried lipid samples prepared as described in section 2.2.15 were removed from the freezer and allotted sufficient time to warm to room temperature. A water bath maintaining 80°C was prepared. Then, 1 mL of 1 normal methanolic hydrochloric acid was added to each sample. Each sample was sonicated for 1 min. The reaction vessel was placed into the 80°C water bath for 1 hour. After one hour, the vessels were removed from the water bath and allotted sufficient time to reach room temperature. Once the samples reached room temperature, 0.5 mL of 0.9% sodium chloride in water was added to each sample and mixed on the vortex for a few seconds. After mixing, three separate additions of 0.5 mL of hexane were added to exact as much of the

organic compounds as possible. Each sample after extraction was dried on a rotary evaporator. The samples were then purged with argon and stored in -80°C freezer until GC/MS injection.

2.2.17. Oxylipin analysis method using HPLC/MS/MS

The LC conditions were optimized to separate all eicosanoids of interest with a desired peak shape and signal intensity using a XBridge BEH C18 2.1x150mm HPLC column. The mobile phase A comprised of 0.1% acetic acid in water. Mobile phase B consisted of acetonitrile:methanol (84:16) with 0.1% glacial acetic acid. Gradient elution was performed at a flow rate of 250 μ L/min. Chromatography was optimized to separate all analytes in 20 min. The autosampler, Waters ACQUITY FTN, was kept at 10°C. The column was connected to a TQXS tandem mass spectrometer (Waters) equipped with Waters Acquity SDS pump and Waters Acquity CM detector. Electrospray was operated as ionization source for negative multiple reaction monitoring (MRM) mode. To generate the best selectivity and sensitivity, each analyte standards were infused into the mass spectrometer and multiple reaction monitoring was used to analyze the desired compound.

2.2.18. Lipidomic analysis method using GC/MS

The fatty acid methyl esters (FAMES) were injected into an Agilent 7010 series gas chromatograph equipped with a 30 \times 0.25-mm DB-23 column (Agilent), N₂ as the carrier gas at 1.4 ml/min, and an Agilent triple-axis high energy diode-electron multiplier (HED-EM) detector. The gas chromatograph was run at initial temperature of 120°C for 1 min, followed by gradient flow of 10°C/min to 190°C, followed by an increase of 2°C/min to 200°C. Electron ionization (EI) was used as the ion source method.

2.2.19. Synthesis of epoxyeicosatetraenoic acid (EEQ) regioisomeric mixture

In a flame-dried 100 mL round bottom flask under Ar atmosphere, eicosapentaenoic acid methyl ester (EPA-ME) (1 gram, 3.16 mmol, 1 equiv.) dissolved in 5 mL methylene chloride was added by syringe. Then, meta-chloroperoxybenzoic acid (mCPBA) (1.01 g, 3.79 mmol, 1.2 equiv.) was dissolved in 10 mL of methylene chloride and added dropwise to the reaction vessel. The reaction mixture was stirred for one hour at room temperature. Aqueous sodium bicarbonate (5%, 10 mL) was added, extracted with methylene chloride (3 x 15 mL), dried with magnesium sulfate, and evaporated under reduced pressure. The methyl epoxyeicosatetraenoate regioisomeric mixture was separated from unreacted starting material and polyepoxides by normal-phase flash chromatography using a hexane: ethyl acetate gradient described in table 2 and tracked by thin layer chromatography (TLC) (hexane: ethyl acetate, 70:30 % volume/volume, $R_f = 0.45$), yielding 726 mg (2.19 mmol, 69% yield) of the methyl epoxyeicosatetraenoate regioisomeric mixture.

Duration (minutes)	%B	Solvent A	Solvent B
3.3	4.9	Hexane	Ethyl Acetate
14.1	26.3	Hexane	Ethyl Acetate
0.1	27.2	Hexane	Ethyl Acetate
0.5	30.0	Hexane	Ethyl Acetate
12	49.8	Hexane	Ethyl Acetate

Table 2: Solvent gradient for EEQ methyl ester separation.

In a flame-dried 100 mL round bottom flask under Ar atmosphere cooled to 0°C in an ice bath, the methyl epoxyeicosatetraenoate regioisomeric mixture (0.726 g, 2.19 mmol, 1 equiv.) was added by syringe. Then, THF: H₂O solvent mixture (8mL, 6.4 mL:1.6 mL) was added to the reaction vessel followed by dropwise addition of 2 M aqueous LiOH (2.19 mL, 4.38 mmol, 2 equiv.). The reaction mixture was warmed to room temperature and stirred for one hour. The reaction was quenched by dropwise addition of neat formic acid until pH~4. Water (10 mL) was

added and extracted three times with ethyl acetate (3 x 15 mL), dried with magnesium sulfate, and evaporated under reduced pressure. The EEQ regioisomeric mixture was separated from unreacted starting material by normal-phase flash chromatography using hexane: ethyl acetate gradient as described in table 3 and tracked by TLC (hexane: ethyl acetate, 70:30 % volume/volume, $R_f = 0.27$), yielding 648 mg of EEQ monoepoxides (2.03 mmol, 93% yield).

Duration (minutes)	%B	Solvent A	Solvent B
1.6	0	Hexane	Ethyl Acetate
12.4	49.8	Hexane	Ethyl Acetate
6.0	69.9	Hexane	Ethyl Acetate
5.0	79.9	Hexane	Ethyl Acetate

Table 3: Solvent gradient for EEQ acid separation.

The monoepoxides were characterized using the HPLC/MS/MS and discussed further in section 2.2.20. The synthetic scheme for EEQ preparation from EPA-ME is illustrated in Figure 19.

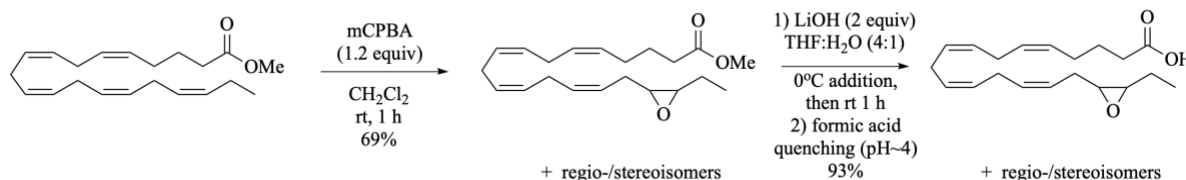


Figure 19: Synthesis of epoxyeicosatetraenoic acid (EEQ) regioisomeric mixture.

2.2.20. Characterization of EEQ mixture by HPLC/MS/MS

Identical HPLC/MS/MS conditions were used for characterization of the EEQ mixture and as used for raw biological samples as described in section 2.2.17. The EEQ mixtures were characterized by matched retention times and MS/MS transition with a known standard of each EEQ regioisomer. The identification was further corroborated by the parent ion mass/charge ratio at the matched retention time. All EEQ regioisomers in negative MRM mode will have a parent ion m/z of 317.2. Figures 20-24 illustrates the initial identification of each regioisomer by retention time comparison to the known standard (top) and mixture (bottom).

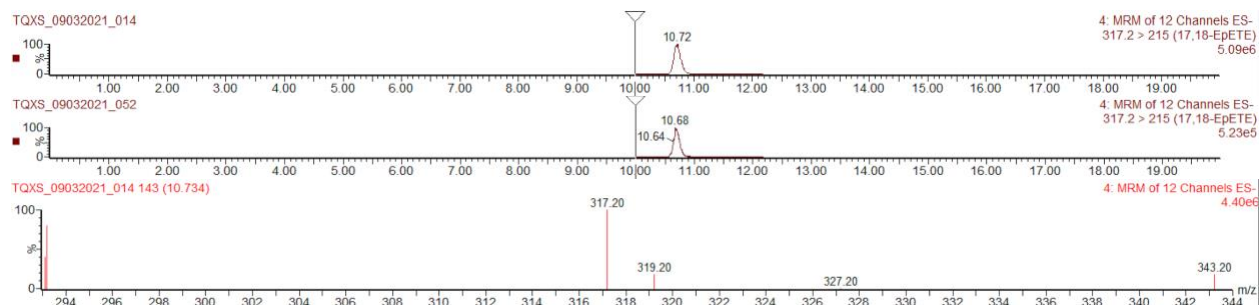


Figure 20: Characterization of 17,18-EEQ (EpETE) by HPLC/MS/MS.

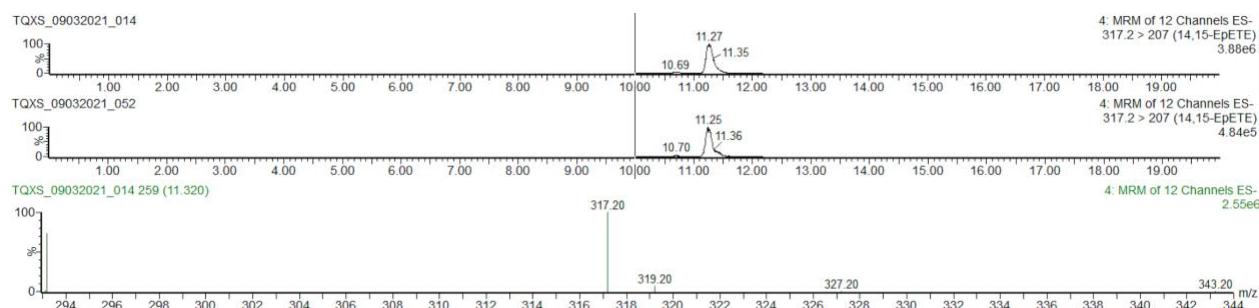


Figure 21: Characterization of 14,15-EEQ (EpETE) by HPLC/MS/MS.

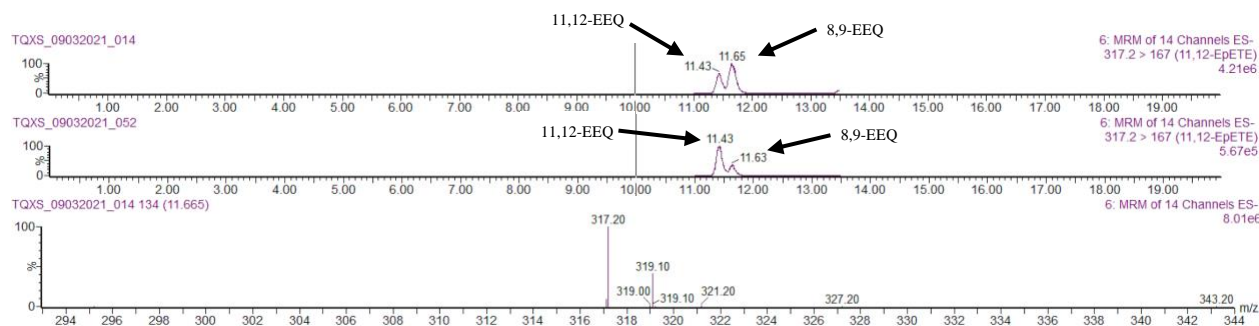


Figure 22: Characterization of 11,12-EEQ (EpETE) by HPLC/MS/MS.

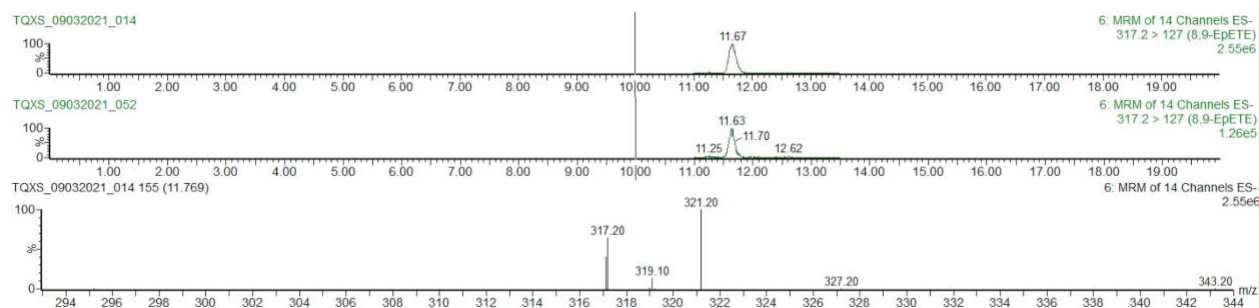


Figure 23: Characterization of 8,9-EEQ (EpETE) by HPLC/MS/MS.

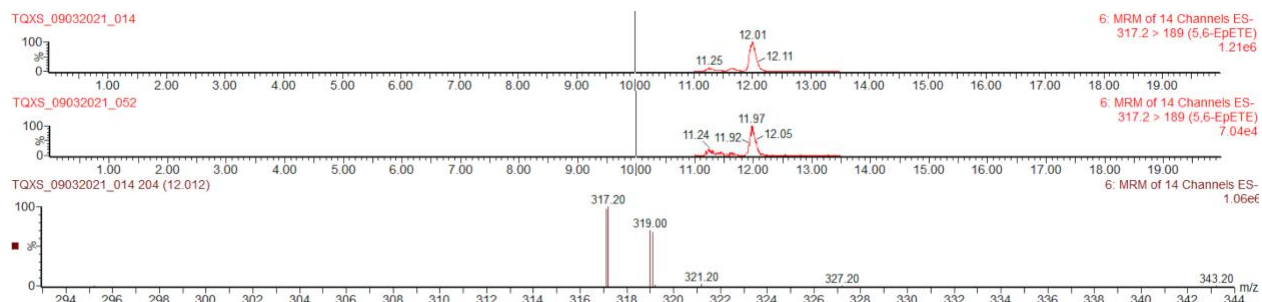


Figure 24: Characterization of 5,6-EEQ (EpETE) by HPLC/MS/MS.

All EEQ regioisomers in mixture match retention times, within 0.05 min, with known standard of each regioisomer. Additionally, the parent ion of 317.2 m/z is present for each regioisomer in the mixture further validating the presence of each isomer. Lastly, 11,12-EEQ overlaps slightly with 8,9-EEQ during separation, which explains the presence of two peaks in the 11,12-EEQ chromatogram. The unique peak at 11.43 is used for quantification.

2.3. Using GFP to assess neural health of glutamatergic neurons in *C. elegans*

2.3.1. Establishing the glutamatergic GFP model

OH11152 [*eat-4::GFP; ttx-3::DsRed*] expresses green fluorescent protein (GFP) in five glutamatergic neurons: BAG, ASE, AWC, AFD, ASG. Figure 25 shows several examples of healthy worms expressing GFP in five glutamatergic neurons.

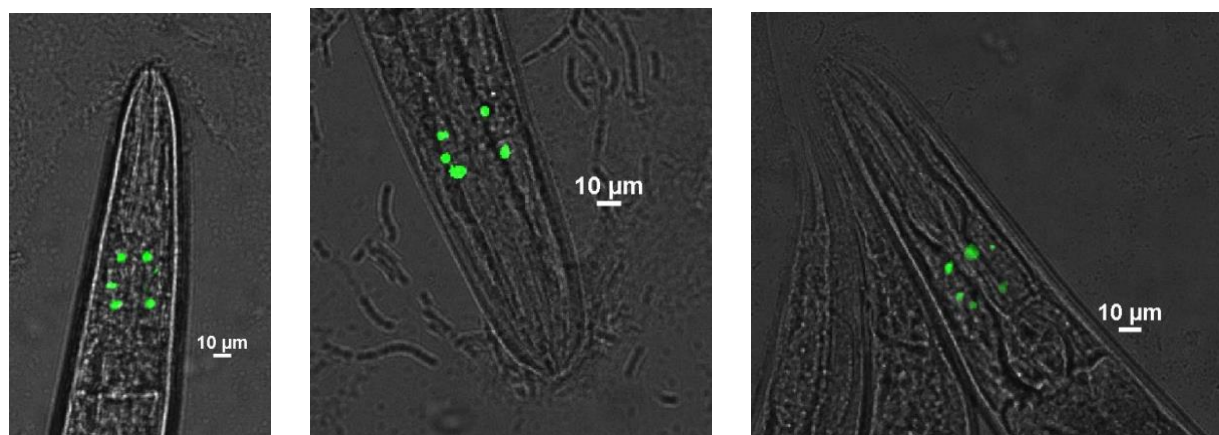


Figure 25: GFP showing glutamatergic neuron somas in healthy *eat-4::GFP C. elegans*.

The imaging assay for *eat-4::GFP; ttx-3::DsRed* involves counting the number of visible cell somas. Any worm that does not express GFP in these five neurons is considered unhealthy.

Results are reported as the percentage of worms that are healthy (expressing GFP in all five GFP tagged neurons).

2.3.2. Transgenic humanized tau *C. elegans* glutamatergic neuron assay

To investigate the effect of tau on glutamatergic neurons, a *eat-4::GFP; ttx-3::DsRed* (expresses GFP in five glutamatergic neurons) was crossed with tau transgenic worms, *aex-3::tau(4R1N); myo-2::DsRed* (CK1441). More detail on the crossing process can be found in sections 2.2.6. and 2.2.7. Imaging analysis of the resulting homozygous population revealed that the tau insertion causes degeneration of the five glutamatergic neurons. The observed effect is reported and illustrated in Figure 26.

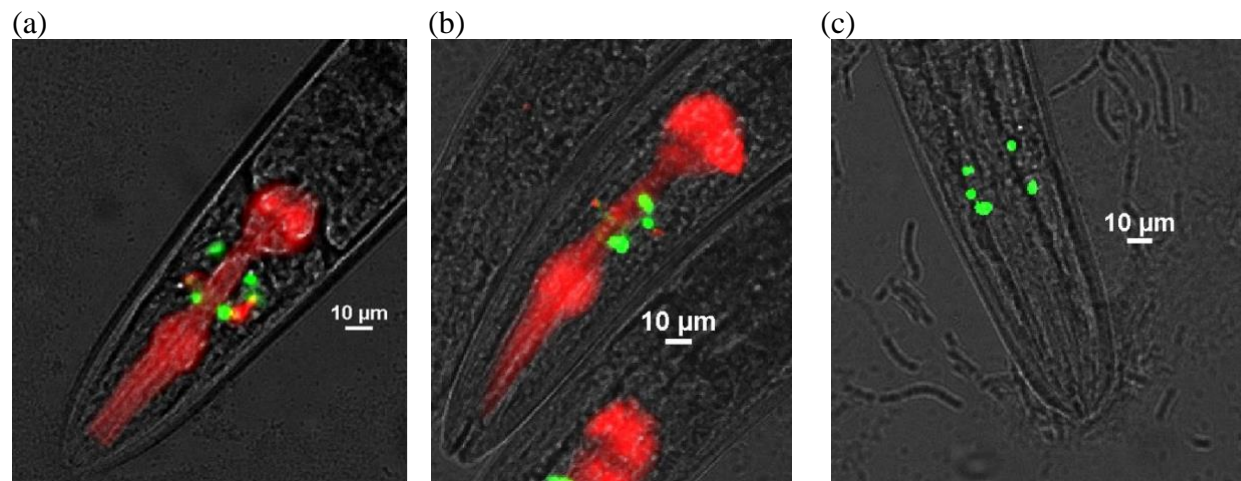


Figure 26: GFP in *eat-4::GFP; aex-3::tau C. elegans*.
(a) Healthy tau worm (b) Unhealthy tau worm (c) Healthy control

The observed neurodegeneration quantified by neural GFP loss in the tau worms (*eat-4::GFP; aex-3::tau*) was quantified. An age synchronized population of control worms (*eat-4::GFP*) and tau worms (*eat-4::GFP; aex-3::tau*) were assayed for neural health by assessing the number of visible somas in each worm. More details on the neural imaging assay can be found in section 2.2.7. Figure 27 shows the quantified results of three separate trials of the control (*eat-4::GFP*) and tau (*eat-4::GFP; aex-3::tau*) strain. The worms were maintained for five days and scored

during the lifespan at days 1, 3 and 5. The tau worms (*eat-4::GFP; aex-3::tau*) exhibit a shortened lifespan making it difficult to maintain a sufficiently large population beyond day 5.

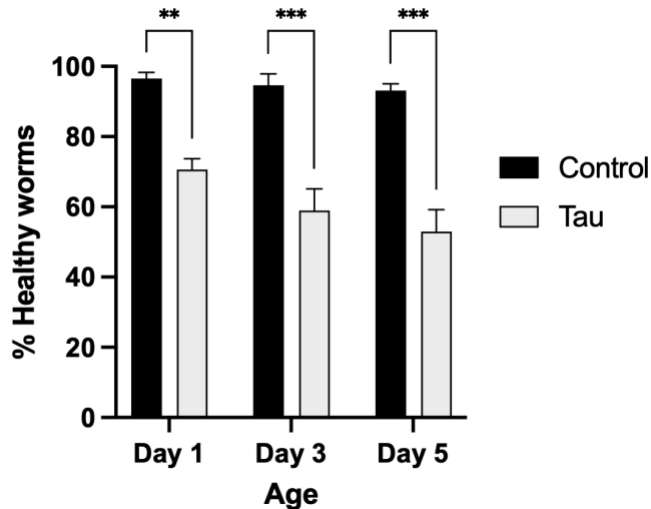


Figure 27: Quantified glutamatergic neural health in *eat-4::GFP* (Control) and *eat-4::GFP; aex-3::tau* (Tau) worms.

Three trials of 20 worms each were performed for each strain at each time point. The % healthy worms for each time point is the average of the triplicate. Error bars are standard error (SEM). Two-way analysis of variance (ANOVA) and Tukey's multiple comparison test was used to analyze the statistical significance of this results. (* $P < 0.05$, ** $P < 0.01$, *** $P < 0.001$, **** $P < 0.0001$).

The control (*eat-4::GFP*) and tau worms (*eat-4::GFP; aex-3::tau*) data demonstrate that tauopathy induces neurodegeneration in glutamatergic neurons through an unidentified mechanism. Therefore, tau worms (*eat-4::GFP; aex-3::tau*) serve as a useful model to investigate potential therapeutics through supplementation.

2.3.3. Glutamatergic neuron assay with epoxide hydrolase inhibitor, AUDA, treatment

There is evidence suggesting that inhibiting soluble epoxide hydrolase in AD models can have a protective effect on the individual³¹. Therefore, to investigate if the same or similar effect can be observed in the *C. elegans* animal model, we supplemented the AD *C. elegans* tau model with 12-[[[(tricyclo[3.3.1.1.3,7]dec-1-ylamino)carbonyl]amino]-dodecanoic acid (AUDA). AUDA is a known soluble epoxide hydrolase inhibitor that has been shown to inhibit the *C. elegans*

epoxide hydrolase homolog (CEEH)³². Therefore, AUDA serves as the best sEH inhibitor to study the effects of epoxide hydrolase inhibition in *C. elegans*. The structure of AUDA is shown in Figure 28.

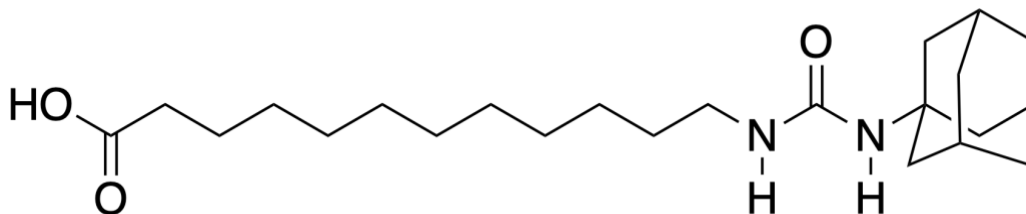


Figure 28: Structure of AUDA.

Separate L4 age synchronized population of control worms (*eat-4::GFP*) tau worms (*eat-4::GFP; aex-3::tau*) were moved to 12 total plates supplemented with AUDA, 3 populations of control (*eat-4::GFP*) with AUDA and vehicle (ethanol) and 3 populations of tau (*eat-4::GFP; aex-3::tau*) with AUDA and vehicle. Sufficient AUDA was dissolved in ethanol and added to a 55°C NGM solution to a final concentration of 100 μ M AUDA. The AUDA plus NGM solution was then used to pour plates and seeded with OP50 using standard methods. Ethanol was added to the NGM plates and used for the vehicle control. Refer to sections 2.2.5. for more details on the seeding and supplementation process. An age synchronized population of worms was generated and maintained using the filtration method illustrated and described in section 2.2.8. and 2.2.9. Twenty worms from each of the 12 age synchronized populations were scored for neuron health by counting the distinct cell somas expressing GFP. Worms missing any of the five glutamatergic neurons were scored as unhealthy, and worms expressing all five were scored as healthy. Figure 29 shows the percentage of healthy worms, expressing GFP in all five glutamatergic neurons, for each population.

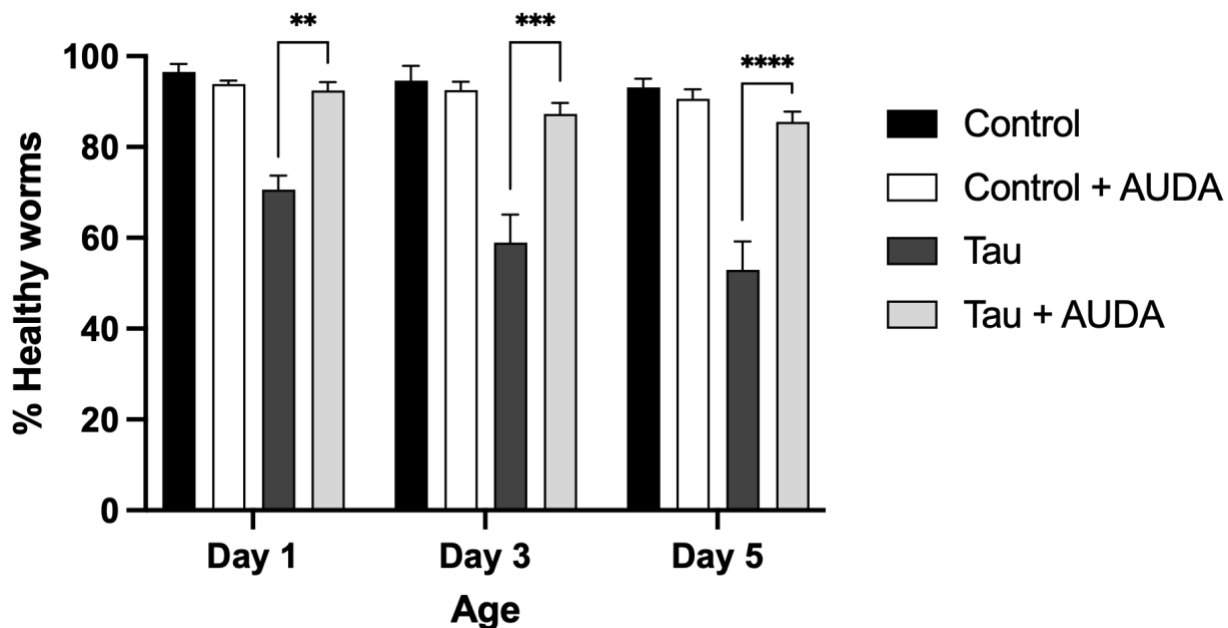


Figure 29: Quantified glutamatergic neural health in *eat-4::GFP* (Control) and *eat-4::GFP; aex-3::tau* (Tau) treated with and without AUDA.

Three trials of 20 worms each were performed for each strain at each time point. The % healthy worms for each time point is the average of the triplicate. Error bars are standard error (SEM). Two-way analysis of variance (ANOVA) and Tukey's multiple comparison test was used to analyze the statistical significance of this results. (* $P < 0.05$, ** $P < 0.01$, *** $P < 0.001$, **** $P < 0.0001$).

Figure 29 illustrates a significant difference between the *eat-4::GFP; aex-3::tau* (Tau) with and without supplementation. The *eat-4::GFP; aex-3::tau* (Tau) worms supplemented with AUDA have significantly healthier glutamatergic neurons, as detected by GFP in the five tagged neurons, than tau worms treated with ethanol control. AUDA is a known inhibitor of epoxide hydrolase in the worms³². Therefore, the recovery effect may be explained by an increased epoxy PUFA concentration and a decrease in 1,2-diol PUFA metabolite concentration.

2.3.4. Glutamatergic neuron assay with ω -3 fatty acid and ω -3 fatty acid metabolite supplements

To investigate if the observed neuronal recovery was caused by an increase in specific ω -3 fatty acids or ω -3 epoxide metabolites, both the control (*eat-4::GFP*) and tau (*eat-4::GFP; aex-3::tau*) were supplemented with eicosapentaenoic acid (EPA) and its epoxide metabolite, ep-

eicosatetraenoic acid (EEQ). EPA is an ω -3 fatty acid, and ω -3 fatty acids have been associated with neuroprotective effects in mammalian studies³³. Additionally, EPA is found in larger concentrations compared to other ω -3 fatty acids such docosahexaenoic (DHA) in *C. elegans*³⁴. EEQ is one of the substrates of CEEH and was tested to assess if the rescued glutamatergic neurons from AUDA treatment are the result of an increase in epoxide metabolites. The L4 age synchronized populations were prepared and placed on NGM plates supplemented with EPA or EEQ. Refer to section 2.2.5. for more details on supplementing NGM plates on the surface of the agar. Age synchronized populations of supplemented worms were maintained by filtration. Twenty worms of each population were scored for the presence of GFP in all five neuron somas. If the worms have all five somas, they are scored as healthy. Otherwise, the worms are scored as unhealthy. Figure 30 shows the quantified results for control (*eat-4::GFP*) supplementation with EPA and EEQ for each population of worms.

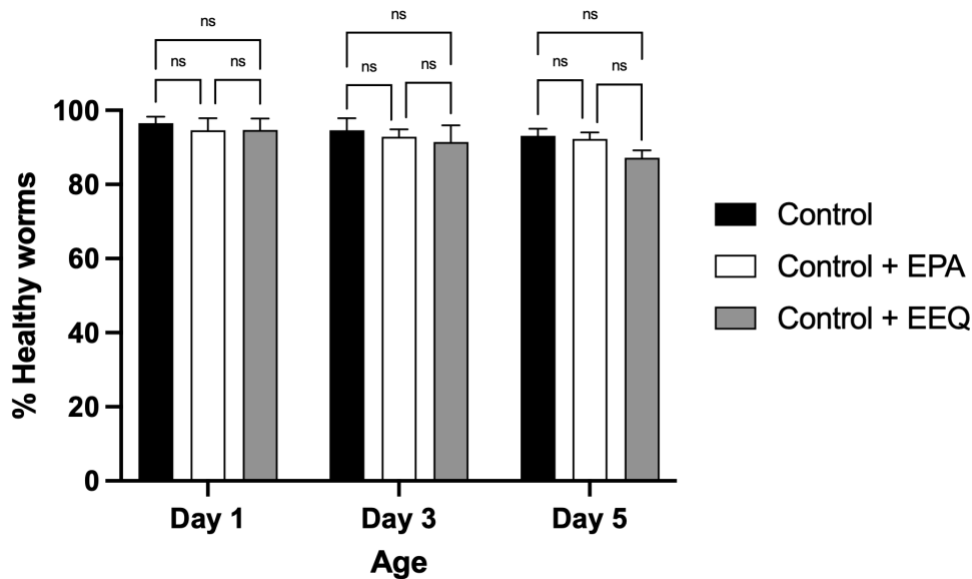


Figure 30: Quantified glutamatergic neural health in *eat-4::GFP* (Control) treated with EPA and EEQ.

Three trials of 20 worms each were performed for each strain at each time point. The % healthy worms for each time point is the average of the triplicate. Error bars are standard error (SEM). Two-way analysis of variance (ANOVA) and Tukey’s multiple comparison test was used to analyze the statistical significance of this results. (* $P < 0.05$, ** $P < 0.01$, *** $P < 0.001$, **** $P < 0.0001$).

Age synchronized population of tau worms (*eat-4::GFP; aex-3::tau*) were placed on plates with vehicle control (ethanol), EPA, or EEQ. Age synchronization and maintenance was performed as previously described in sections 2.2.8. and 2.2.9. The glutamatergic neural health was assayed as previously described in section 2.3.2. Figure 31 shows the results for tau worms (*eat-4::GFP; aex-3::tau*) supplementation with EPA and EEQ for each population of worms.

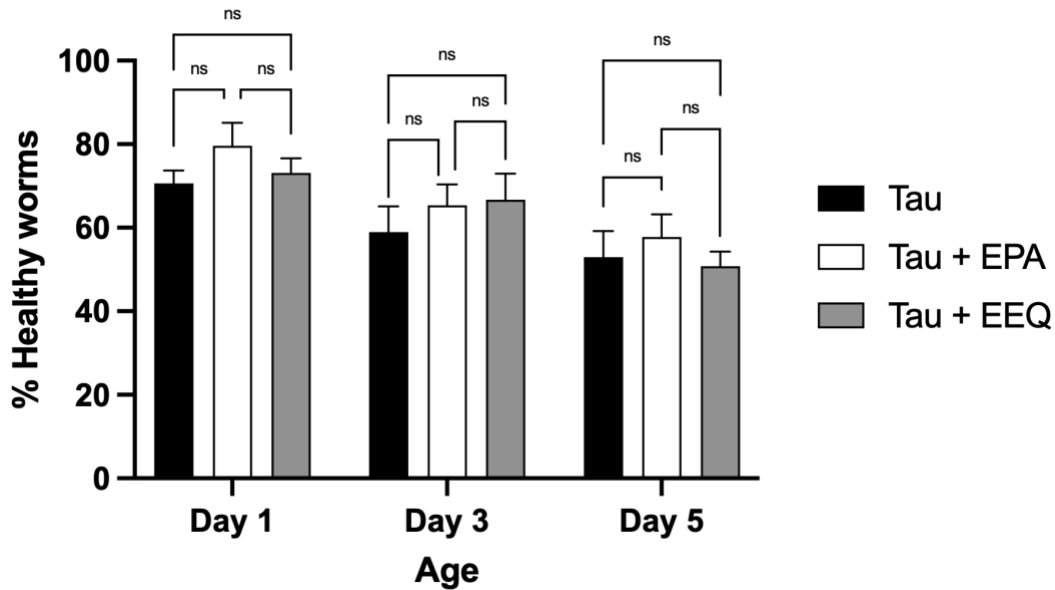


Figure 31: Quantified glutamatergic neural health in *eat-4::GFP; aex-3::tau* (Tau) treated with EPA and EEQ.

Three trials of 20 worms each were performed for each strain at each time point. The % healthy worms for each time point is the average of the triplicate. Error bars are standard error (SEM). Two-way analysis of variance (ANOVA) and Tukey's multiple comparison test was used to analyze the statistical significance of this results. (* $P < 0.05$, ** $P < 0.01$, *** $P < 0.001$, **** $P < 0.0001$).

Figure 32 shows both strains, control (*eat-4::GFP*) and tau (*eat-4::GFP; aex-3::tau*) with supplementations for a direct comparison.

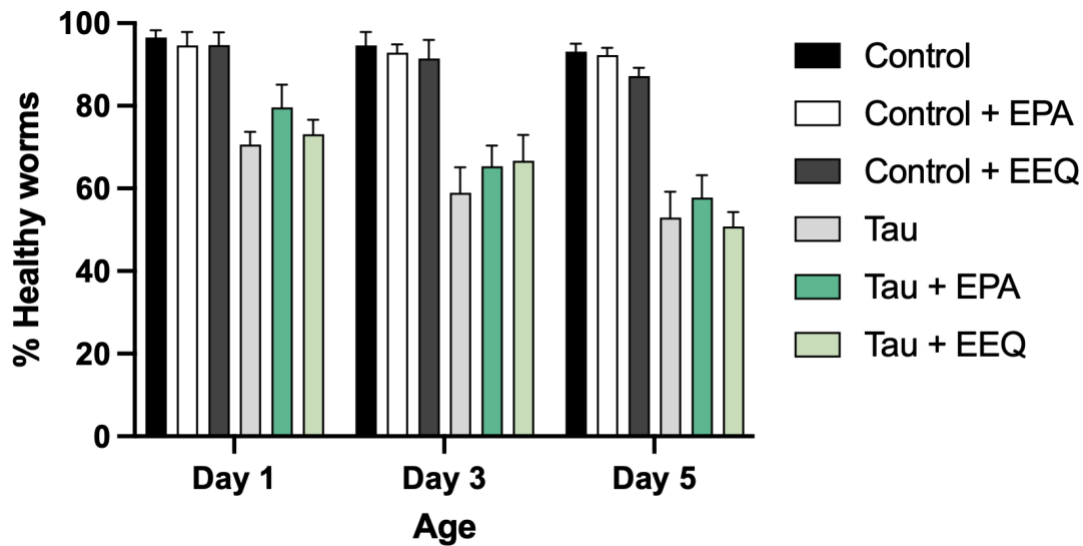


Figure 32: Quantified glutamatergic neural health in *eat-4::GFP* (Control) and *eat-4::GFP; aex-3::tau* (Tau) treated with EPA and EEQ.

Three trials of 20 worms each were performed for each strain at each time point. The % healthy worms for each time point is the average of the triplicate. Error bars are standard error (SEM). Two-way analysis of variance (ANOVA) and Tukey's multiple comparison test was used to analyze the statistical significance of this results. (* $P < 0.05$, ** $P < 0.01$, *** $P < 0.001$, **** $P < 0.0001$).

Figure 32 illustrates that there are significant differences between the control (*eat-4::GFP*) and tau (*eat-4::GFP; aex-3::tau*) groups. The result illustrated in Figure 32 might be explained by limited absorption of EPA and EEQ through supplementation directly on the surface of the agar as outlined in section 2.2.5 or that EPA and EEQ do not rescue neurodegeneration of glutamatergic neurons. To test the absorption hypothesis, lipid and oxylin profiles were determined by GC/MS and HPLC/MS/MS discussed further in sections 2.5.1 and 2.5.2.

It is possible that supplementation with EPA and EEQ leads to increased metabolism in the worms, which may result in a relatively constant ratio of epoxide and diol metabolites. If the epoxide to diol ratio remains constant, a limited or no rescuing effect is expected. To investigate the constant epoxide to diol ratio hypothesis, dual supplementations were performed with PUFA or PUFA metabolites and AUDA. Treatment with AUDA will inhibit the function of epoxide

hydrolase, increasing the epoxy-PUFAs concentrations. An age synchronized population of control worms (*eat-4::GFP*) were placed on plates with AUDA plus vehicle (ethanol), EPA, or EEQ. Age synchronization and maintenance was performed as previously described in sections 2.2.8. and 2.2.9. Glutamatergic neural health was assayed as previously described in section 2.3.2. Figure 33 illustrates the results for control worms (*eat-4::GFP*) supplemented with EPA + AUDA and EEQ + AUDA.

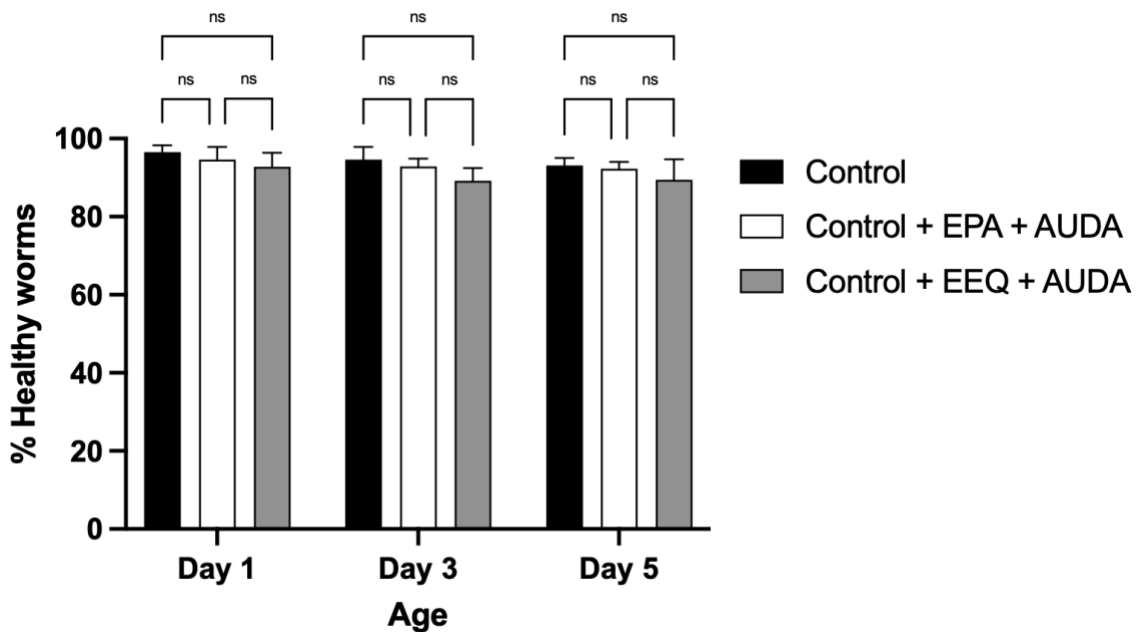


Figure 33: Quantified glutamatergic neural health in *eat-4::GFP* (Control) with cotreatment of EPA + ADUA and EEQ + AUDA.

Three trials of 20 worms each were performed for each strain at each time point. The % healthy worms for each time point is the average of the triplicate. Error bars are standard error (SEM). Two-way analysis of variance (ANOVA) and Tukey’s multiple comparison test was used to analyze the statistical significance of this results. (* $P < 0.05$, ** $P < 0.01$, *** $P < 0.001$, **** $P < 0.0001$).

There is no statically significant difference between the control (*eat-4::GFP*) or worms supplemented with AUDA along with either EPA or EEQ. The null result was expected as there is not a significant loss in glutamatergic neurons until much later in the lifespan, day 10 and later. However, supplementation on the control (*eat-4::GFP*) at the early time points, days 1, 3,

and 5, is necessary for comparisons with the tau worms (*eat-4::GFP; aex-3::tau*), which have a much shorter lifespan.

To test if a similar effect is observed in tau worms (*eat-4::GFP; aex-3::tau*) when AUDA plus EPA or EEQ, an age synchronized population of tau worms (*eat-4::GFP; aex-3::tau*) were placed on plates with AUDA along with vehicle control (ethanol), EPA or EEQ. Age synchronization and maintenance was performed as previously described in sections 2.2.8. and 2.2.9. The glutamatergic neural health was assayed as previously described in section 2.3.2.

Figure 34 shows the quantified results for tau cross supplemented with EPA + AUDA and EEQ + AUDA.

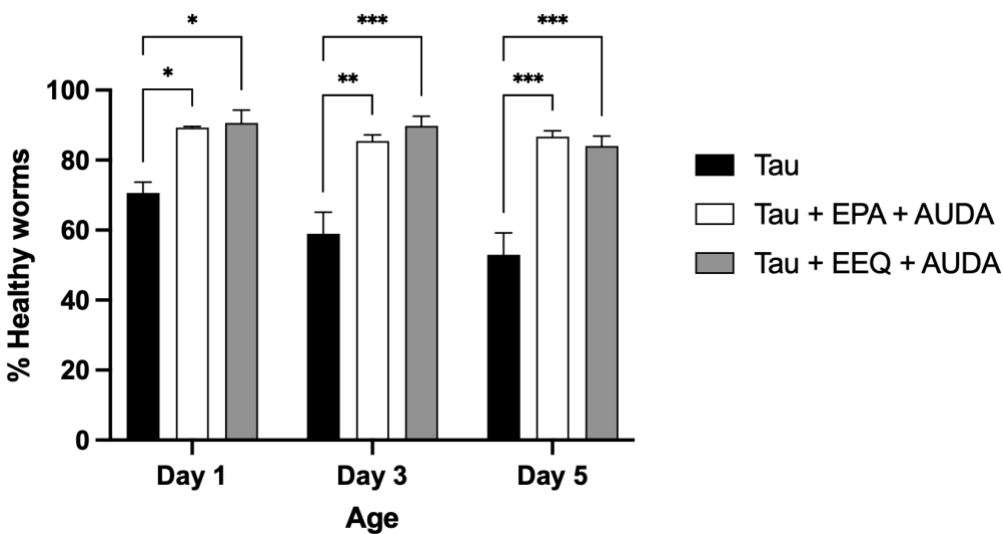


Figure 34: Quantified glutamatergic neural health in *eat-4::GFP; aex-3::tau* (Tau) with cotreatment EPA + ADUA and EEQ + AUDA.

Three trials of 20 worms each were performed for each strain at each time point. The % healthy worms for each time point is the average of the triplicate. Error bars are standard error (SEM). Two-way analysis of variance (ANOVA) and Tukey’s multiple comparison test was used to analyze the statistical significance of this results. (*P< 0.05, **P< 0.01, ***P< 0.001, ****P< 0.0001).

Figure 34 suggests that AUDA along with EPA and EEQ can significantly rescue glutamatergic neurons in tau worms (*eat-4::GFP; aex-3::tau*), although EPA and EEQ alone did not rescue the glutamatergic neurons. However, supplementation with AUDA alone does recue the

glutamatergic neurons, and AUDA may rescue the neurons to a point that any additive or synergistic effects from EPA and EEQ are undetectable. While the additive or synergistic effects cannot be ruled out, it is unlikely as EPA and EEQ supplementation alone did not rescue glutamatergic neurons. Additionally, Figure 35 illustrates the results of EEQ + AUDA and EPA + AUDA on control (*eat-4::GFP*) and tau worms (*eat-4::GFP; aex-3::tau*).

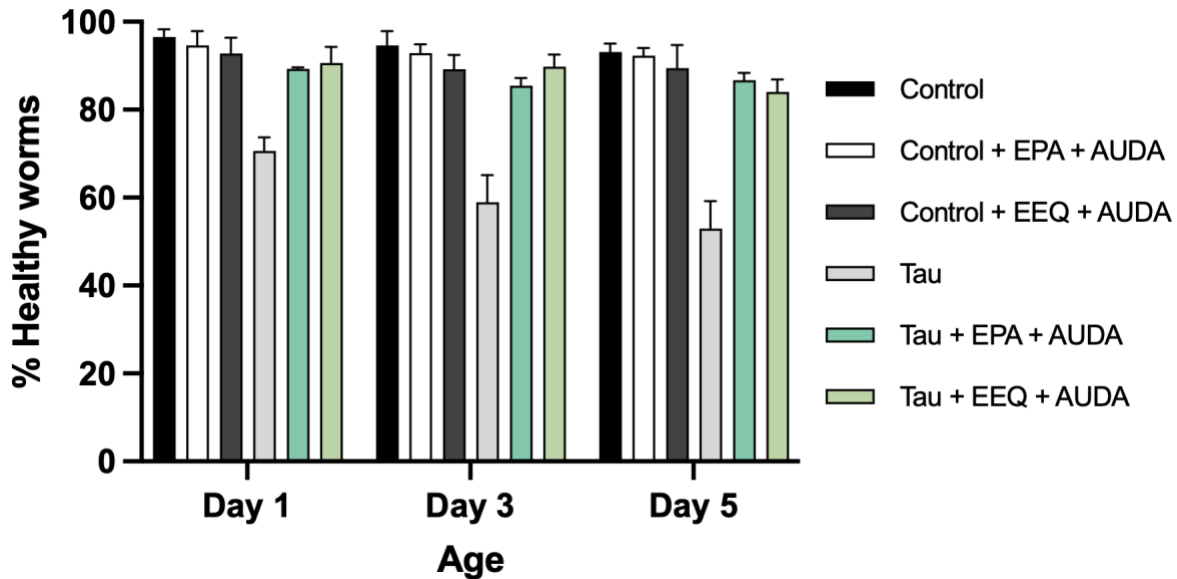


Figure 35: Quantified glutamatergic neural health in *eat-4::GFP* (Control) and *eat-4::GFP; aex-3::tau* (Tau) with cotreatment of EPA + AUDA and EEQ + AUDA.

Three trials of 20 worms each were performed for each strain at each time point. The % healthy worms for each time point is the average of the triplicate. Error bars are standard error (SEM). Two-way analysis of variance (ANOVA) and Tukey's multiple comparison test was used to analyze the statistical significance of this results. (* $P < 0.05$, ** $P < 0.01$, *** $P < 0.001$, **** $P < 0.0001$).

Figure 35 illustrates that treating the tau worms (*eat-4::GFP; aex-3::tau*) with AUDA rescues glutamatergic neurons to control (*eat-4::GFP*) levels. EPA and EEQ seem to have no statistically significant effect, and the observed recovery is largely due to epoxide hydrolase inhibition with AUDA.

To investigate if AUDA was responsible for rescuing glutamatergic neuron health in the tau worms (*eat-4::GFP; aex-3::tau*) treated with EPA + AUDA and EEQ + AUDA, each tau

worm group (*eat-4::GFP; aex-3::tau*) treated with AUDA were compared to each other and to the tau vehicle control (ethanol only). Figure 36 illustrates the result of this comparison.

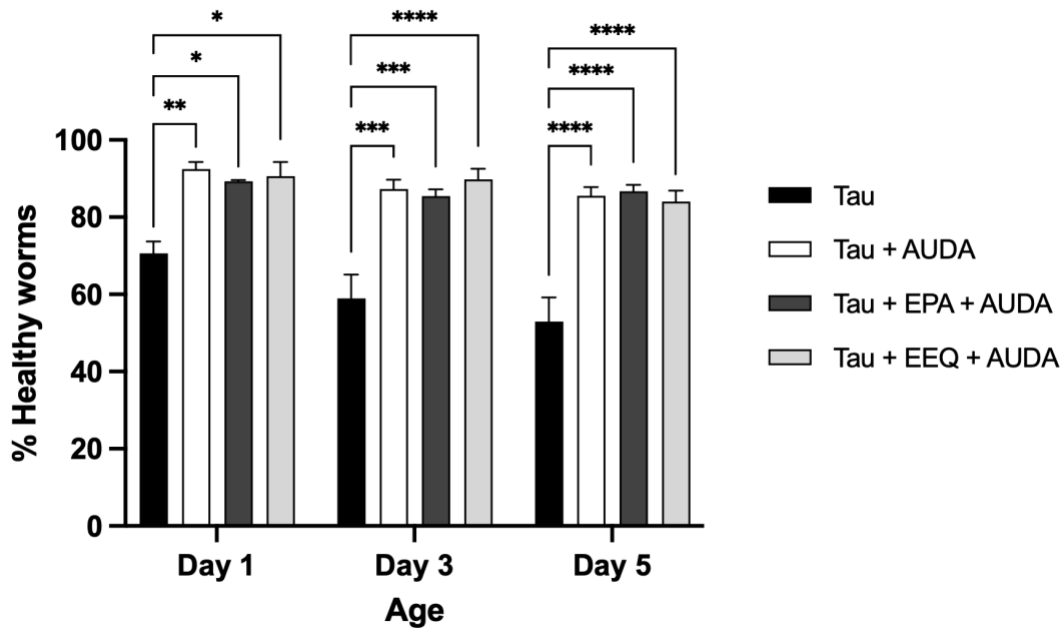


Figure 36: Quantified glutamatergic neural health in *eat-4::GFP; aex-3::tau* (Tau) treated with AUDA, EPA + AUDA, and EEQ + AUDA.

Three trials of 20 worms each were performed for each strain at each time point. The % healthy worms for each time point is the average of the triplicate. Error bars are standard error (SEM). Two-way analysis of variance (ANOVA) and Tukey's multiple comparison test was used to analyze the statistical significance of this results. (* $P < 0.05$, ** $P < 0.01$, *** $P < 0.001$, **** $P < 0.0001$).

Figure 36 shows statistical differences between the control groups (ethanol) and each treatment group in which AUDA was included. Comparisons between AUDA, EPA + AUDA, and EEQ + AUDA show no significant difference suggesting that AUDA alone is likely responsible for the observed rescued glutamatergic neurons. Furthermore, Figure 32 shows that EPA and EEQ alone do not significantly rescue glutamatergic neurons. Therefore, the most likely explanation is that AUDA is responsible for the observed effect, and EPA and EEQ are not contributing or weakly contributing.

2.3.5. Glutamatergic neuron assay with ferroptosis inhibitor, LIP-1, treatment

To investigate if ferroptosis is involved in the observed glutamatergic cell death, worms were supplemented with known ferroptosis inhibitor, liproxstatin-1 (LIP-1)³⁵. The structure of liproxstatin-1 is shown in Figure 37.

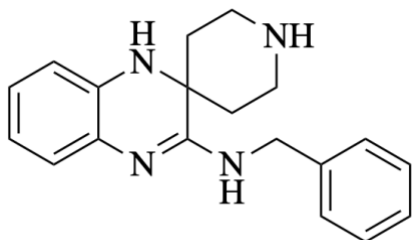


Figure 37: Structure of liproxstatin-1 (LIP-1).

Separate L4 age synchronized populations of control (*eat-4::GFP*) and tau worms (*eat-4::GFP; aex-3::tau*) were moved to 12 total plates supplemented with LIP-1, 3 populations of control (*eat-4::GFP*) with supplement (LIP-1) and vehicle (ethanol) and 3 populations of tau (*eat-4::GFP; aex-3::tau*) with supplement (LIP-1) and vehicle (ethanol). Sufficient LIP-1 was dissolved in ethanol to produce a final concentration of 250 μ M LIP-1 solution. Standard NGM plates were prepared as described in section 2.2.1. Then, 10 μ L of 250 μ M LIP-1 solution was added to each supplementation plate. The plate was then quickly seeded with OP50 to avoid any oxidation from air exposure. Refer to section 2.2.5 for more information on supplementation on the surface of the plate. An age synchronized population of each strain was maintained by filtration as described in section 2.2.8. and 2.2.9. Each population was assayed for glutamatergic neural health as previously described in section 2.3.1. Figure 38 shows the results for control supplementation with LIP-1.

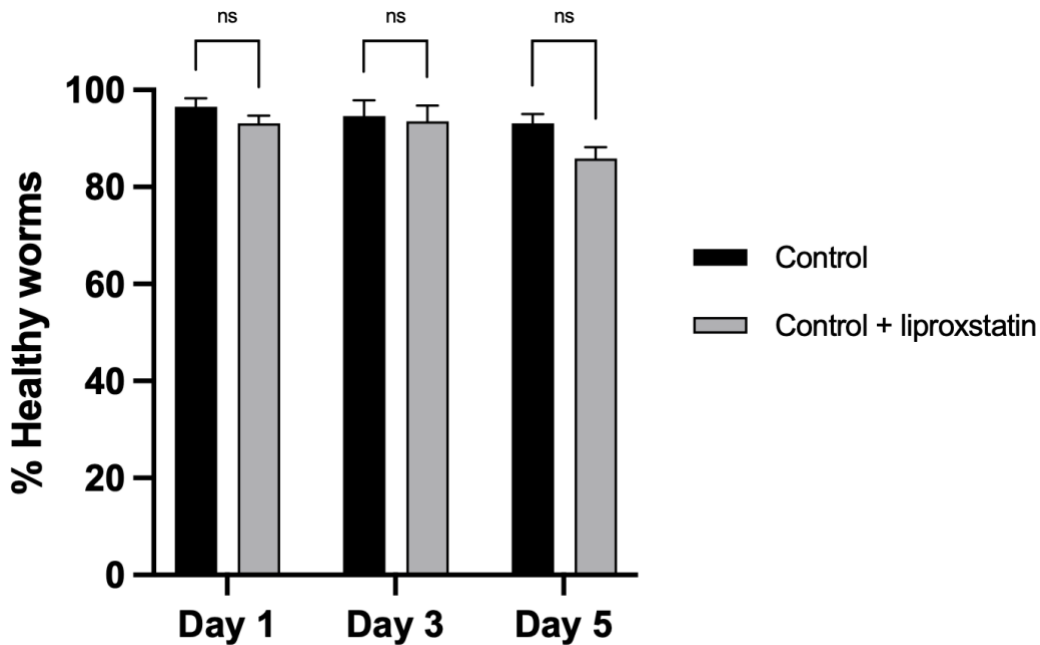


Figure 38: Quantified glutamatergic neural health in *eat-4::GFP* (Control) treated with LIP-1.

Three trials of 20 worms each were performed for each strain at each time point. The % healthy worms for each time point is the average of the triplicate. Error bars are standard error (SEM). Two-way analysis of variance (ANOVA) and Tukey's multiple comparison test was used to analyze the statistical significance of this results. (* $P < 0.05$, ** $P < 0.01$, *** $P < 0.001$, **** $P < 0.0001$).

Figure 38 shows no significant difference with LIP-1 treatment, which is expected because ferroptosis is not a significant cell death mechanism until later in life or under increased iron conditions in wild-type animals. Therefore, treatment with LIP-1 does not affect the glutamatergic neurons in the control (*eat-4::GFP*) and serve as a control for any observed effects in the tau worms (*eat-4::GFP; aex-3::tau*)

To investigate if ferroptosis is involved in the glutamatergic cell death observed in our tau model, a synchronized population of tau expressing worms were placed on plates with 10 μL of 250 μM LIP-1. An age synchronized population of supplemented worms were maintained by filtration. A glutamatergic neuron health was assayed as previously described in section 2.3.1. Figure 39 illustrates the results of LIP-1 treatment in the tau worms (*eat-4::GFP; aex-3::tau*).

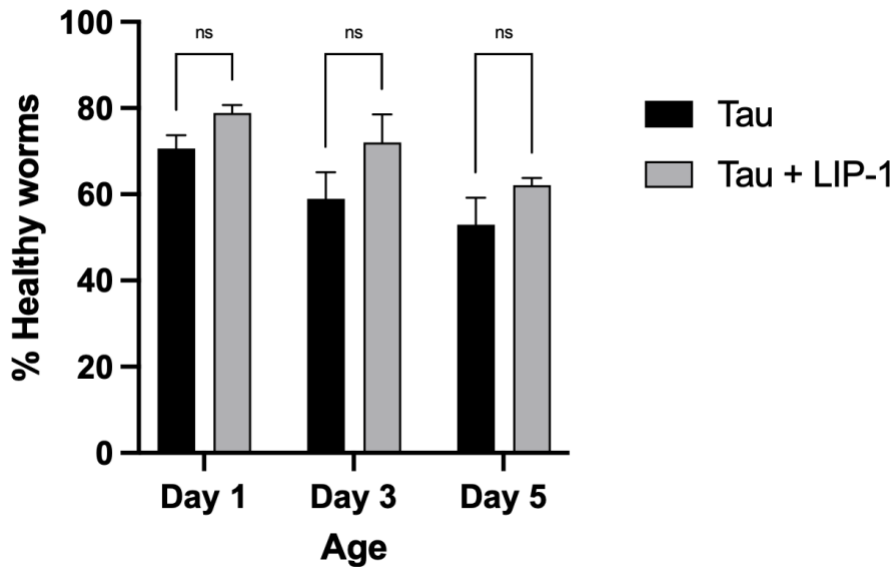


Figure 39: Quantified glutamatergic neural health in *eat-4::GFP; aex-3::tau* (Tau) treated with LIP-1.

Three trials of 20 worms each were performed for each strain at each time point. The % healthy worms for each time point is the average of the triplicate. Error bars are standard error (SEM). Two-way analysis of variance (ANOVA) and Tukey's multiple comparison test was used to analyze the statistical significance of this results. (* $P < 0.05$, ** $P < 0.01$, *** $P < 0.001$, **** $P < 0.0001$).

Figure 39 shows that there is not a significant difference between tau (*eat-4::GFP; aex-3::tau*) treated with ethanol and tau treated with LIP-1. Therefore, ferroptosis is not likely the main cause of neuronal cell death and suggests another mechanism of cell death, such as glutamate excitotoxicity, must be responsible for the observed effect of neurodegeneration in our tau (*eat-4::GFP; aex-3::tau*) model.

2.4. Assessing fitness using the thrashing assay

2.4.1. Establishing the thrashing model in wildtype

The *C. elegans* thrashing assay assesses the swimming ability of the worms, providing an assessment of the fitness of the worms. To perform the thrashing assay, 20 age synchronized worms of a desired age were transferred by pick to 10 μ L of s-basal on a NGM plate. The worms were allotted 15 seconds to swim removing any bacteria on the cuticle. After 15 seconds, the

movement of the worm was recorded for 30 seconds using a camera. The videos were analyzed and scored for the number of “thrashes” each worm performed in the 30 second video. Thrashing was scored as described in section 2.2.11. and illustrated in Figure 13.

To investigate and establish the thrashing phenotype, several aging studies were performed. Age synchronized populations of N2 (wildtype) worms were generated as outlined in section 2.2.8. The age synchronized population was maintained by filtration as outlined in section 2.2.9. Twenty worms were assayed for thrashing at specific timepoints throughout their lifespan at days 1, 4, 8, 12, and 16. The result is illustrated in Figure 40.

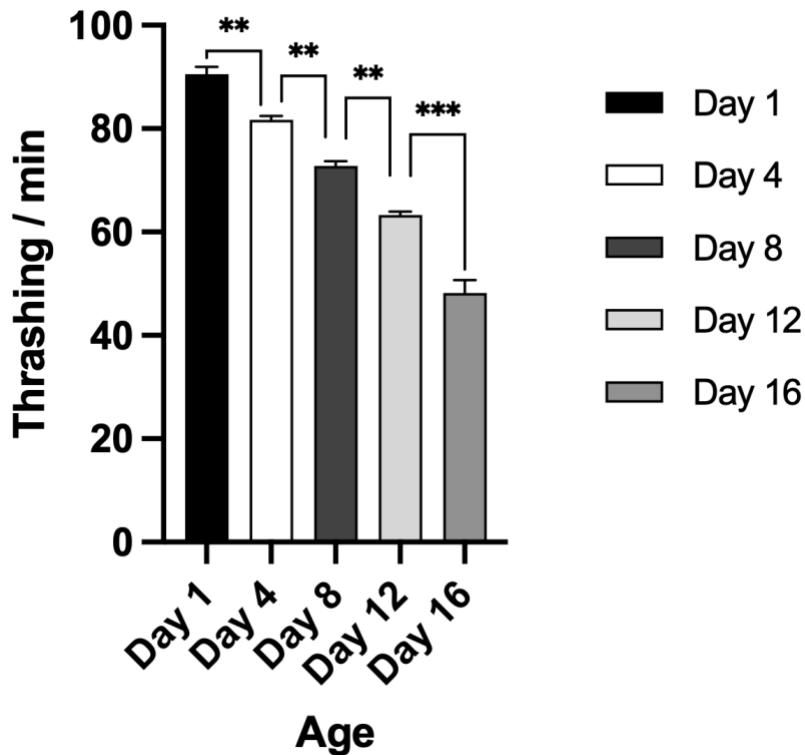


Figure 40: Quantified thrashing of N2 during the aging process.

Three trials of 20 worms each were performed for each strain at each time point. The average thrashing of the triplicate is reported. Error bars are standard error (SEM). A one-way analysis of variance (ANOVA) was used to analyze the statistical significance of this result (* $P < 0.05$, ** $P < 0.01$, *** $P < 0.001$, **** $P < 0.0001$).

Figure 40 shows statistically significant differences between all aging worm groups when compared to the younger timepoints. The aging process causes the worms to thrash significantly less and therefore, decreased thrashing is a normal and expected part of the aging process that must be considered when interpreting thrashing assay results. To conclude that there any other factors causing decreased thrashing, the decrease in thrashing must be significantly greater than the normal aging effect.

2.4.2. Transgenic humanized *C. elegans* thrashing assay

To further investigate the affects that human tau has in the *C. elegans* animal model, thrashing assays were performed on the control (*eat-4::GFP*) and tau worms (*eat-4::GFP; aex-3::tau*). To investigate any fitness effects tauopathy may cause, plates were prepared with ethanol supplementation on the surface of the agar before seeding the plate with bacteria. Treatment with ethanol serves as a vehicle control because PUFA and PUFA metabolites are dissolved in ethanol. An age synchronized population of control (*eat-4::GFP*) and tau worms (*eat-4::GFP; aex-3::tau*) were prepared as described in sections 2.2.8. Three separate age synchronized populations of L4 control worms (*eat-4::GFP*) and tau worms (*eat-4::GFP; aex-3::tau*) were placed on separate ethanol supplemented plates. The age synchronized population was maintained by filtration as previously described in section 2.2.9. The worms were scored for thrashing on days 1, 3, and 5 of their lifespans. After day 5, tau (*eat-4::GFP; aex-3::tau*) populations are nearly all dead, which makes it difficult to assay at later timepoints. Figure 41 illustrates the results of thrashing for control (*eat-4::GFP*) and tau worms (*eat-4::GFP; aex-3::tau*).

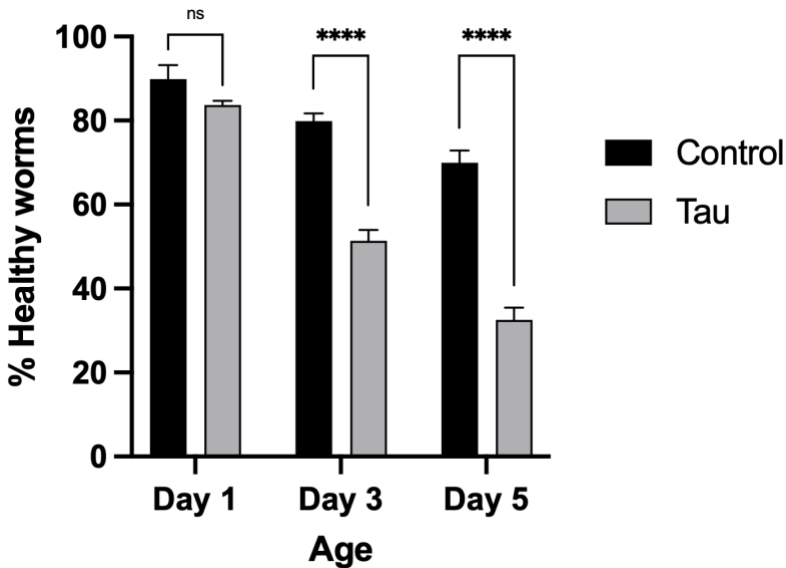


Figure 41: Quantified thrashing of *eat-4::GFP* (Control) and *eat-4::GFP; aex-3::tau* (Tau). Three trials of 20 worms each were performed for each strain at each time point, and the average thrashing of the triplicate was reported. Error bars are standard error (SEM). Two-way analysis of variance (ANOVA) and Tukey's multiple comparison test was used to analyze the statistical significance of this results. (* $P < 0.05$, ** $P < 0.01$, *** $P < 0.001$, **** $P < 0.0001$).

Figure 41 illustrates significant differences in thrashing between the tau worms (*eat-4::GFP; aex-3::tau*) and the control worms (*eat-4::GFP*) starting at day 3 and continuing in day 5. As previously mentioned, the assays become extremely difficult to perform beyond day 5 for the tau strain (*eat-4::GFP; aex-3::tau*) because the population size has dwindled significantly to ~10% of the starting population. Additionally, if the assays were performed with a population older than day 5, the results may vary because the healthier worms that live longer than average are selectively assayed. Figure 41 suggests that thrashing can be used to investigate the differences in fitness between control (*eat-4::GFP*) and tau (*eat-4::GFP; aex-3::tau*) worms throughout the lifespan. Therefore, it is feasible to track supplementation effects on fitness of the worms through thrashing

2.4.3. Thrashing assay with epoxide hydrolase inhibitor, AUDA, treatment

To investigate the role of epoxide hydrolase activity in thrashing quantity, worms were treated with AUDA supplementation to inhibit epoxide hydrolase. To prepare AUDA

supplemented plates, sufficient AUDA was dissolved in ethanol and was added to a 55°C NGM solution after autoclave to a final concentration of 100 μ M. First, it was established that AUDA supplementation does not have a significant effect on thrashing of the control worms (*eat-4::GFP*). Figure 42 illustrates the result of supplementing the control worms (*eat-4::GFP*) with AUDA.

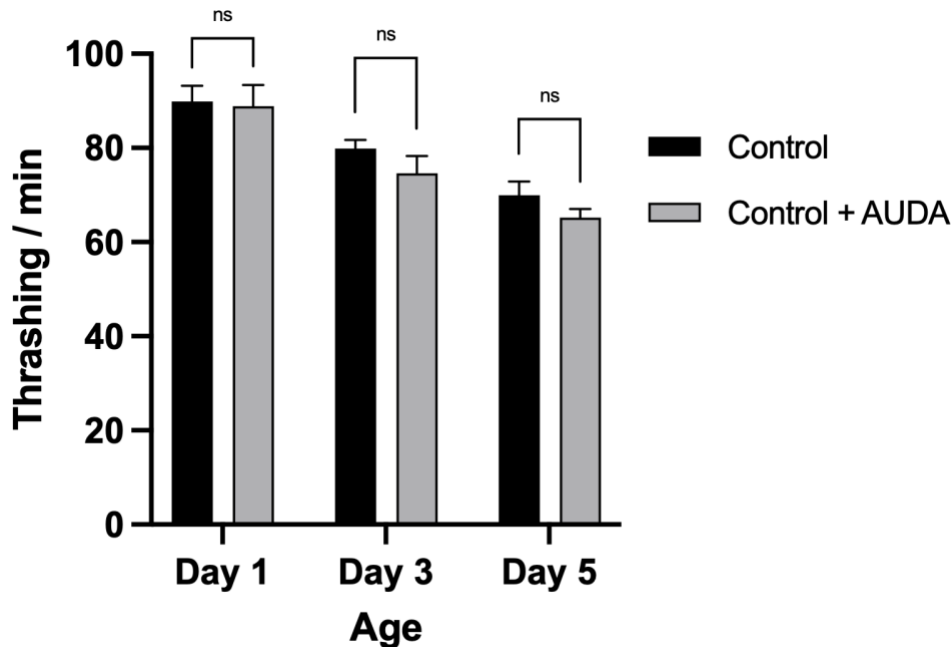


Figure 42: Quantified thrashing of *eat-4::GFP* (Control) supplemented with AUDA.

Three trials of 20 worms each were performed for each strain at each time point, and the average thrashing of the triplicate was reported. Error bars are standard error (SEM). Two-way analysis of variance (ANOVA) and Tukey’s multiple comparison test was used to analyze the statistical significance of this results. (* $P < 0.05$, ** $P < 0.01$, *** $P < 0.001$, **** $P < 0.0001$).

Figure 42 illustrates that AUDA has no significant effect on thrashing in control worms (*eat-4::GFP*). Therefore, supplementation with AUDA in the tau (*eat-4::GFP; aex-3::tau*) and control worms (*eat-4::GFP*) can be compared to assess the role of epoxide hydrolase inhibition in fitness of the worms.

To investigate if AUDA-mediated inhibition of epoxide hydrolase can affect thrashing in tau worms (*eat-4::GFP; aex-3::tau*), an age synchronized population of control (*eat-4::GFP*)

and tau worms (*eat-4::GFP; aex-3::tau*) were prepared as described in section 2.2.8. Age synchronized populations of L4 control (*eat-4::GFP*) and tau (*eat-4::GFP; aex-3::tau*) were placed on AUDA supplemented plates and ethanol (vehicle) supplemented plates. The age synchronized populations were maintained by filtration as described in section 2.2.9. The worms were scored for thrashing on days 1, 3, and 5 of the lifespan. Figure 43 illustrates the effects of AUDA supplementation on thrashing.

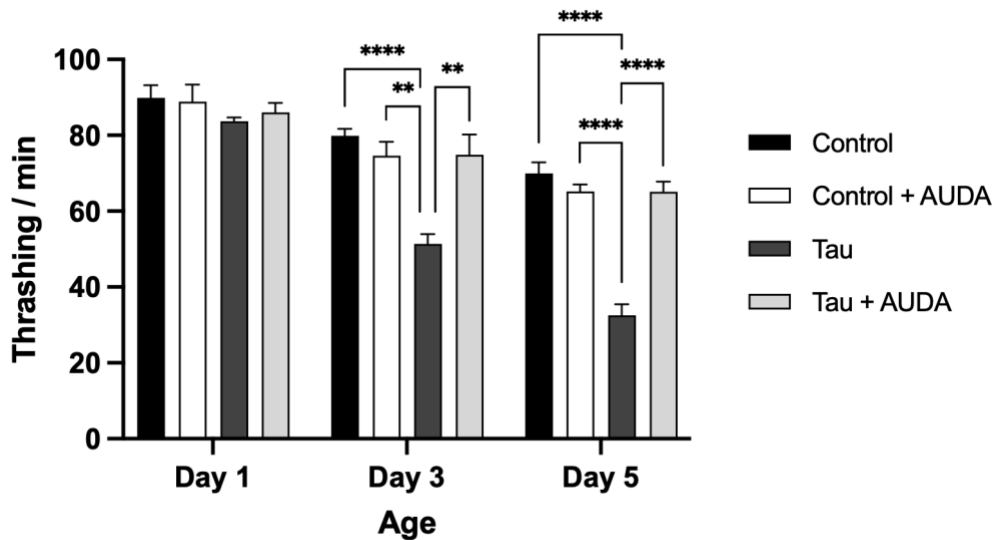


Figure 43: Quantified thrashing of *eat-4::GFP* (Control) and *eat-4::GFP; aex-3::tau* (Tau) supplemented with AUDA.

Three trials of 20 worms each were performed for each strain at each time point, and the average thrashing of the triplicate was reported. Error bars are standard error (SEM). Two-way analysis of variance (ANOVA) and Tukey's multiple comparison test was used to analyze the statistical significance of this results. (* $P < 0.05$, ** $P < 0.01$, *** $P < 0.001$, **** $P < 0.0001$).

Figure 43 shows that there is no significant difference between the control (*eat-4::GFP*) and tau worms (*eat-4::GFP; aex-3::tau*) supplemented with AUDA. Additionally, Figure 43 illustrates that thrashing in tau worms (*eat-4::GFP; aex-3::tau*) can be rescued with AUDA treatment.

Therefore, epoxide hydrolase activity and PUFA metabolite concentration play a significant role in the healthspan of the worms as observed by the thrashing phenotype.

2.4.4. Thrashing assay with ω -3 fatty acid and ω -3 fatty acid metabolite supplements

To investigate if the observed fitness recovery was caused by an increase in specific ω -3 fatty acids or ω -3 epoxide metabolites, both the control (*eat-4::GFP*) and tau worms (*eat-4::GFP; aex-3::tau*) were supplemented with EPA and EEQ. L4 age synchronized populations were prepared and placed on NGM plates supplemented with EPA or EEQ. Age synchronized populations were prepared and maintained as previously described in sections 2.2.8 and 2.2.9. Each population was assayed for thrashing at days 1, 3, and 5. The result of the control worms (*eat-4::GFP*) supplemented with EPA and EEQ is illustrated in Figure 44.

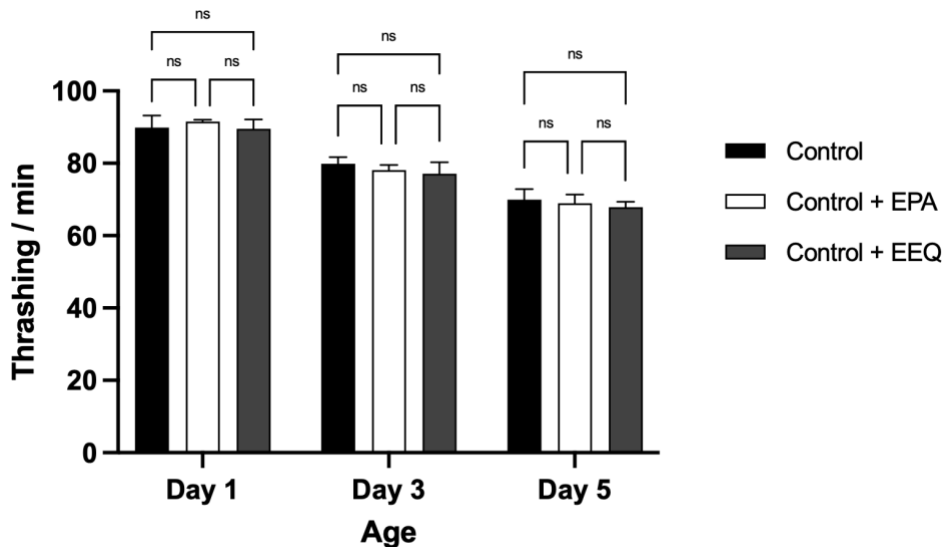


Figure 44: Quantified thrashing of *eat-4::GFP* (Control) supplemented with EPA and EEQ.

Three trials of 20 worms each were performed for each strain at each time point, and the average thrashing of the triplicate was reported. Error bars are standard error (SEM). Two-way analysis of variance (ANOVA) and Tukey's multiple comparison test was used to analyze the statistical significance of this results. (* $P < 0.05$, ** $P < 0.01$, *** $P < 0.001$, **** $P < 0.0001$).

Figure 44 suggests that EPA and EEQ supplementation on control worms (*eat-4::GFP*) did not significantly affect worm fitness as observed in thrashing. The result is anticipated as the control worms (*eat-4::GFP*) exhibit no detectable defects in thrashing at day 5 of the lifespan. However,

it is necessary to assess thrashing in the control worms (*eat-4::GFP*) at the early timepoints to serve as a control for compare with the tau worms (*eat-4::GFP; aex-3::tau*).

To investigate if the ω -3 PUFAs and ω -3 PUFA metabolites affect the thrashing phenotype in the tau worms (*eat-4::GFP; aex-3::tau*), an age synchronized population of the tau worms (*eat-4::GFP; aex-3::tau*) were supplemented with EPA and EEQ. The age synchronized population was maintained by filtration as previously described in section 2.2.8 and 2.2.9. The worms were assayed for thrashing on days 1, 3, and 5. The results of supplementing the tau (*eat-4::GFP; aex-3::tau*) with EPA and EEQ are shown in Figure 45.

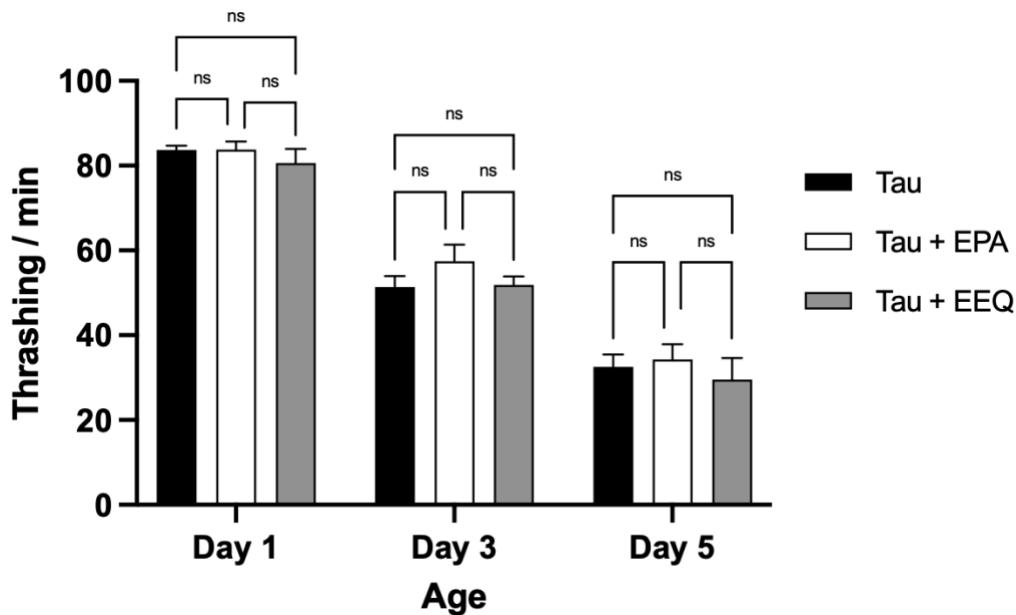


Figure 45: Quantified thrashing of *eat-4::GFP; aex-3::tau* (Tau) supplemented with EPA and EEQ.

Three trials of 20 worms each were performed for each strain at each time point, and the average thrashing of the triplicate was reported. Error bars are standard error (SEM). Two-way analysis of variance (ANOVA) and Tukey's multiple comparison test was used to analyze the statistical significance of this results. (* $P < 0.05$, ** $P < 0.01$, *** $P < 0.001$, **** $P < 0.0001$).

Figure 45 suggests that EPA and EEQ supplementation in the tau worms (*eat-4::GFP; aex-3::tau*) did not significantly affect worm fitness as observed in thrashing. The result may be explained by limited absorption of EPA and EEQ through the cuticle of the worm. Therefore,

EPA and EEQ concentrations in the worm are investigated and discussed in sections 2.5.1 and 2.5.2.

It is possible that supplementation with EPA and EEQ leads to increased metabolism in the worms, which may result in a relatively constant ratio of epoxide and diol metabolites. If the ratio remains constant, the null result is expected because of the suspected rescuing effect of EEQ, as shown by AUDA rescuing thrashing, and the detrimental effect of the diol. To investigate the constant epoxide to diol ratio hypothesis, cotreatments were performed with PUFA or PUFA metabolites and AUDA. Treatment with AUDA will inhibit the function of epoxide hydrolase leading to an increase in the epoxy PUFAs concentrations. An age synchronized population of control (*eat-4::GFP*) and tau worms (*eat-4::GFP; aex-3::tau*) were supplemented with vehicle control (ethanol), EPA + AUDA, or EEQ + AUDA. Age synchronized populations were prepared and maintained as previously described. Figure 46 shows the quantified results for control worms supplemented with EPA + AUDA and EEQ + AUDA.

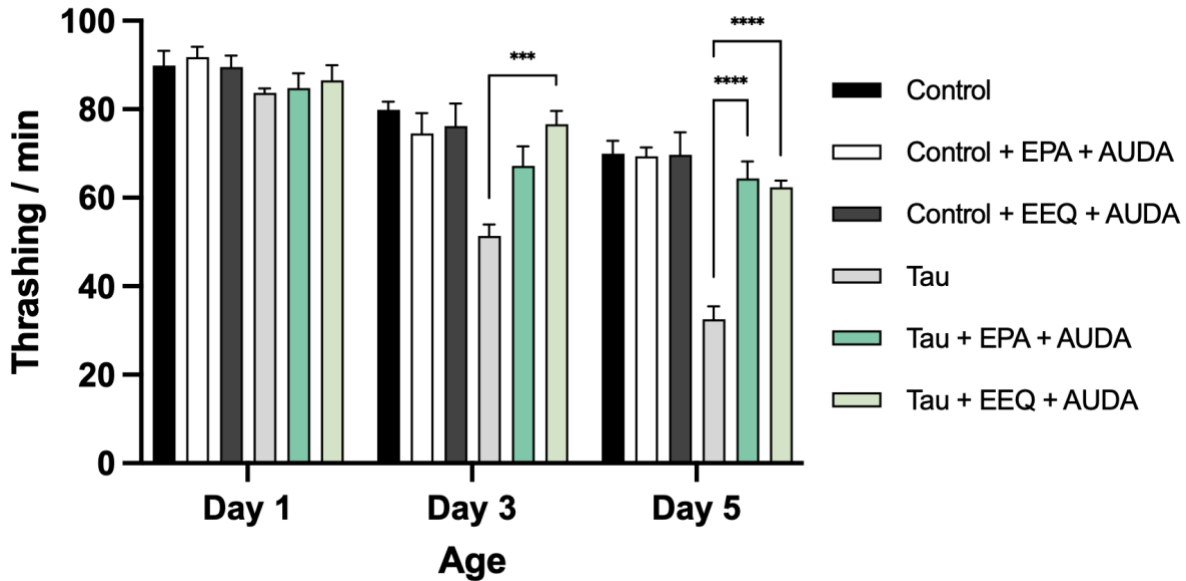


Figure 46: Quantified thrashing of *eat-4::GFP* (control) and *eat-4::GFP; aex-3::tau* (Tau) supplemented with EPA/AUDA and EEQ/AUDA.

Three trials of 20 worms each were performed for each strain at each time point, and the average thrashing of the triplicate was reported. Error bars are standard error (SEM). Two-way analysis of variance (ANOVA) and Tukey's multiple comparison test was used to analyze the statistical significance of this results. (* $P < 0.05$, ** $P < 0.01$, *** $P < 0.001$, **** $P < 0.0001$).

Figure 46 shows that there is no significant difference in control worms (*eat-4::GFP*) when cotreated with EPA+AUDA and EEQ+AUDA, which is consistent with Figure 42 and Figure 44 as both represent no change when control worms (*eat-4::GFP*) are treated with EPA, EEQ, or AUDA alone. Additionally, Figure 46 illustrates significant rescuing of thrashing in tau worms (*eat-4::GFP; aex-3::tau*) when treated with EPA + AUDA or EEQ + AUDA. However, Figure 45 shows that supplementing the tau worms (*eat-4::GFP; aex-3::tau*) with EPA or EEQ only does not significantly rescue thrashing. Taken together, it is likely that AUDA alone is responsible for the increased thrashing. Therefore, AUDA can rescue physical fitness, as measured by thrashing, but EPA or EEQ alone cannot.

2.5. Assessing lipid and lipid metabolite profiles using mass spectrometry

2.5.1. Lipidomic profiling using GC/MS

To confirm that treatment with PUFA fatty acids on the surface of the agar leads to an increase in PUFA levels in the worms, lipidomic analysis using a GC/MS method was performed. To investigate the PUFA levels for GC/MS, approximately 3-5 mg of whole worm lysates were collected. Sufficiently large populations of both control (*eat-4::GFP*) and tau worms (*eat-4::GFP; aex-3::tau*) were prepared using approximately seven plates per strain and supplementation pair. Six total conditions were prepared for lipidomic analysis namely, control (*eat-4::GFP*) and tau worms (*eat-4::GFP; aex-3::tau*) with ethanol control, EPA, or, DGLA. The populations were treated with 10 μ L of ethanol, 100 μ M EPA, or 100 μ M DGLA. DGLA concentrations have been linked to ferroptosis and are quantified to further investigate if ferroptosis is involved in the neuronal cell death in glutamatergic neurons³⁶. Refer to sections 2.2.12, 2.2.13, 2.2.15, 2.2.16, and 2.2.18 for more details on the lipidomic preparation and GC/MS injection method. Figure 47 shows the results of DGLA quantification for each population.

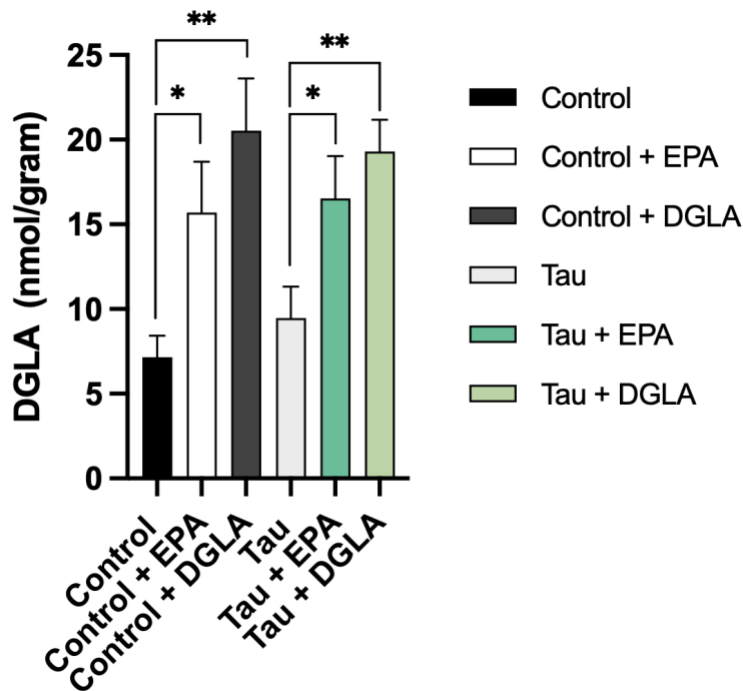


Figure 47: Quantification of DGLA in *eat-4::GFP* (Control) and *eat-4::GFP; aex-3::tau* (Tau) using GC/MS.

Three trials of whole worm lysates greater than 3 mg were used for each condition, and the average concentration for each triplicate is reported. Error bars are standard error (SEM). Two-way analysis of variance (ANOVA) and Tukey's multiple comparison test was used to analyze the statistical significance of this result (* $P < 0.05$, ** $P < 0.01$, *** $P < 0.001$, **** $P < 0.0001$).

Figure 47 illustrates that supplementation with both EPA and DGLA significantly increases the concentration of DGLA in the worm samples. The increase in DGLA after supplementation with EPA can be explained by the extensive PUFA synthesis and metabolism biological machinery that *C. elegans* possess. The worms can convert between all PUFAs. Additionally, in *C. elegans*, EPA is the end of the PUFA synthetic pathway and therefore, additional supplementation forces the worms to maintain homeostasis by possibly converting EPA to DGLA. Figure 48 illustrates the results of EPA quantification for each population.

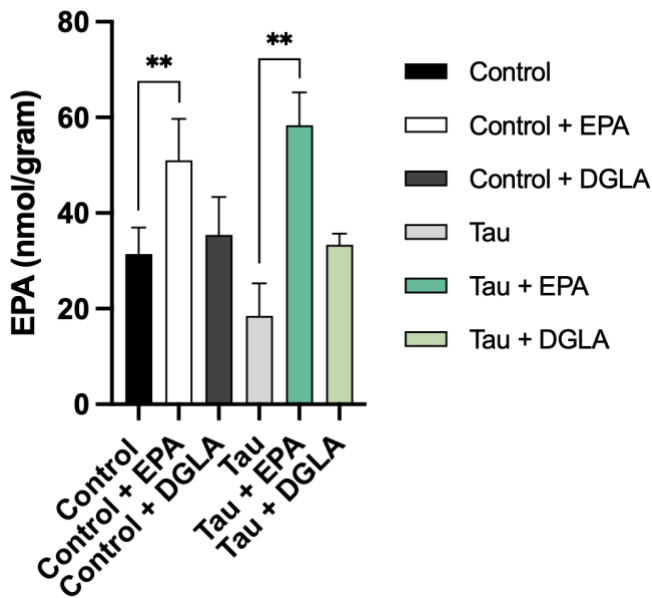


Figure 48: Quantification of EPA in *eat-4::GFP* (Control) and *eat-4::GFP; aex-3::tau* (Tau) using GC/MS.

Three trials of whole worm lysates greater than 3 mg were used for each condition, and the average concentration for each triplicate is reported. Error bars are standard error (SEM). Two-way analysis of variance (ANOVA) and Tukey's multiple comparison test was used to analyze the statistical significance of this result (* $P < 0.05$, ** $P < 0.01$, *** $P < 0.001$, **** $P < 0.0001$).

Figure 48 illustrated a significant increase in the EPA concentration for each population supplemented with EPA. Therefore, EPA supplementation on the plates leads to a detectable and significant increase in the EPA levels in the worms, validating that PUFA supplementation leads to an increase of PUFA concentration in the worm.

2.5.2. Oxylin profile using HPLC/MS/MS

To confirm that treatment with ep-PUFAs, such as EEQ, on the surface of the agar plates leads to an increase in the EEQ and their metabolite levels in the worms, oxylin analysis using a HPLC/MS/MS method was used. To investigate the oxylin profile of the worms, approximately 5 mg of whole worm lysates must be collected for each strain and supplement pair. Sufficiently large populations of both control (*eat-4::GFP*) and tau worms (*eat-4::GFP; aex-3::tau*) were prepared using approximately 7 plates per trial for each group. Four total

conditions were prepared for oxylipin analysis namely, control (*eat-4::GFP*) and tau worms (*eat-4::GFP; aex-3::tau*) with ethanol and EEQ. Each plate for every population was treated with 10 μ L of ethanol or 10 μ L of 100 μ M EEQ. Refer to sections 2.2.12, 2.2.13, 2.2.14, and 2.2.17 for more details on oxylipin preparation and HPLC/MS/MS injection. Figure 49 illustrates the results for all detectable EPA metabolites.

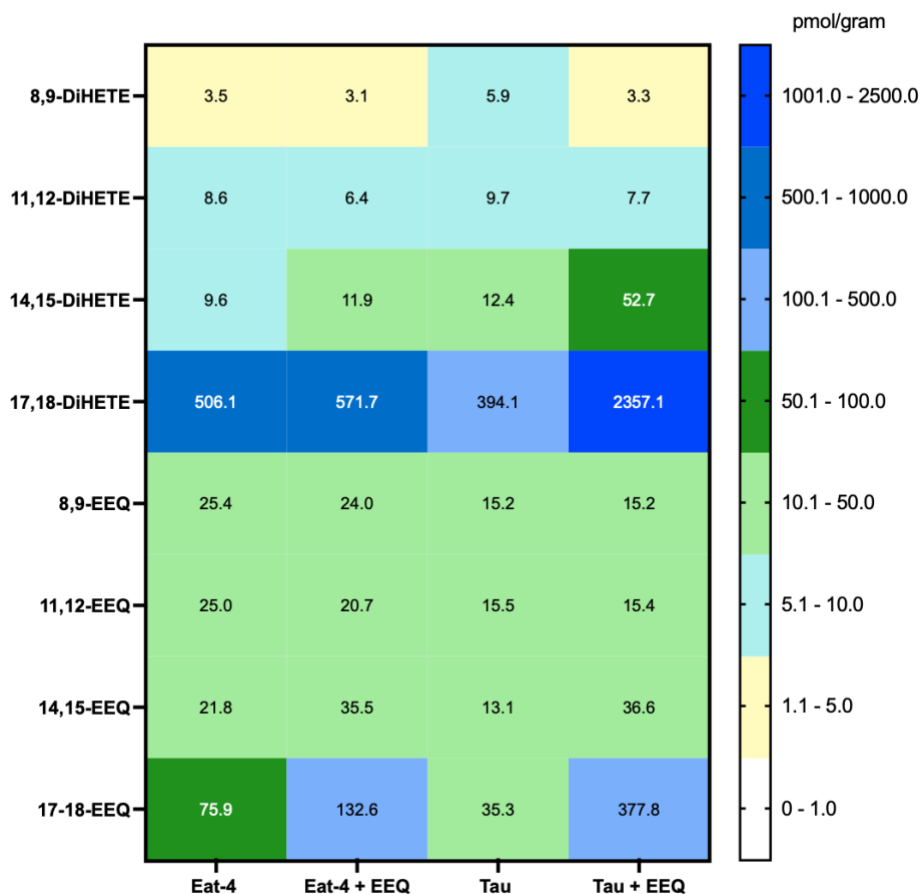


Figure 49: Oxylipin quantification of EPA diol and epoxide metabolites.

Each reported value is the average of three independent populations of whole worm lysate that were 5 mg or greater for each condition.

Figure 49 illustrates significant increases for two specific EEQ regioisomers namely, 14,15 EEQ and 17,18 EEQ, when treated with EEQ supplement. Additionally, DiHETE, the product of EEQ metabolism by epoxide hydrolase, is significantly increased for the same regioisomeric positions,

14,15-DiHETE and 17,18-DiHETE. Therefore, the method of EEQ supplementation does lead to increased levels of EEQ and EEQ metabolites in the worms. However, it is not consistent across all regioisomers as there is no such increase for the 8,9- and 11,12-regioisomers for either the epoxide or diol derivative. Lastly, it is important to note that the 5,6-regioisomer is not reported because the 5,6-epoxide is susceptible to intramolecular lactonization. To further assess the EEQ increase through supplementation, the 14,15- and 17,18-regioisomers were compared directly and reported in Figure 50.

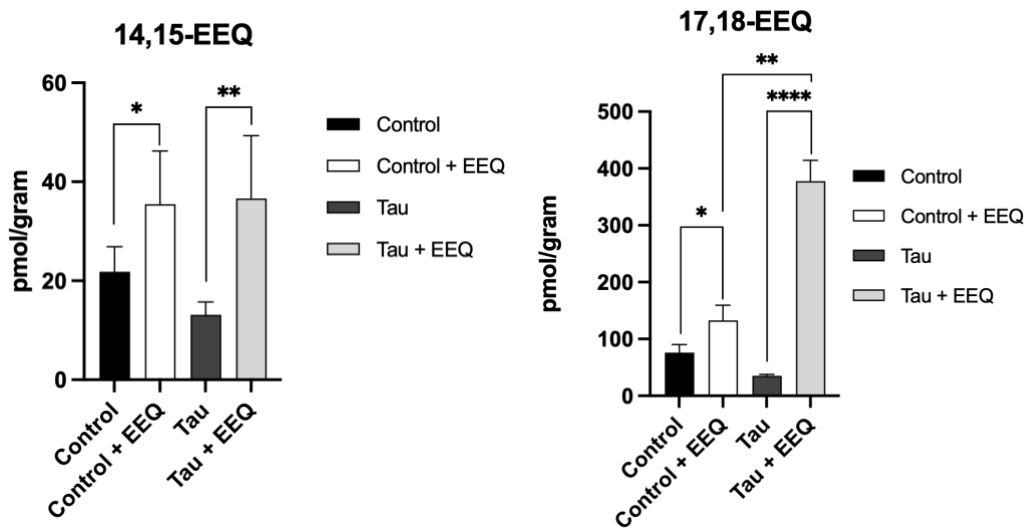


Figure 50: Direct comparison of 14,15-EEQ and 17,18-EEQ concentrations in each treatment group.

Each value is reported as an average of three independent populations of whole worm lysates. The average concentration for each group is reported for each triplicate. Error bars are standard error (SEM). Two-way analysis of variance (ANOVA) and Tukey's multiple comparison test was used to analyze the statistical significance of this result (* $P < 0.05$, ** $P < 0.01$, *** $P < 0.001$, **** $P < 0.0001$).

Figure 50 illustrates a statistically significant increase in the 14,15- and 17,18-EEQ regioisomers suggesting that the supplementation method increases the EEQ levels in the worms. However, as previously mentioned, the observed increase is not consistent in all EEQ regioisomers.

Additionally, the 17,18-EEQ regioisomer is significantly increased in the tau worms (*eat-4::GFP; aex-3::tau*) supplemented with EEQ when compared to control worms (*eat-4::GFP*)

with the same supplementation, suggesting that the tau worms may have altered EEQ metabolism. To further assess the effects of EEQ supplementation on the oxylin profile, the 14,15- and 17,18-DiHETE metabolite of EEQ were directly compared and reported in Figure 51.

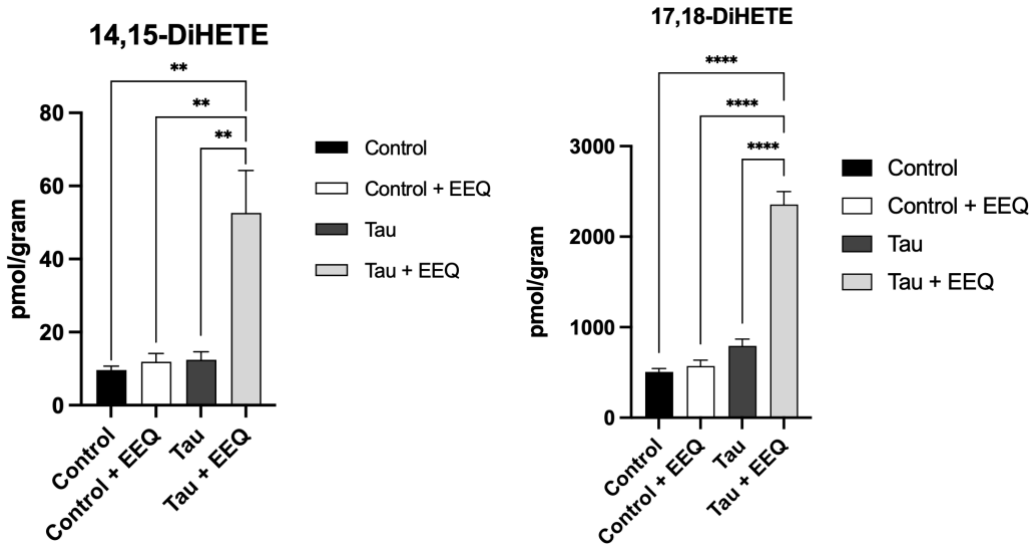


Figure 51: Direct comparison of 14,15-DiHETE and 17,18-DiHETE concentrations in each treatment group.

Each value is reported as an average of three independent populations of whole worm lysates. The average concentration for each group is reported for each triplicate. Error bars are standard error (SEM). Two-way analysis of variance (ANOVA) and Tukey's multiple comparison test was used to analyze the statistical significance of this result (* $P < 0.05$, ** $P < 0.01$, *** $P < 0.001$, **** $P < 0.0001$).

Figure 51 illustrates a significant increase of 14,15- and 17,18-DiHETE in the tau worms (*eat-4::GFP; aex-3::tau*) treated with EEQ. There are minor increases observed in the control strain (*eat-4::GFP*) supplemented with EEQ, but the difference is not statistically significant.

Therefore, Figure 51 suggests that the tau worms (*eat-4::GFP; aex-3::tau*) have increased epoxide hydrolase function, through increased activity or expression, as the DiHETE metabolite of EEQ is dramatically increased when supplemented with EEQ. Additionally, comparing control (*eat-4::GFP*) to the tau worms (*eat-4::GFP; aex-3::tau*) treated with vehicle show a minor and not statistically significant increase in both 14,15-DiHETE and 17-18-DiHETE,

further suggesting increased epoxide hydrolase function, through increased activity or expression, is specific to the tau worms (*eat-4::GFP; aex-3::tau*).

2.6. Discussion of the *eat-4::GFP* model

2.6.1. Neurological effects

Figure 27 illustrates that the tau worms (*eat-4::GFP; aex-3::tau*) exhibit significant neurodegeneration in glutamatergic neurons compared to control worms (*eat-4::GFP*) as quantified by the number of distinct somas. The specific neurodegeneration of glutamatergic neurons in the tau worms (*eat-4::GFP; aex-3::tau*) has not been previously reported and mimics neurodegeneration observed in AD patients. Additionally, our lab has shown that the neurodegeneration is not observed in all sensory neurons, as dopaminergic neurons in the *dat-1::GFP; aex-3::tau* strain exhibit no quantifiable neurodegeneration³⁷. Therefore, the observed neurodegeneration due to tauopathy in the *eat-4::GFP; aex-3::tau* worms is specific to the glutamatergic neurons and not a result of global neurodegeneration of all neuron types. The observed neurodegeneration of glutamatergic neurons in tau worms (*eat-4::GFP; aex-3::tau*) establishes a useful model to investigate the mechanism of tauopathy in AD.

Inhibition of EH in AD animal models have shown significant cognitive improvement with no clear mechanism³⁸. To begin investigating the mechanism, the tau worms (*eat-4::GFP; aex-3*) were treated with known CEEH inhibitor, AUDA. It was found that AUDA treatment rescued neurodegeneration in the tau worms (*eat-4::GFP; aex-3::tau*) as shown in Figure 29. The EH inhibition-induced rescuing effect of the tau (*eat-4::GFP; aex-3::tau*) AD model mimics similar EH inhibition rescuing effects observed in mammalian AD models. However, the mechanism of AUDA rescue and potential lipid mediators responsible for the positive effect must still be identified. The rescued glutamatergic neurons in AUDA treated tau worms (*eat-*

eat-4::GFP; aex-3::tau) may be explained by an increase in epoxy-PUFA metabolites and/or a decrease in the 1,2 diol metabolites. To investigate whether the epoxy-PUFA metabolites are responsible for the positive effects, the tau worms (*eat-4::GFP; aex-3::tau*) were treated with EPA and EEQ. EPA and its epoxide metabolite, EEQ, were chosen because EPA is found in the highest concentration of all PUFAs in *C. elegans*, and it is an ω -3 PUFA, which may have neuroprotective effects. Treatment of both the control (*eat-4::GFP*) and tau worms (*eat-4::GFP; aex-3::tau*) with EPA and EEQ lead to no significant neurodegeneration as observed in Figures 24, 25, and 26. One possible explanation for the null result may be because EPA and EEQ are not significantly absorbed through the cuticle of the worm. To investigate the limited absorption hypothesis, the oxylipin and lipidomic profile of worms supplemented with and without EPA and EEQ were quantified by HPLC/MS/MS and GC/MS, respectively. Figure 44 illustrates that specific regioisomers, 14,15-EEQ and 17-18-EEQ, are found in much higher concentrations in both control (*eat-4::GFP*) and tau worms (*eat-4::GFP; aex-3::tau*) when supplemented with EEQ. Therefore, the increased concentration of specific EEQ regioisomers suggest that EEQ is absorbed into the worm, which suggests that the limited rescuing effect of EEQ is not due to an absorption issue. Additionally, Figure 48 illustrates that EPA is found in significantly higher concentrations when both control (*eat-4::GFP*) and tau worms (*eat-4::GFP; aex-3::tau*) were treated with EPA. Therefore, the supplementation method as described in sections 2.2.5 lead to an increase in EPA and EEQ concentrations in the worms, and therefore, the confounding factor of cuticle absorption can be ruled out. However, EPA and EEQ supplementation do not significantly rescue glutamatergic neurons from tauopathy-induced neurodegeneration. It is possible that EPA and EEQ alone are not sufficient for rescuing neurodegeneration. AUDA

inhibits CEEH function, and EEQ is not the only substrate of CEEH. Therefore, AUDA may rescue neurodegeneration through another ep-PUFA mediator or through off target effects.

To further investigate the role of EPA and EEQ on glutamatergic neuronal health, control (*eat-4::GFP*) and tau worms (*eat-4::GFP; aex-3::tau*) were supplemented with EPA + AUDA and EEQ + AUDA. Figure 36 illustrates that EPA + AUDA and EEQ + AUDA rescues glutamatergic neurons from neurodegeneration. However, Figure 32 shows EPA and EEQ alone does not rescue the glutamatergic neurons. Therefore, it is possible that EPA and EEQ do not significantly rescue glutamatergic neurons from degeneration. However, AUDA may reach a maximum effect that prevents the detection of any synergistic effects from EPA and EEQ supplementation. It is possible that EPA and EEQ contribute to rescuing neurodegeneration in a small way that is undetectable when cotreated with AUDA.

To further investigate PUFA effects on glutamatergic neurons, control (*eat-4::GFP*) and tau worms (*eat-4::GFP; aex-3::tau*) worms were treated with a known ferroptosis inhibitor, LIP-1. Ferroptosis is a potential cell death mechanism responsible for neurodegeneration in AD patients³⁹. The primary evidence for the ferroptosis hypothesis is that iron accumulates in NFTs, and the accumulation has been linked to cognitive decline^{39,40}. Additionally, AUDA treatment significantly alters the PUFA metabolism profile, and therefore, may indirectly prevent lipid peroxidation, which is associated with ferroptosis. Therefore, treatment with LIP-1 provides a way to assess a potential mechanism of AUDA rescuing neurodegeneration. Figure 39 illustrates that LIP-1 treatment does not rescue tau worms (*eat-4::GFP; aex-3::tau*) from glutamatergic neurodegeneration. Therefore, ferroptosis is not the primary cell death mechanism observed in the tau (*eat-4::GFP; aex-3::tau*) AD model. Additionally, the null result of LIP-1 treatment suggests that AUDA rescue of neurodegeneration is functioning through another mechanism,

possibly glutamate excitotoxicity. Glutamate excitotoxicity may be prevented by AUDA supplementation because it has been shown that an increase in ep-PUFA metabolites inhibit the NMDA receptor activity, which is closely linked in glutamate excitotoxicity⁴¹. However, to unambiguously determine the cell death mechanism for glutamatergic neurodegeneration, further experiments must be performed.

In conclusion, genetic insertion of the human tau protein causes significant neurodegeneration as quantified by distinct somas present in the worms. Therefore, the tau model (*eat-4::GFP; aex-3::tau*) provides a useful model to investigate the cell death mechanism associated with tauopathy. Additionally, neurodegeneration can be rescued by supplementation with AUDA. However, the mechanism of the rescuing effect remains elusive. Treatment with the ferroptosis inhibitor, LIP-1, did not rescue the glutamatergic neurons from degeneration, which suggests that ferroptosis is not the primary cell death mechanism during the assessed time points. Additionally, treatment with EEQ and EPA did not rescue the glutamatergic neurons. Therefore, it is unlikely that any of the EEQ lipid mediators are responsible for the rescuing effect. However, AUDA inhibits CEEH entirely, and EEQ is not the only substrate of CEEH. Therefore, another lipid mediator derived from another parent PUFA may be responsible for the neuroprotection. Additionally, it is possible that AUDA protects against another cell death mechanism entirely, such as glutamate excitotoxicity. The increased ep-PUFA concentration from AUDA treatment may inhibit NMDA receptor activity, preventing glutamate excitotoxicity⁴¹. Nevertheless, further investigation is necessary to determine the lipid mediators and cell death mechanism(s) involved in the glutamatergic neurodegeneration.

2.6.2. Physical fitness effects

Figure 41 illustrates that at day 3 and later, tau worms (*eat-4::GFP; aex-3::tau*) exhibit significant fitness defects as quantified by thrashing. Therefore, tauopathy may be involved in the fitness defects, suggesting that tauopathy does not only affect sensory neurons as previously discussed. To begin investigating the mechanism responsible for fitness defects, the tau worms (*eat-4::GFP; aex-3::tau*) were supplemented with AUDA. Figure 43 illustrates that AUDA supplementation rescues the worms from the fitness defects, observed by increased thrashing. Figure 42 shows that supplementing the control strain with 100 μ M of AUDA results in no overt toxic effects because the control worms (*eat-4::GFP*) are similarly fit with and without AUDA treatment. The rescued fitness as observed by thrashing in tau worms (*eat-4::GFP; aex-3::tau*) supplemented with AUDA may be explained by neuroprotection of motor neurons. However, the health of motor neurons was not investigated, and therefore we cannot conclude that this rescue in fitness is due to neuroprotection.

To investigate the mechanism leading to rescued fitness of the tau worms (*eat-4::GFP; aex-3::tau*), the tau worms (*eat-4::GFP; aex-3::tau*) were supplemented with EPA and EEQ. If one or multiple EEQ regioisomers are the lipid mediators responsible for the neuroprotection, EEQ treatment will rescue the tau worms (*eat-4::GFP; aex-3::tau*) from the fitness defects observed in thrashing. Treatment of both the control (*eat-4::GFP*) and tau worms (*eat-4::GFP; aex-3::tau*) with EPA and EEQ yielded no significant protection from the fitness defects caused by tauopathy as observed in Figures 38 and 39. Therefore, the five EEQ regioisomers are likely not the lipid mediators involved in the suggested neuroprotection. However, it is possible that another epoxy-PUFA is the lipid mediator responsible for the proposed neuroprotection. Additionally, the concentrations of EEQ and EPA that pass the cuticle was detected by GC/MS

and HPLC/MS/MS, which eliminates any absorption issues. Further investigation is required to determine which lipid mediator(s) are responsible for the increased fitness.

To further investigate the mechanism of AUDA protection from fitness defects, control (*eat-4::GFP*) and tau worms (*eat-4::GFP; aex-3::tau*) were supplemented with EPA + AUDA and EEQ + AUDA. Figure 46 illustrates significant rescuing in fitness as observed by thrashing of tau worms (*eat-4::GFP; aex-3::tau*) when cotreated with EPA + AUDA, and EEQ + AUDA supplementation. However, EPA and EEQ alone did not rescue fitness alone as shown in Figure 45. Therefore, AUDA is likely responsible for the protection from fitness defects as EPA and EEQ alone did not rescue any of the defects. However, it is possible that AUDA protection reaches a maximum that prevents the detection of any synergistic or additive effects of EPA or EEQ.

In conclusion, genetic insertion of the human tau protein causes fitness defects as observed by thrashing. Additionally, the defects can be rescued by supplementation with AUDA. The mechanism of recovery may be neuroprotection of motor neurons. It is possible that specific lipid mediators, but not the five tested EEQ regioisomers, are regulated by AUDA treatment, and these mediators contribute to neuroprotection of motor neurons. However, motor neuron health was not assayed in this work, and therefore, we cannot conclude that this rescue in fitness is due to neuroprotection.

2.6.3. Experimental limitations

One significant limitation of the tau model (*eat-4::GFP; aex-3::tau*) is that this model investigates the effects of human tau alone. The current literature investigating AD suggests that tau and A β function synergistic in neurodegeneration⁴². The model proposed in this work can only assess the role of tau and tauopathy in neurodegeneration. To build upon the tau model (*eat-*

eat-4::GFP; aex-3::tau), we can generate a new strain that expresses both human tau and A β to determine if the effects of tauopathy are exacerbated by the presence of A β . Furthermore, there is an inherent limitation in the glutamatergic neuronal GFP assay as only five specific glutamatergic neurons are tagged with the EAT-4 GFP. The limited number of neuron somas is both an advantage and a disadvantage. The limited number allows for easier distinct between somas and overlapped axons and dendrites. However, *C. elegans* contain 78 known glutamatergic neurons¹⁷. Therefore, the current tau model (*eat-4::GFP; aex-3::tau*) discussed in this work are only a small representation of all glutamatergic neurons in *C. elegans*. Therefore, conclusions of neurodegeneration in the glutamatergic system needs further support in AD models that tag more neurons of the system.

2.6.4. Future directions

The mechanism of glutamatergic neurodegeneration observed in this worked has yet to be elucidated. Ferroptosis is not likely the major cell death mechanism during the observed time points, as treatment of tau worms (*eat-4::GFP; aex-3::tau*) with ferroptosis inhibitor, LIP-1, did not protect the glutamatergic neurons from degeneration. However, AUDA treatment did rescue the tau worms (*eat4::GFP; aex-3::tau*) worms from neurodegeneration. Therefore, AUDA is directly or indirectly preventing another form of cell death. Besides ferroptosis, the current AD literature suggests that glutamate excitotoxicity may be involved in AD related neurodegeneration, specially through overactivation of the NMDA glutamate receptor⁴³. *C. elegans* contain several glutamate receptors, but only two of the NMDA family, NMR-1 and NMR-2⁴⁴. Genetic knockouts of the two *C. elegans* NMDA glutamate receptors, NMR-1 and NMR-2, are available. To further investigate the cell death mechanism responsible for glutamatergic neurodegeneration, new strains crossing the tau model (*eat-4::GFP; aex-3::tau*)

with each glutamate NMDA receptor, NMR-1 and NMR-2, will be generated. The new strains containing tau and the genetic mutation preventing NMDA receptor will be assayed for glutamatergic neuron function using the GFP assay previously described. If neurodegeneration is not observed when NMR-1 and/or NMR-2 is not present, glutamate excitotoxicity would be suggested as the most likely cell death mechanism of neurodegeneration. However, without further investigation, glutamate excitotoxicity can only be hypothesized as the major cell death mechanism in glutamatergic neurodegeneration.

REFERENCES

REFERENCES

- (1) Institute of Medicine (US) Forum on Neuroscience; Disorders, N. S. *Introduction*; National Academies Press (US), 2011.
- (2) Doble, A. *Pharmacol. Ther.* **1999**, *81* (3), 163–221.
- (3) Herman, M. A.; Nahir, B.; Jahr, C. E. *PLoS One* **2011**, *6* (11), e26501.
- (4) Cortese, B. M.; Phan, K. L. *CNS Spectr.* **2005**, *10* (10), 820–830.
- (5) Bechtholt-Gompf, A. J.; Walther, H. V.; Adams, M. A.; Carlezon, W. A., Jr; Ongür, D.; Cohen, B. M. *Neuropsychopharmacology* **2010**, *35* (10), 2049–2059.
- (6) Dobi, A.; Margolis, E. B.; Wang, H.-L.; Harvey, B. K.; Morales, M. *J. Neurosci.* **2010**, *30* (1), 218–229.
- (7) Juge, N.; Gray, J. A.; Omote, H.; Miyaji, T.; Inoue, T.; Hara, C.; Uneyama, H.; Edwards, R. H.; Nicoll, R. A.; Moriyama, Y. *Neuron* **2010**, *68* (1), 99–112.
- (8) Daniels, R. W.; Miller, B. R.; DiAntonio, A. *Neurobiol. Dis.* **2011**, *41* (2), 415–420.
- (9) Belov Kirdajova, D.; Kriska, J.; Tureckova, J.; Anderova, M. *Front. Cell. Neurosci.* **2020**, *14*, 51.
- (10) Wang, R.; Reddy, P. H. *J. Alzheimers. Dis.* **2017**, *57* (4), 1041–1048.
- (11) Hynd, M. R.; Scott, H. L.; Dodd, P. R. *Neurochem. Int.* **2004**, *45* (5), 583–595.
- (12) Kashani, A.; Lepicard, E.; Poirel, O.; Videau, C.; David, J. P.; Fallet-Bianco, C.; Simon, A.; Delacourte, A.; Giros, B.; Epelbaum, J.; Betancur, C.; El Mestikawy, S. *Neurobiol. Aging* **2008**, *29* (11), 1619–1630.
- (13) Chen, K.; Jiang, X.; Wu, M.; Cao, X.; Bao, W.; Zhu, L.-Q. *Front Cell Dev Biol* **2021**, *9*, 704298.
- (14) Dixon, S. J. *Immunol. Rev.* **2017**, *277* (1), 150–157.
- (15) Chen, X.; Comish, P. B.; Tang, D.; Kang, R. *Front Cell Dev Biol* **2021**, *9*, 637162.
- (16) Dysken, M. W.; Guarino, P. D.; Vertrees, J. E.; Asthana, S.; Sano, M.; Llorente, M.; Pallaki, M.; Love, S.; Schellenberg, G. D.; McCarten, J. R.; Malphurs, J.; Prieto, S.; Chen, P.; Loreck, D. J.; Carney, S.; Trapp, G.; Bakshi, R. S.; Mintzer, J. E.; Heidebrink, J. L.; Vidal-Cardona, A.; Arroyo, L. M.; Cruz, A. R.; Kowall, N. W.; Chopra, M. P.; Craft, S.; Thielke, S.; Turvey, C. L.;

- Woodman, C.; Monnell, K. A.; Gordon, K.; Tomaska, J.; Vatassery, G. *Alzheimers. Dement.* **2014**, *10* (1), 36–44.
- (17) Serrano-Saiz, E.; Poole, R. J.; Felton, T.; Zhang, F.; De La Cruz, E. D.; Hobert, O.. *Cell* **2013**, *155* (3), 659–673.
- (18) Kraemer, B. C.; Zhang, B.; Leverenz, J. B.; Thomas, J. H.; Trojanowski, J. Q.; Schellenberg, G. D. *Proc. Natl. Acad. Sci. U. S. A.* **2003**, *100* (17), 9980–9985.
- (19) http://www.wormbook.org/chapters/www_strainmaintain/strainmaintain.html, Maintenance of *C. elegans*, accessed Feb. 12, 2022.
- (20) Ke, T.; Santamaría, A.; Tinkov, A. A.; Bornhorst, J.; Aschner, M. *Curr. Protoc. Toxicol.* **2020**, *84* (1), e94.
- (21) Brenner, S. *Genetics* **1974**, *77* (1), 71–94.
- (22) Taggart-Murphy, L.; Kim, C.; Richards, D.; Narin, A. Tips and Tricks for Successful Worm Picking <https://invivobiosystems.com/view-from-the-bench/tips-and-tricks-for-successful-worm-picking>, accessed Feb. 18, 2022.
- (23) Wang, H.; Zhao, Y.; Zhang, Z. *Biochem. Biophys. Res. Commun.* **2019**, *509* (3), 694–699.
- (24) Deline, M. L.; Vrablik, T. L.; Watts, J. L. *J. Vis. Exp.* **2013**, No. 81.
- (25) Anderson, J. L.; Morran, L. T.; Phillips, P. C. *J. Hered.* **2010**, *101 Suppl 1*, S62–S74.
- (26) Schafer, W. R. *Egg-Laying*; WormBook, 2005.
- (27) Gruber, J.; Ng, L. F.; Poovathingal, S. K.; Halliwell, B. Effects. *FEBS Lett.* **2009**, *583* (21), 3377–3387.
- (28) Handbook - Introduction <https://www.wormatlas.org/hermaphrodite/introduction/mainframe.htm>, accessed Jun. 19, 2022.
- (29) Caldwell, K. A.; Willicott, C. W.; Caldwell, G. A. *Dis. Model. Mech.* **2020**, *13* (10).
- (30) Shivers, J.; Uppaluri, S.; Brangwynne, C. P. *Microfluid. Nanofluidics* **2017**, *21* (9), 149.
- (31) Shen, H. C.; Hammock, B. D. *J. Med. Chem.* **2012**, *55* (5), 1789–1808.
- (32) Harris, T. R.; Aronov, P. A.; Jones, P. D.; Tanaka, H.; Arand, M.; Hammock, B. D. *Arch. Biochem. Biophys.* **2008**, *472* (2), 139–149.
- (33) Wall, R.; Ross, R. P.; Fitzgerald, G. F.; Stanton, C. *Nutr. Rev.* **2010**, *68* (5), 280–289.

- (34) Zhang, F.; Sarparastzardoudi, M.; Dattmore, D. Unpublished lipidomic analysis from the Lee Lab
- (35) Jenkins, N. L.; James, S. A.; Salim, A.; Sumardy, F.; Speed, T. P.; Conrad, M.; Richardson, D. R.; Bush, A. I.; McColl, G. *Elife* **2020**, *9*.
- (36) Perez, M. A.; Magtanong, L.; Dixon, S. J.; Watts, J. L. *Dev. Cell* **2020**, *54* (4), 447–454.e4.
- (37) Sarparastzardoudi, M. Unpublished *C. elegans* dopaminergic neuron assay from the Lee Lab
- (38) Griñán-Ferré, C.; Codony, S.; Pujol, E.; Yang, J.; Leiva, R.; Escolano, C.; Puigoriol-Illamola, D.; Companys-Aleman, J.; Corpas, R.; Sanfeliu, C.; Pérez, B.; Loza, M. I.; Brea, J.; Morisseau, C.; Hammock, B. D.; Vázquez, S.; Pallàs, M.; Galdeano, C. *Neurotherapeutics* **2020**.
- (39) Tao, Y.; Wang, Y.; Rogers, J. T.; Wang, F. *J. Alzheimers. Dis.* **2014**, *42* (2), 679–690.
- (40) Ayton, S.; Wang, Y.; Diouf, I.; Schneider, J. A.; Brockman, J.; Morris, M. C.; Bush, A. I. *Mol. Psychiatry* **2020**, *25* (11), 2932–2941.
- (41) Zhang, E.; Kim, J.-J.; Shin, N.; Yin, Y.; Nan, Y.; Xu, Y.; Hong, J.; Hsu, T. M.; Chung, W.; Ko, Y.; Lee, W.; Lim, K.; Kim, D. W.; Lee, S. Y. *J. Med. Food* **2017**, *20* (6), 535–541.
- (42) Tripathi, T.; Kalita, P. *ACS Chem. Neurosci.* **2019**, *10* (3), 1129–1130.
- (43) Wang, R.; Reddy, P. H. *J. Alzheimers. Dis.* **2017**, *57* (4), 1041–1048.
- (44) Brockie, P. J.; Maricq, A. V. *WormBook* **2006**, 1–16.

CHAPTER THREE:

INVESTIGATION OF TAU FEEDING MODEL IN *C. ELEGANS*

3. TAU FEEDING MODEL

3.1. Introduction of PIMAX model

3.1.1. Using PIMAX to produce tau and hyperphosphorylated tau in *E. coli*

Many pathogenic proteins are underrepresented in proteomics and biochemical studies because of the difficulty of their production in *E. coli*. The underrepresented proteins may undergo posttranslational modifications vital to their function both pathologically and physiologically¹. One such protein of particular interest to this thesis is the tau protein and its posttranslational phosphorylation that is closely linked to AD pathology². Efficient production of the protein with the posttranslational modification requires a well-defined “facilitator” such as the protein responsible for the modification and the natural physiological partner within a well-studied dimeric complex¹. The Kuo lab developed a method, protein interaction module-assisted function X (PIMAX) to address and overcome the obstacles of generating specific posttranslational modified proteins in *E. coli*¹.

PIMAX functions by inserting two proteins of interest on a pair of well-studied protein-protein interaction modules¹. The protein-protein interaction brings the two proteins of interest into proximity of one another. The proximity facilitates efficient modification of the physiological partner by the modification protein. The PIMAX model was used to generate hyperphosphorylated tau in *E. coli*. The model takes advantage of the specific heterodimerization of the proteins Jun and Fos. The researchers then modified Fos by inserting GSK-3 β , glycogen synthase kinase 3 β , into *E. coli* by recombinant gene generation and ligation-independent cloning. Additionally, Jun was modified by inserting human tau, 4R1N isoform, into *E. coli* by

recombinant gene generation and ligation-independent cloning. Two *E. coli* strains of interest were generated tau only (Jun modification with Tau), and hyperphosphorylated tau (Jun modification with tau and Fos modification with GSK-3 β). The protein-protein interaction used in PIMAX is specific heterodimerization of the proteins Jun and Fos¹. The two different *E. coli* strains provide tau without posttranslational modification and tau with posttranslational modification *in vitro*, which provides a potential use in *C. elegans* as the nematodes consume *E. coli*.

To release the protein of interest, tau and hyperphosphorylated tau, the researchers took advantage of the specific protease from tobacco etch virus (TEV). TEV protease is a highly sequence-specific cysteine protease³. Therefore, TEV protease can be used to specifically cleave the tau protein from the Jun/Fos dimer after posttranslational modification has occurred. The inserted a TEV protease cleavage site between the Fos/Jun protein and the protein of interest, tau or GSK-3 β . To release hyperphosphorylated tau, one can culture the *E. coli* strain with both modifications, Fos with kinase and Jun with tau, for 24 hours. Then, *E. coli* expressing TEV protease to the hyperphosphorylated tau was added, producing bacteria to initiate protein cleavage of hyperphosphorylated tau from the Fos/Jun dimer. Figure 52 illustrates the PIMAX model used in hyperphosphorylated tau production in *E. coli*. PIMAX provides an efficient method to investigate hyperphosphorylated tau in *in vitro* models. Therefore, *C. elegans* were feed tau and hyperphosphorylated tau producing bacteria to investigate the viability of feeding delivery as a method to model AD in *C. elegans*.

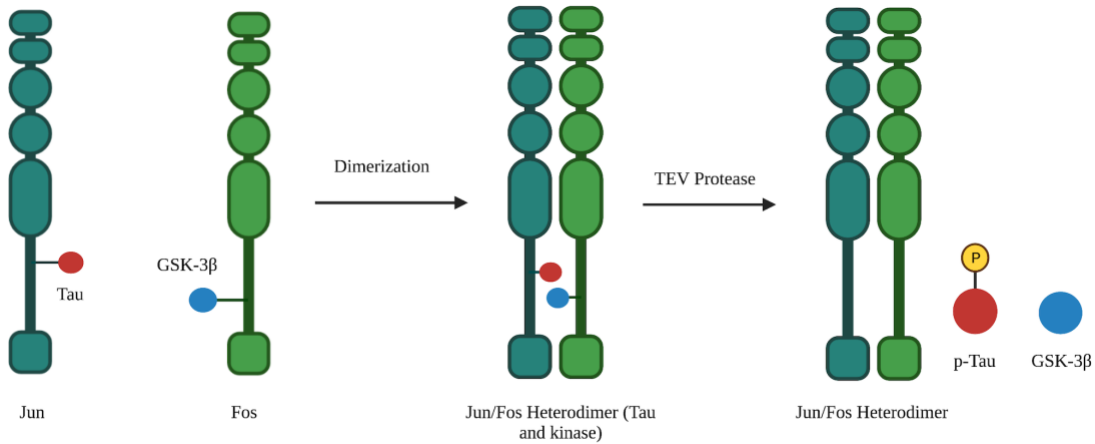


Figure 52: PIMAX model producing free hyperphosphorylated tau in *E. coli*.

3.2. Experimental

3.2.1. Growing healthy bacteria stocks

Overnight cultures of *E. coli* producing tau, p-tau, vector, and TEV (Tobacco Etch Virus) protease was prepared by mixing 10 mL of LB, 2 μ L of bacteria, and sufficient ampicillin to generate a final concentration of 5 μ g/mL in separate containers. The bacteria solution was moved to a shaker set to 37°C and allowed to shake overnight. The overnight culture was diluted by mixing 40 μ L bacterial stock with 2 mL LB and sufficient ampicillin to generate a final concentration of 5 μ g/mL. The diluted bacteria solution was moved to the shaker at 37°C for 2 hours. Then, 20 μ L of 100 mM stock of isopropyl β -D-1-thiogalactopyranoside (IPTG) was added to the diluted bacteria to induce expression of the protein of interest. After addition of IPTG, the diluted bacteria culture was moved to the shaker at 37°C for 3 hours. Equal parts of the TEV culture was mixed with each bacteria type. The mixed bacteria solutions were then seeded onto NGM plates coated with 5 μ g/mL of ampicillin and 1 mM of IPTG. The bacteria were left out at room temperature to grow overnight¹. The resulting plates were used for all assays involving the tau feeding model. The plates were stored in a box sealed with aluminum foil to prevent light exposure to stabilize IPTG⁴.

3.2.2. Making IPTG and ampicillin plates

NGM plates containing ampicillin and IPTG were created in groups of 15 by mixing 1125 μL of IPTG and sufficient ampicillin to generate a final concentration of 5 $\mu\text{g}/\text{mL}$. Then, 82.5 μL of the mixed solution was added to the surface of each NGM plate and spread with a glass rod. Each bacterial type of tau, p-tau and vector were seeded to each plate on top of the dried ampicillin and IPTG. Refer to 2.2.5. for more details on the supplementing process. The plates were left overnight at room temperature to dry and allow for bacterial growth. All plates generated in this way were stored in aluminum foil covered boxes to prevent IPTG light exposure⁴.

3.2.3. Serotonin (5-HT) assay

A 1 mM solution of serotonin was prepared by mixing 2 mg serotonin per 5 mL of s-basal medium. The total volume varied depending on the number of serotonin assays to be ran. Then, 200 μL of the 1 mM serotonin solution was added to several wells of a 96-well plate. Next, 5 worms were placed into each well plate for the assay. Each group of worms was transferred simultaneously, and the exposure time was monitored. The worms were assayed for paralysis at a 10-minute exposure time⁵. One trial consists of 4 wells with 5 worms each. The serotonin assay is illustrated in Figure 53.

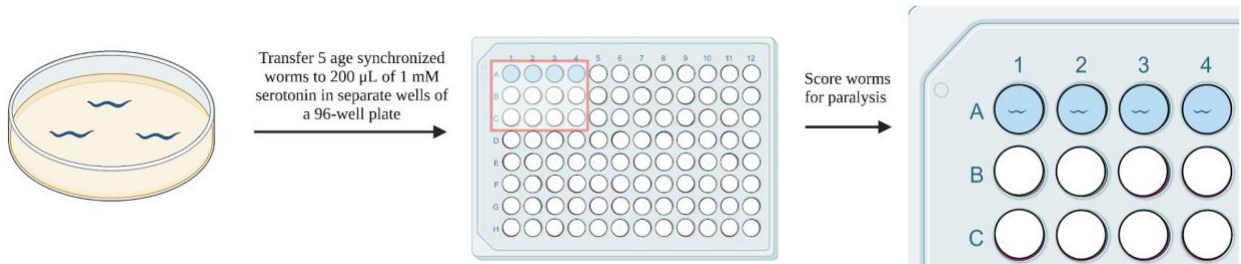


Figure 53: Serotonin assay.

3.2.4. Cold tolerance assay

Age-synchronized worms (25-100) worms were placed directly in a refrigerator at 4°C. The worms were left at 4°C for 24-36 hours. After this exposure to the cold temperature, the worms were removed from the refrigerator and allotted approximately 1 hour to equilibrate to room temperature. The worms were then assayed for viability by gently tapping each worm with a pick and observing movement or lack thereof^{6,7}. The cold tolerance assay is illustrated in Figure 54.

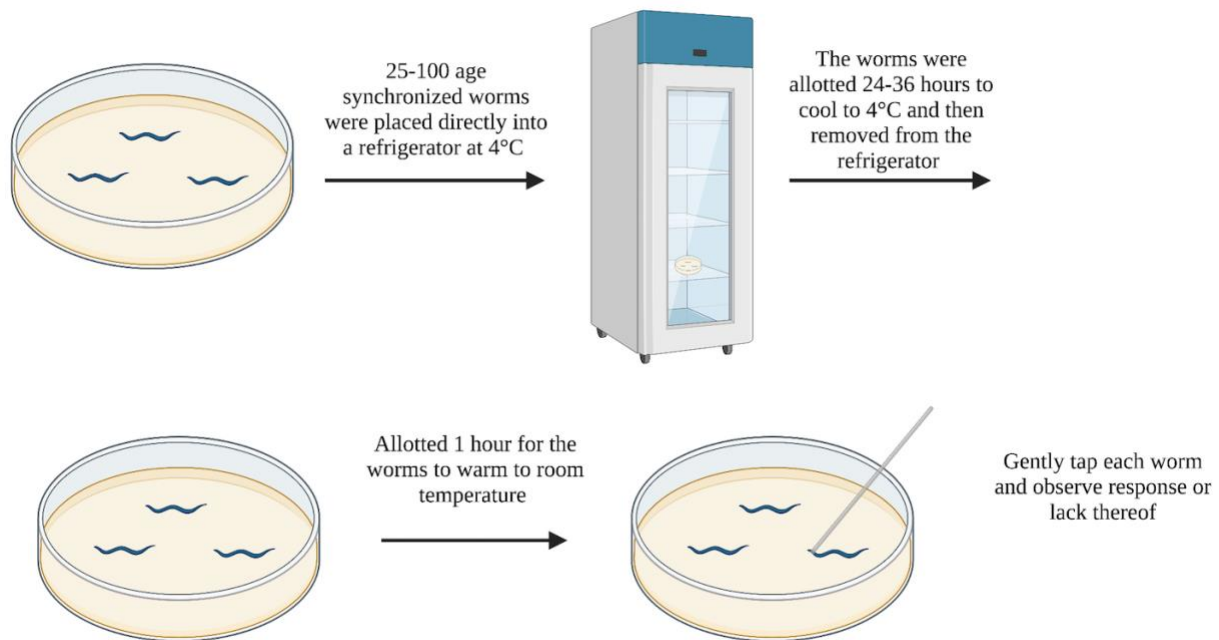


Figure 54: Cold tolerance.

3.3. Thrashing assay results

3.3.1. *C. elegans* fed PIMAX DH5 α *E. coli* producing human tau

To investigate the viability of a tau feeding model, an L4 age synchronized population of wildtype N2 worms were prepared. The age synchronized population was transferred to plates seeded with three different DH5 α bacteria: vector control (Jun/Fos), tau (Jun/Fos with tau), and p-tau (Jun/Fos with tau and kinase). Each age synched population was maintained by filtration.

Twenty worms from each population were placed in 10 μ L of s-basal on an NGM only plate, and their thrashing was recorded. The thrashing results of each population are illustrated in Figure 55.

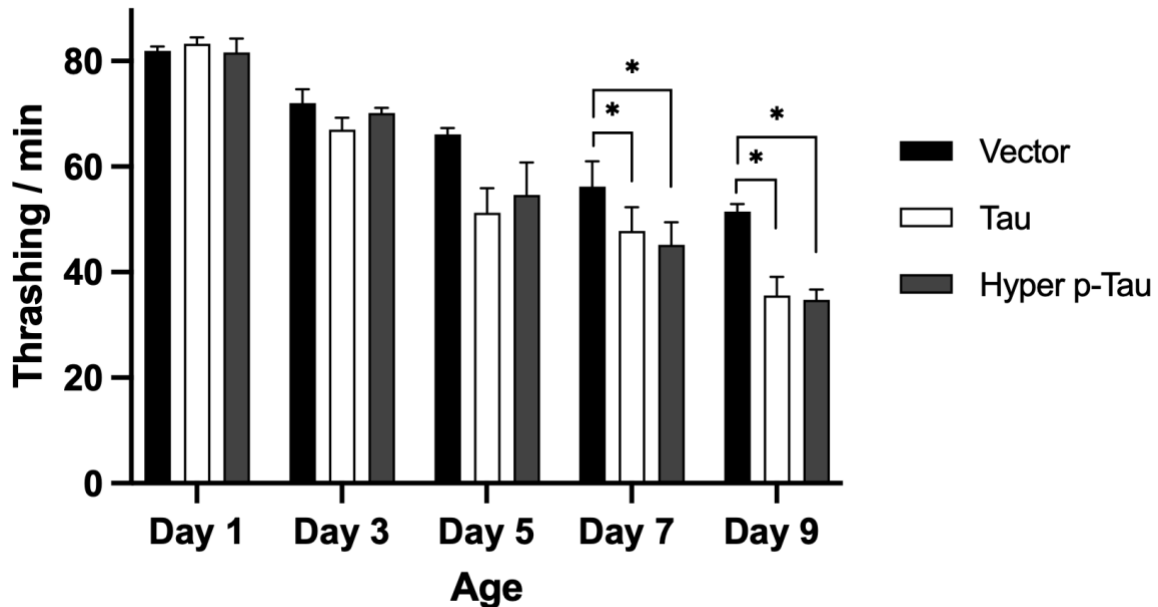


Figure 55: Quantified thrashing of N2 fed different PIMAX bacterial types.

Three trials of 20 worms each were performed for each strain at each time point. The average thrashing of the triplicate Error bars are standard error (SEM). Two-way analysis of variance (ANOVA) and Tukey's multiple comparison test was used to analyze the statistical significance of this results. (* $P < 0.05$, ** $P < 0.01$, *** $P < 0.001$, **** $P < 0.0001$).

Figure 55 suggests that there is a statistically significant difference between the vector and both the tau and p-tau populations starting at day 7 and continuing into day 9. The observed lack of thrashing may be due to a neurological disorder induced by the consumption of tau and p-tau from the bacteria. However, there is no evidence that simply consuming the tau and p-tau protein can lead to tau aggregation in the neurons. It is also possible that the observed effect is caused by accumulation of Jun/Fos dimer, tau, and p-tau throughout the body, which is not specific in the neurons. Further investigation is necessary to differentiate the most likely explanation for the observed changes. Additionally, there is no difference between the tau and p-tau populations at

any point in the lifespan of the worms. Hyperphosphorylated tau is thought to be the more toxic protein in several neurological disorders especially Alzheimer's disease. Therefore, the result showing that tau and p-tau are comparably toxic to *C. elegans* is surprising. A potentially confounding factor is that the tau bacteria expresses approximately twice as much tau protein as the p-tau bacteria. Therefore, the additional expression of tau in the "tau" bacteria must be accounted to reach accurate conclusions.

3.3.2. *C. elegans* feed PIMAX DH5 α *e. coli* producing human tau controlling for expression levels

To investigate if the observed lack of difference between tau and p-tau was due to the expression levels, the tau bacteria were diluted with vector bacteria in equal parts to attempt to mitigate the variable expression. An L4 age synchronized population of wildtype N2 worms were prepared. Plates of each bacteria type vector, tau, and p-tau were prepared in the same manner as before except that the "tau" population was diluted with equal parts of the vector to control for the increased expression of tau. The age synchronized population of worms was transferred to plates seeded with three different DH5 α bacteria namely, vector control (Jun/Fos), tau dilution (Jun/Fos with tau), and p-tau (Jun/Fos with tau and kinase). Each age synched population was maintained by filtration. Twenty worms of each population were placed in 10 μ L of s-basal on an NGM only plate, and their thrashing was recorded. The thrashing results of each population are illustrated in Figure 56.

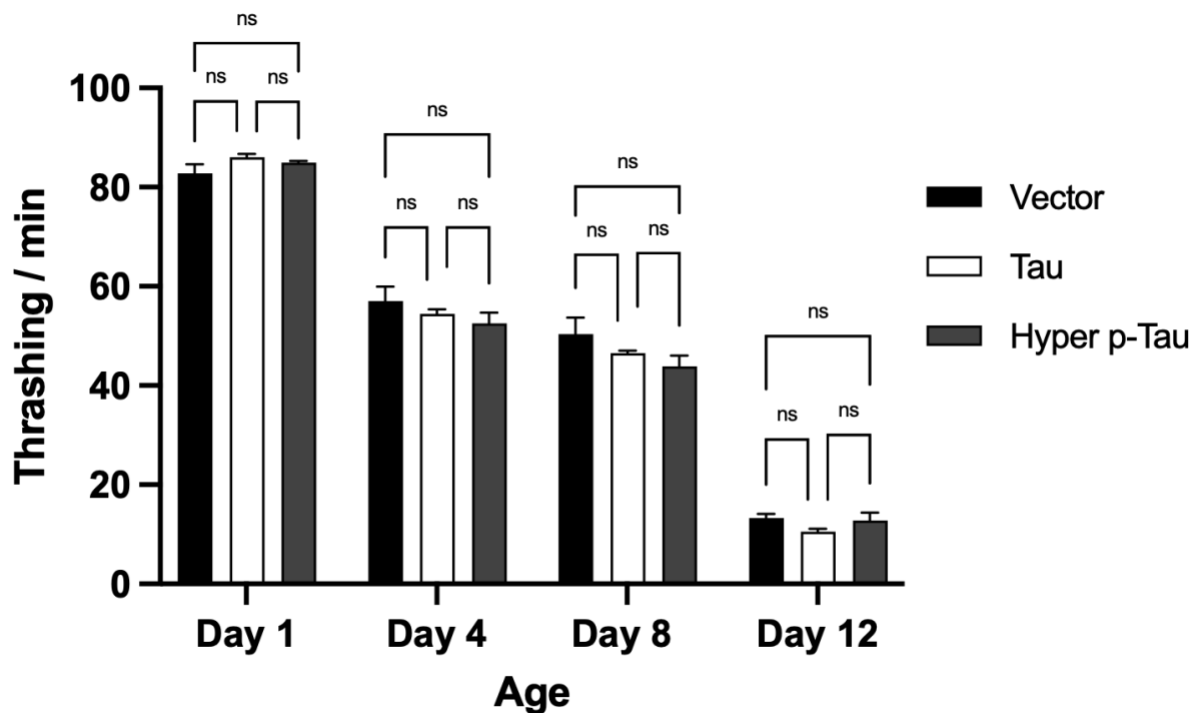


Figure 56: Quantified thrashing of N2 fed different PIMAX bacterial types controlling for expression levels.

Three trials of 20 worms each were performed for each strain at each time point. The average thrashing of the triplicate is reported. Error bars are standard error (SEM). Two-way analysis of variance (ANOVA) and Tukey's multiple comparison test was used to analyze the statistical significance of this results. (* $P < 0.05$, ** $P < 0.01$, *** $P < 0.001$, **** $P < 0.0001$).

Figure 56 shows that there is no statistically significant difference between any of the populations at the same age. There is an aging effect that seems to cause a decrease in total thrashing as the worms age. The observed decrease seen in Figure 56 is more drastic than that of wildtype worms feed the standard OP50 bacteria. Therefore, there seems to be some additional effect leading to the observed fitness phenotype observed by thrashing. One possible explanation is buildup of the protein dimer Jun/Fos, which is used in the PIMAX model to generate tau and hyperphosphorylated tau in the DH5 α bacteria. To investigate protein buildup was causing the lack of thrashing phenotype, another study with several control bacteria was performed. Specifically, OP50, DH5 α , vector, tau, and p-tau were used to control for two more factors. First, DH5 α without the Jun/Fos dimer is necessary to investigate the role of the Jun/Fos dimer on the

thrashing phenotype. Secondly, OP50 control is used as a secondary control to investigate the role of DH5 α on the thrashing phenotype. An L4 age synchronized population of wildtype N2 worms were generated. The age synchronized populations were transferred to separate plates seeded with OP50 and four different DH5 α bacteria namely, DH5 α only, vector control (Jun/Fos), tau (Jun/Fos with tau), and p-tau (Jun/Fos with tau and kinase). Each age synchronized population was maintained by filtration. Twenty worms of each population were placed in 10 μ L of s-basal on an NGM only plate, and their thrashing was recorded. The thrashing results of each population are illustrated in Figure 57.

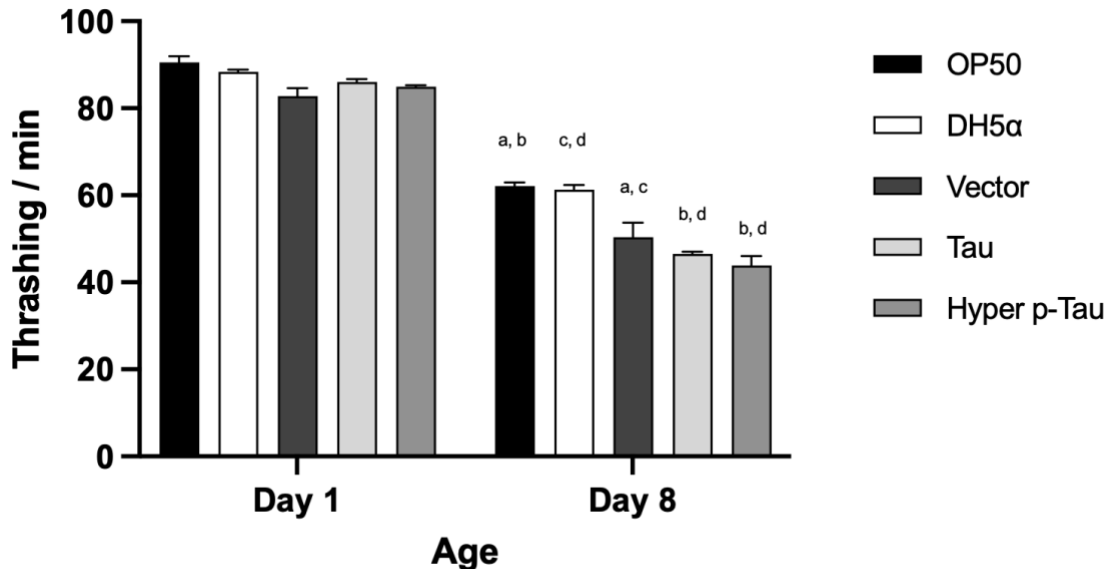


Figure 57: Quantified thrashing of N2 fed different PIMAX and control bacterial types. Three trials of 20 worms each were performed for each strain at each time point. The average thrashing for each group of 20 is reported for the individual value of that trial. Error bars are SEM. A 2-way ANOVA was used to analyze the statistical significance of this result. Groups marked with “a” are ***P < 0.001, with “b” are ****P < 0.0001, with “c” are ****P < 0.0001 and “d” are ****P < 0.0001.

Figure 57 illustrates minimal difference between any bacterial type in day 1. At day 8, the only significant differences are between all Jun/Fos producing bacteria (vector, tau, and hyper p-tau) and the two controls (OP50 and DH5 α). It is difficult to make any conclusions from day 1

thrashing data. However, some conclusions can be made from day 8 thrashing data. First, there is no difference between OP50 and DH5 α , which suggests that DH5 α is not responsible for the decreased thrashing. Additionally, there is a significant difference between worms fed DH5 α and each Jun/Fos bacteria, suggesting that the Jun/Fos dimer is responsible for the decreased thrashing. Furthermore, worms fed OP50 thrashed considerably more than each Jun/Fos producing bacteria (vector, tau, and hyper p-tau), which further suggests that the Jun/Fos dimer is responsible for the decreased thrashing. Lastly, there is not a significant difference between any of the Jun/Fos producing bacteria (vector, tau, and hyper p-tau) Therefore, all thrashing evidence suggests that the presence of the Jun/Fos dimer has a toxic effect on the worms' fitness, which does not appear to be exacerbated by the presence of tau or hyperphosphorylated tau.

3.4. Serotonin assay results

3.4.1. Introduction to the serotonin assay

Serotonin or 5-hydroxytryptamine (5-HT) is a monoamine neurotransmitter. Serotonin is biochemical derived from the amino acid tryptophan. The biological function of serotonin is multifaceted and not completely understood^{8,9}. However, many of the functions have been linked to the activation and inactivation of 5-HT receptors¹⁰. The 5-HT receptors are G protein-coupled receptor and ligand-gated ion channels found in the CNS. The serotonin receptors modulate the release of many neurotransmitters including glutamate^{10,11}. Therefore, serotonin exposure is linked to neurological function of many neuron types. Additionally, serotonin signaling pathways have been detected in *C. elegans*^{12,13}. Several behavioral phenotypes, such as locomotion, have been linked to 5-HT exposure. Furthermore, paralysis induced by serotonin exposure has been observed in many neurological disorder models in *C. elegans*¹⁴. It is thought that the observed paralysis is caused from overstimulation of 5-HT receptors, which causes

calcium influx into the neurons¹⁴. The paralysis occurs more quickly in organisms with unhealthy neurological function, as there is less biological machinery to handle the excessive serotonin exposure. Therefore, paralysis in response to 5-HT exposure can be used as an indication of neurological health.

3.4.2. Serotonin assay in *C. elegans* fed PIMAX DH5 α *E. coli* producing human tau

To further investigate the effects of feeding tau producing bacteria on the healthspan of the worms, the 5-HT assay was performed. The 5-HT assay provides information about the neural health of the worms that were exposed to 5-HT. Worms with healthy neurological function can be exposed to 5-HT for a short time (~10 minutes) without paralysis. However, worms with abnormal neurological function will become paralyzed during the 10-minute exposure. Therefore, the number of observed healthy worms after the 10-minute exposure are recorded.

To perform the 5-HT assay, an L4 age synchronized population of wildtype, N2, worms were prepared. Plates of each bacteria type vector, tau, and p-tau were prepared in the same manner as before except that the “tau” population was now diluted with equal parts of the vector in an attempt to control for the overexpression of the tau protein in “tau” bacterium. The age synchronized population was transferred to plates seeded with three different DH5 α bacteria: vector control (Jun/Fos), tau dilution (Jun/Fos with tau), and p-tau (Jun/Fos with tau and kinase). Each age synched population was maintained by filtration. Twenty worms of each population were placed 96-well plates containing 200 μ L of 1 mM 5-HT. Worms were exposed to the 5-HT for 10 minutes, and the number of moving worms were scored. The results of the 5-HT assay are shown in Figure 58.

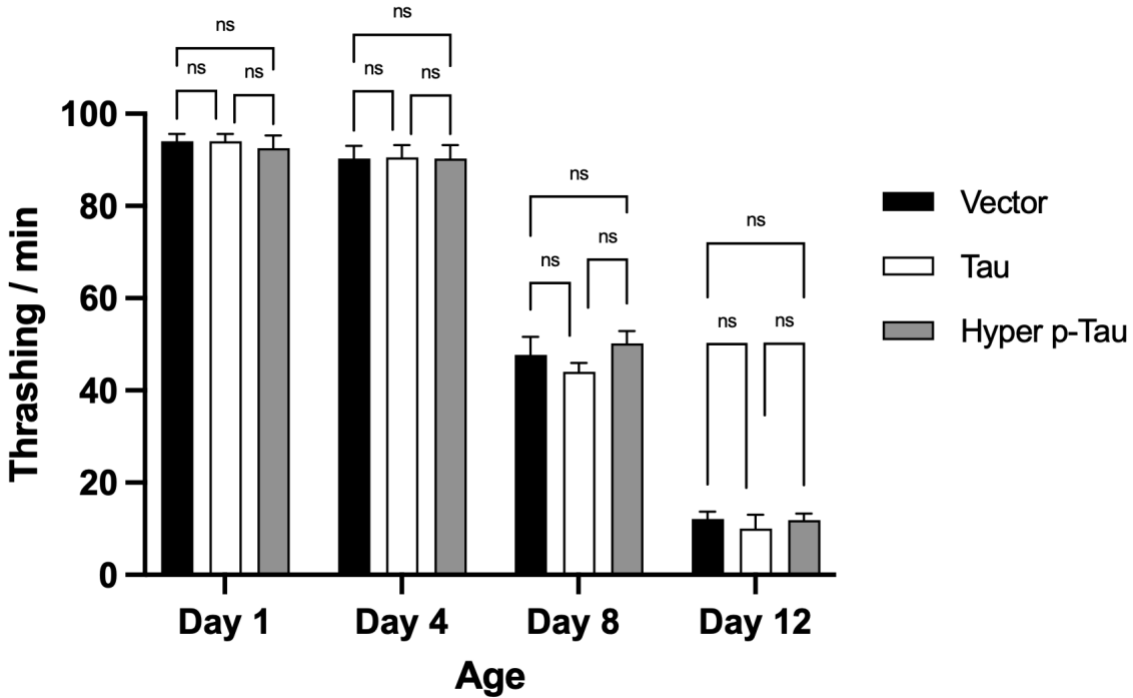


Figure 58: Quantified healthy N2 worms after 10-minute 5-HT exposure.

Three trials of 20 worms each were performed for each strain at each time point. The percent healthy for each group of 20 is reported for the individual value of that trial. Error bars are the SEM. A 2-way ANOVA was used to analyze the statistical significance of this result (* $P < 0.05$, ** $P < 0.01$, *** $P < 0.001$, **** $P < 0.0001$).

Figure 58 illustrates that there are no statistically significant differences present in any of the age synchronized populations. Therefore, feeding worms the Jun/Fos dimer, tau, and/or hyperphosphorylated does not affect the neurological health of the worms observed in the 5-HT assay. It is possible that the fed tau or hyperphosphorylated tau never enters the neurons of the worms, and therefore, neurological effects are not observed.

3.5. Cold tolerance assay results

3.5.1. Introduction to the cold tolerance assay

Wildtype *C. elegans* raised at 16°C can survive a sudden shift to a cold temperature of 4°C. Animals raised at 20-25°C cannot survive a similar sudden temperature change¹¹. A pair of neurons, ASJL and ASJR, have been identified as the primary temperature shock sensory neurons. When ASJL and ASJR are disrupted by laser ablation and genetic mutation, the ablated

or mutated worms survive the temperature shock more effectively¹⁵. Sensory neurons initiate a signaling cascade that leads to a change in the lipid profile in the intestines. Worms lacking functional ASJL and ASJR neurons retain a more cold-resistant profile¹⁶. Therefore, it is expected that worms with neurodegeneration will be more resistant to sudden temperature changes.

3.5.2. Cold Tolerance assay in *C. elegans* fed PIMAX DH5 α *E. coli* producing human tau

To further investigate the effects of feeding tau producing bacteria on the healthspan of the worms, a cold tolerance assay was performed. To perform the cold tolerance assay, an L4 age synchronized population of wildtype N2 worms were prepared. Plates of each bacteria type vector, tau, and p-tau were prepared in the same manner as before except that the “tau” population was now diluted with equal parts of the vector in an attempt to control for the overexpression of the tau protein in “tau” bacterium. The age synchronized population was transferred to plates seeded with three different DH5 α bacteria namely, vector control (Jun/Fos), tau dilution (Jun/Fos with tau), and p-tau (Jun/Fos with tau and kinase). Each age synched population was maintained by filtration. Approximately 50 worms were moved, while remaining on their agar plate, from 25°C to 4°C and left in 4°C for 24 hours. The worms were then placed back in 25°C for 1 hour. The population was then scored for viability. The results of the cold tolerance assay are shown in Figure 59.

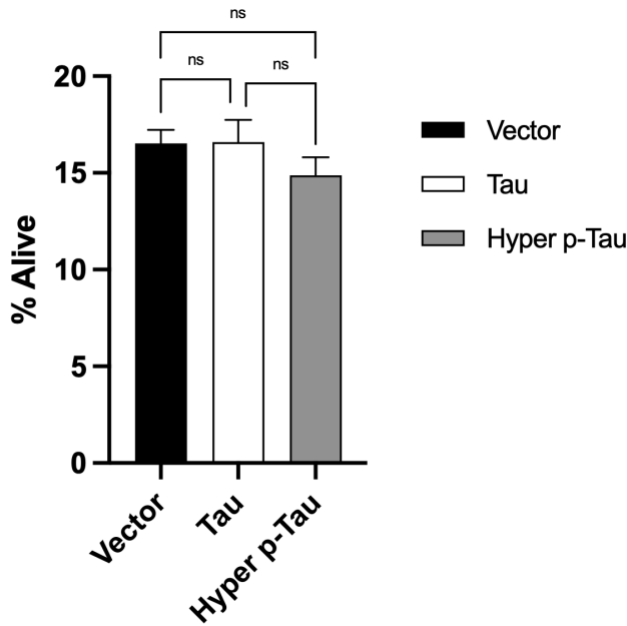


Figure 59: Quantified alive N2 worms after exposure to 4°C.

Three trials of 50 worms each were performed for each strain at each time point. The percent alive for each group of 50 is reported for the individual value of that trial. Error bars are the SEM. A 2-way ANOVA was used to analyze the statistical significance of this result (* $P < 0.05$, ** $P < 0.01$, *** $P < 0.001$, **** $P < 0.0001$).

Figure 59 illustrates that there is no statistically significant difference between any of the different bacterial types. Therefore, feeding worms the Jun/Fos dimer, tau, and/or hyperphosphorylated tau does not affect the neurological health of the worms as observed in the cold tolerance assay. It is possible that the fed tau or hyperphosphorylated tau never enters the neurons of the worms or even the worms in general, and therefore, neurological effects are not observed.

3.6. Discussion of the PIMAX feeding model

3.6.1. Physical fitness effects

Figure 55 shows that there is a statistically significant difference between the vector and tau, vector, and p-tau, but not between tau and p-tau. The differences between vector, tau and p-tau were promising, as it suggests that the feeding model producing a lack of fitness phenotype that can be observed in thrashing. However, the lack of difference between tau and p-tau was

surprising because mammalian models have shown that hyperphosphorylated tau has been more convincingly linked to AD pathology. Therefore, further investigation and discussion with our collaborator in the Kuo lab was prompted. It was suggested that the “tau” bacteria produced approximately twice as much tau as the hyperphosphorylated “p-tau” bacteria. To investigate if the lack of difference between “tau” and “p-tau” bacteria was due to the difference in expression, and the experiment was repeated by diluting the “tau” bacteria with equal parts of the vector to attempt to control for the expression levels. Figure 56 shows no statistically significant difference between any groups, which questions the results of the first bacteria feeding study. It is possible that the difference observed in the thrashing assay without dilution was an anomaly as the level of confidence in the difference is rather weak. However, Figure 56 suggests that there is some level of toxicity in the worms feed the Jun/Fos dimer bacteria alone. The toxicity is especially present at day 12 where the worms have considerably less thrashing compared to wildtype worms of the same age. Therefore, the observed toxicity prompted us to conduct another study to investigate several other controls namely, OP50 (normal *C. elegans* food in lab) and DH5 α (the strain of *E. coli*. used to generate the tau and p-tau producing bacteria). Investigation of OP50 and DH5 α in parallel with vector, tau, and p-tau shed light on the effects of Jun/Fos on the fitness of the worms. Figure 57 shows a difference between OP50 and all Jun/Fos dimer bacteria and DH5 α and all Jun/Fos dimer bacteria. However, it does not show any significant differences between Jun/Fos dimers themselves nor between OP50 and DH5 α . Therefore, the most likely explanation for the difference observed between OP50, DH5 α , and the Jun/Fos dimer bacteria is due to accumulation of the Jun/Fos and possible tau and p-tau in the body of the worms. While this is interesting, it is not useful to study neurological disorders, but it can be used to model disease in which protein accumulation is a large part of the pathology.

3.6.2. Neurological effects

Figure 58 shows no statistically significant difference between any of the different populations. Therefore, neurological effects due to feeding tau and p-tau could not be observed using the 5-HT assay. Additionally, Figure 59 shows no statistically significant difference between any populations tested. The lack of difference suggest further that the neurological health of the worms feed the different bacterial types was not affected in a significant way. Therefore, this specific feeding model cannot mimic aspects of AD as initially intended.

3.6.3. Model limitations

The primary limitation of the model is that tau and especially p-tau builds up in the neurons of patients diagnosed with AD. However, the feeding model would only simulate AD if the feeding tau and p-tau can migrate to the neurons after consumption. The lack of neurological phenotypes observed in 5-HT and cold tolerance assays suggests that tau and p-tau do not end up in the neurons or are not uptaken at all. Therefore, the model cannot be used to study AD as initially intended. However, if a method can be developed to migrate the tau and p-tau directly to the neurons, the model may have value. Without further development, the model is insufficient as an AD model.

3.6.4. Future directions

Figure 57 suggests that consumption of the Jun/Fos dimer has a negative effect on the overall fitness of the worms observed in a lack of thrashing phenotype. The most likely explanation for the lack of thrashing is from protein accumulation of Jun/Fos and potentially tau and p-tau in the worms after consumption of the bacteria. Therefore, the model can be used to investigate certain aspects of disease that have significant protein aggregation as a part of the disease pathology like certain myopathies. Additionally, further investigation into an alternative

delivery may be fruitful. If the delivery system can lead to accumulation of tau and p-tau in the neurons, specific aspects of AD can be directly mimicked.

REFERENCES

REFERENCES

- (1) Sui, D.; Xu, X.; Ye, X.; Liu, M.; Mianecky, M.; Rattanasinchai, C.; Buehl, C.; Deng, X.; Kuo, M.-H. *Mol. Cell. Proteomics* **2015**, *14* (1), 251–262.
- (2) Sengoku, R. *Neuropathology* **2020**, *40* (1), 22–29.
- (3) Cesaratto, F.; Burrone, O. R.; Petris, G. *J. Biotechnol.* **2016**, *231*, 239–249.
- (4) Reverse genetics
http://www.wormbook.org/chapters/www_introreversegenetics/introreversegenetics.html,
accessed Feb. 20, 2022.
- (5) Law, W.; Wuescher, L. M.; Ortega, A.; Hapiak, V. M.; Komuniecki, P. R.; Komuniecki, R. *PLoS Pathog.* **2015**, *11* (4).
- (6) Okahata, M.; Ohta, A.; Mizutani, H.; Minakuchi, Y.; Toyoda, A.; Kuhara, A. *Natural J. Comp. Physiol. B* **2016**, *186* (8), 985–998.
- (7) Dosanjh, L. E.; Brown, M. K.; Rao, G.; Link, C. D.; Luo, Y. *J. Alzheimers. Dis.* **2010**, *19* (2), 681–690.
- (8) Mohammad-Zadeh, L. F.; Moses, L.; Gwaltney-Brant, S. M. Serotonin: A Review. *J. Vet. Pharmacol. Ther.* **2008**, *31* (3), 187–199.
- (9) Lv, J.; Liu, F. *Front. Cell. Neurosci.* **2017**, *11*, 74.
- (10) Barnes, N. M.; Neumaier, J. F. *Tocris Biosci Sci Rev Ser* **2011**, *34*, 1–16.
- (11) Stiedl, O.; Pappa, E.; Konradsson-Geuken, Å.; Ögren, S. O. *Front. Pharmacol.* **2015**, *6*, 162.
- (12) Murakami, H.; Bessinger, K.; Hellmann, J.; Murakami, S. *Neurobiol. Aging* **2008**, *29* (7), 1093–1100.
- (13) Murakami, H.; Murakami, S. *Aging Cell* **2007**, *6* (4), 483–488.
- (14) Wu, Y.; Wu, Z.; Butko, P.; Christen, Y.; Lambert, M. P.; Klein, W. L.; Link, C. D.; Luo, Y. *J. Neurosci.* **2006**, *26* (50), 13102–13113.
- (15) Ash, P. E. A.; Zhang, Y.-J.; Roberts, C. M.; Saldi, T.; Hutter, H.; Buratti, E.; Petrucelli, L.; Link, C. D. *Hum. Mol. Genet.* **2010**, *19* (16), 3206–3218.
- (16) Dosanjh, L. E.; Brown, M. K.; Rao, G.; Link, C. D.; Luo, Y. *J. Alzheimers. Dis.* **2010**, *19* (2), 681–690.

CHAPTER FOUR:

INVESTIGATION OF ULTRASOUND AS TRAUMATIC BRAIN INJURY MODEL IN

C. ELEGANS

4. ULTRASOUND EXPOSURE TBI MODEL

4.1. Introduction to traumatic brain injury (TBI)

4.1.1. General TBI relevance in humans and tauopathy

Traumatic brain injury (TBI) has been suggested as a risk factor for tauopathies by triggering disease onset and facilitating its progression¹. Approximately 10 million TBI cases are reported worldwide each year^{2,3}. A moderate to severe TBI will produce systemic complications and can create long-term adverse effects^{4,5}. The primary injury can trigger alterations in the brain that result in molecular and cellular deviations, which disrupt the overall CNS environment^{6,7}. For example, phosphorylated tau and NFTs can be detected as early as 6 hours after the initial brain injury⁸. Additionally, TBI severity has been closely linked to the risk of AD^{3,7}. One possible explanation for the link is due to an increase of phosphorylated tau and NFT accumulation post injury⁸. Therefore, the normal function of tau is disrupted in response to TBI and can be investigated further to provide some insight of TBI and AD pathology.

4.1.2. *C. elegans* tauopathy model

To investigate *C. elegans* as a viable AD model, researchers have developed a transgenic worm that expresses human tau. The transgenic *C. elegans* contain the molecular machinery to produce human tau *in vivo*. The first such model was based on the overexpression of human 1N4R tau pan-neuronally through the *Paex-3* promoter^{9,10}. The mutant worms show reduced survival, reduced thrashing rate, and they accumulate detergent-insoluble tau¹⁰. TBI disrupts the normal function of tau in humans, as increased phosphorylated tau and NFTs are observed in

TBI patients⁸. Therefore, one can expose the transgenic *C. elegans* to a TBI event and monitor any phenotypes related to tau such as survival and thrashing.

4.1.3. Ultrasound as a TBI model in *C. elegans*

Ultrasound exposure to *C. elegans* has been investigated in recent years to understand any bioeffects that may be observed because of the exposure¹¹. One such method used includes surface acoustic wave (SAW) ultrasound irradiation to investigate TBI in *C. elegans*¹². Using this method the researchers found a significant reduction in mobility of the worms¹². The lack of movement phenotype can be tracked to follow the progression of TBI symptoms in the worms. Additionally, another model investigated the effects of medical grade ultrasound exposure on *C. elegans* lifespan and healthspan¹³. The researchers found that worms exposed to the intense ultrasound had reduced lifespans, thrashing, and locomotion¹³. The two models suggest that ultrasound exposure affects the worms in significant and measurable ways. Therefore, if the observed effects mimic TBI events, then ultrasound exposure to transgenic human tau producing *C. elegans* can provide insight into the pathology of TBI.

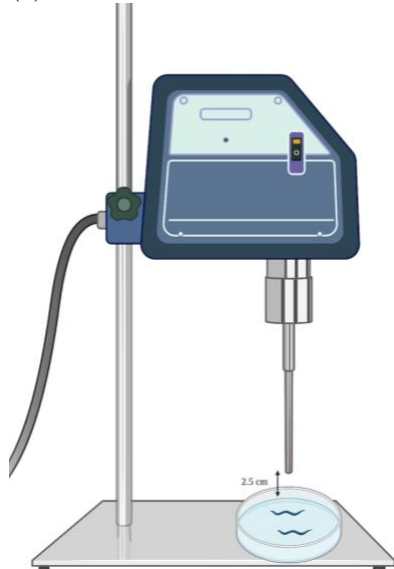
4.2. Thrashing Results after ultrasound exposure through 2.5 cm gap

4.2.1. Model description

Age synchronized worms were transferred to a 50 mm plate filled with s-basal medium. Using a 4710 series ultrasonic homogenizer, the worms in this petri dish were exposed to 1-MHz ultrasound for 15 minutes at 50% duty with a pulse frequency of 100 Hz. The ultrasonic conditions have been used previously to induce mild TBI symptoms in *C. elegans*¹³. The ultrasound finger was placed 2.5 cm away from the surface of the s-basal solution. Sham worms were moved to the s-basal for the same 15-minute duration, but the sham worms were not

exposed to ultrasound^{19,20}. The process of ultrasound exposure is illustrated in Figure 60. All worms were maintained on NGM plates with OP50.

(a)



(b)

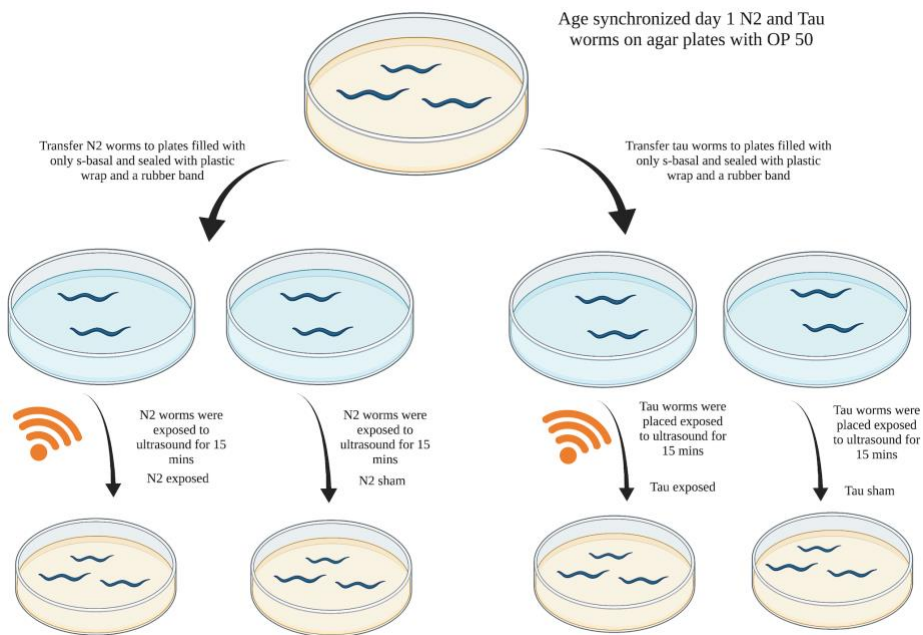


Figure 60: Ultrasound exposure model through a 2.5 cm space.

(a) Image of the experimental apparatus illustrating the 2.5 cm space between the worms in buffer and the ultrasound finger. (b) Details illustrating appropriate separation and ultrasound exposure time for sham and exposure groups.

4.2.2. Thrashing results

To investigate the ultrasound model, worms were assayed for thrashing after exposure to ultrasound. To perform the assay, an L4 age synchronized population of wildtype, N2, and tau worms (*aex-3::tau*) were prepared. The “exposed group” age synchronized population were transferred to plates full of 10 ml of s-basal medium and exposed to ultrasound for 15 minutes. The “sham” group age synchronized population were transferred to plates full of s-basal medium for 15 minutes without exposure to ultrasound to control for any effects from the buffer. Both populations, “sham” and “exposed” of each strain, were then transferred to standard NGM plates seeded with bacteria. Each age synched population was maintained by filtration. Twenty worms of each population were placed in 10 μ L of s-basal medium on an NGM only plate, and their thrashing was recorded. The thrashing results of each population are illustrated in Figure 61.

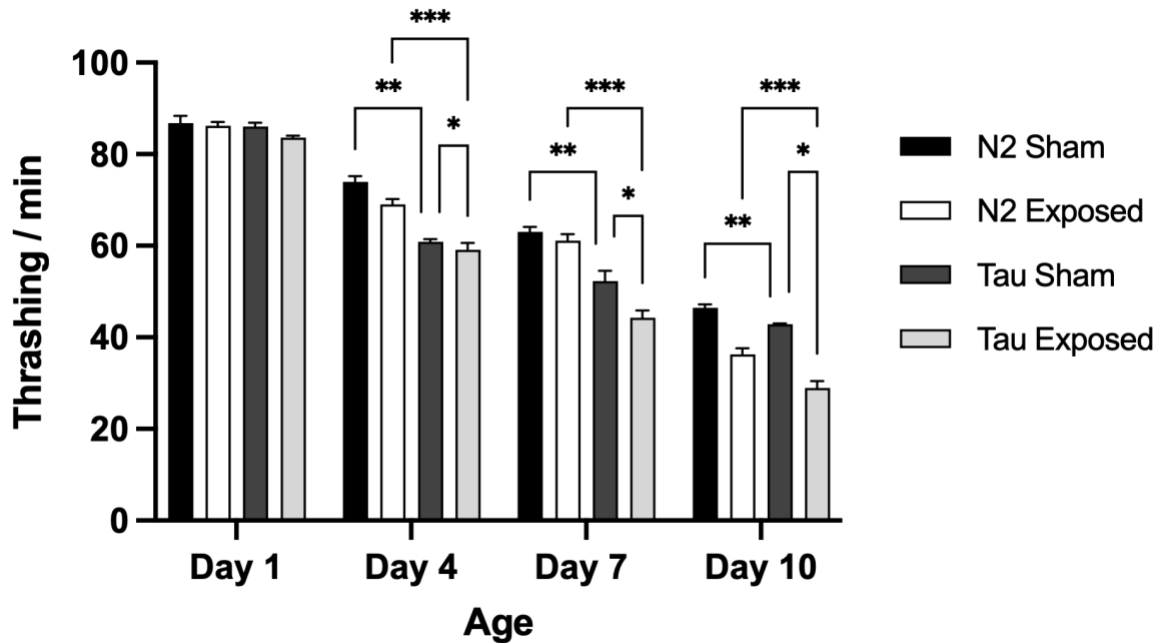


Figure 61: Quantified thrashing of N2 and *aex-3::tau* (Tau) with and without exposure to ultrasound.

Three trials of 20 worms each were performed for each strain at each time point. The average thrashing from each group of 20 is reported for the individual value of that trial. Error bars are the SEM. A 2-way ANOVA was used to analyze the statistical significance of this result (* $P < 0.05$, ** $P < 0.01$, *** $P < 0.001$, **** $P < 0.0001$).

Figure 61 illustrates that there is no statistically significant difference between any population at day 1. However, statistically significant differences are observed later in life, therefore aging may play a role. Additionally, there is no statistically significant difference between N2 sham and N2 exposed until day 10, which further suggests a relationship between aging and the TBI (ultrasound) effect. Furthermore, there are differences between the N2 and tau groups starting at day 4, which continue throughout the lifespan. The decreased fitness of the tau worms (*eat-4::GFP; aex-3::tau*) compared to control (*eat-4::GFP*), as observed in thrashing, is expected and discussed in more detail in chapter 2. However, there is a significant difference between tau sham and tau exposed starting at day 7 and continued in day 10. The presence of tau exacerbates the effect of ultrasound exposure, which suggests some potential interaction between the exposure and tau. The interaction between ultrasound exposure and tau is consistent with the observed effects seen in humans who have experienced traumatic brain injury as described in section 4.1. Therefore, the observed interaction provides more justification for the use of the *C. elegans* model for investigation of TBI.

4.3. Thrashing results in solution

4.3.1. Model description

Age synchronized worms were transferred with s-basal medium to a 14 mL polystyrene test tube. After approximately five minutes, the ultrasound finger was placed directly into the liquid. The five-minute waiting period allows for the worms to fall to the bottom of the test tube so the finger will more homogeneously expose the worms to the ultrasonic waves. Separate populations of worms were exposed to ultrasound for a distinct time, ranging from 1 to 6 seconds^{19,20}. The process of ultrasound exposure through the solution is illustrated in Figure 62. All worms were maintained on NGM plates with OP50.

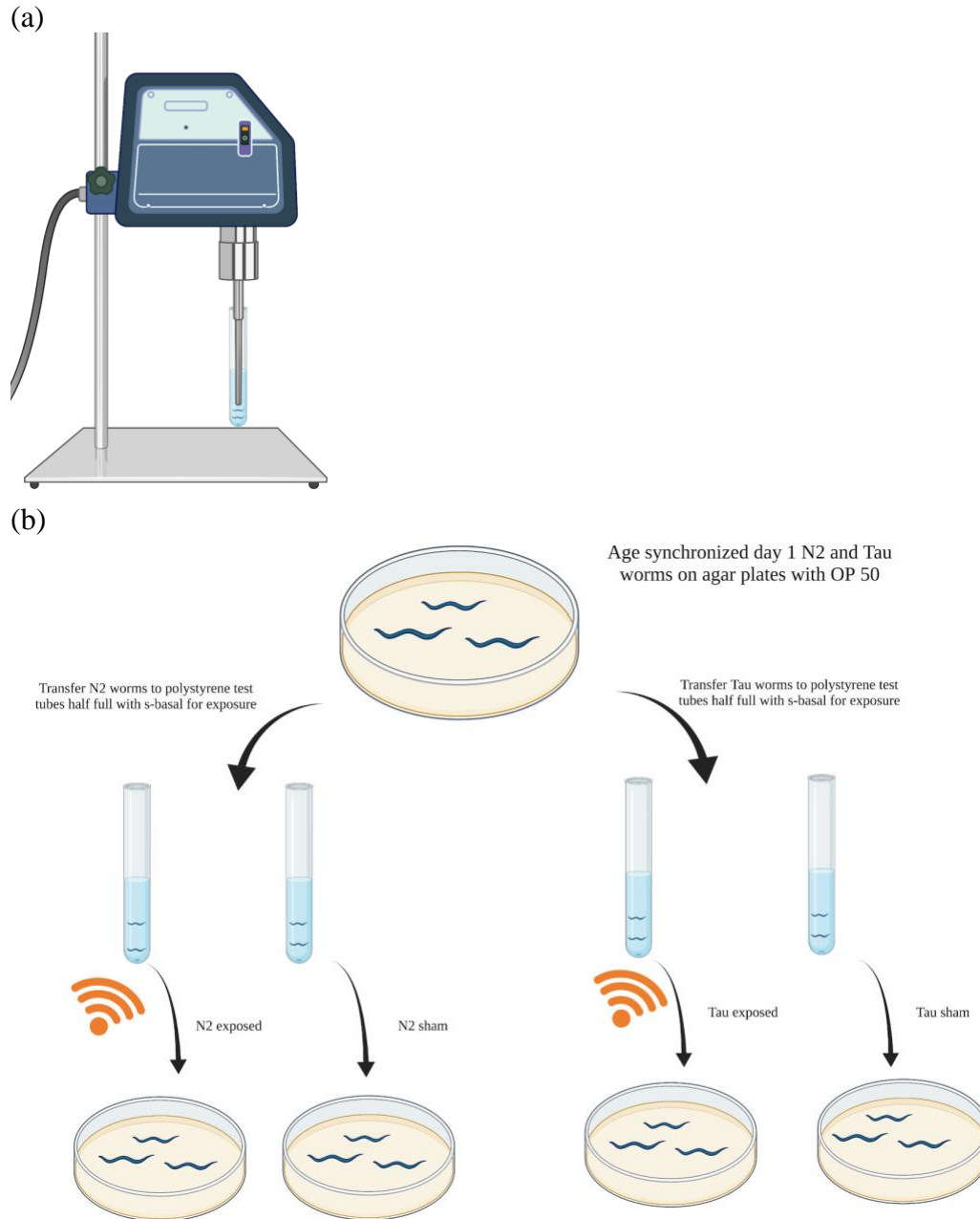


Figure 62: Ultrasound exposure directly in the buffer solution.

(a) Image of the experimental apparatus illustrating the 2.5 cm space between the worms in buffer and the ultrasound finger. (b) Details illustrating appropriate separation and ultrasound exposure time for sham and exposure groups.

4.3.2. Optimization of exposure time results

To further investigate the ultrasound TBI model, the apparatus was changed from the through space model described in 4.3.1. to direct ultrasound exposure in the buffer. Placing the

ultrasound finger directly in the buffer will greatly increase the exposure of ultrasound that the worms in the buffer are experiencing. Therefore, more severe TBI is expected, which can be tracked in the thrashing phenotype. To perform the exposure optimization thrashing assay, an L4 age synchronized population of wildtype, N2, and tau worms (*aex-3::tau*) were prepared. The “exposed” group age synchronized population were transferred to polystyrene test tubes with 7 mL s-basal and exposed to ultrasound using a 4710 series ultrasonic homogenizer programmed to 1-MHz ultrasound for varying durations between 1-6 seconds at 50 % duty with a pulse frequency of 100 Hz. Both populations were then transferred to standard NGM plates seeded with bacteria. Twenty worms of each population were placed in 10 μ L of s-basal on an NGM only plate, and their thrashing was recorded. The thrashing results of each population are illustrated in Figure 63.

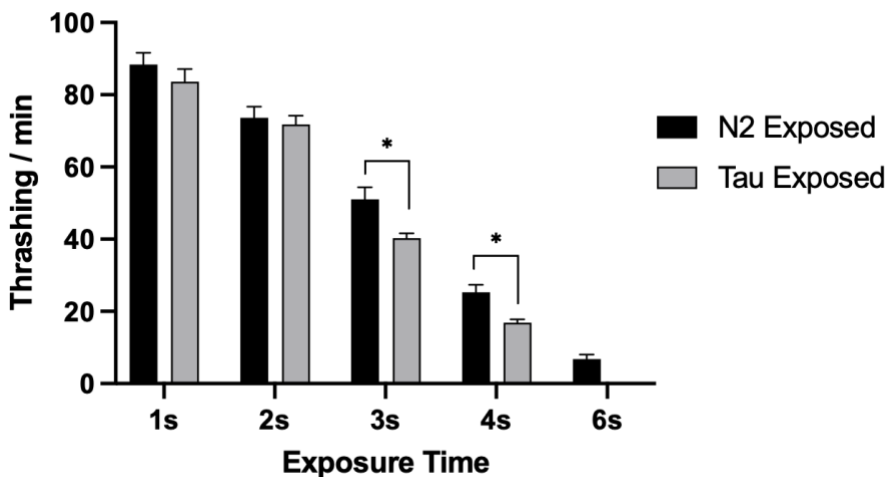


Figure 63: Quantified thrashing of N2 and *aex-3::tau* (Tau) exposed to varying duration of ultrasound.

One trial of ~50 worms each were used for each exposure duration and strain. Error bars are standard deviation. A Student’s t-Test was performed to analyze statistical significance. (* $P < 0.05$, ** $P < 0.01$, *** $P < 0.001$, **** $P < 0.0001$).

Figure 63 illustrates that 3 s and 4 s exposure leads to a difference between N2 exposed group and the tau exposed group. It is important to mention that Figure 63 only shows the results of one

trial of fifty worms. However, even with one trial of ~50 worms, a statistically significant difference was observed, and because of this, 3 s was selected as the optimized exposure time for the ultrasound model with the ultrasound finger placed directly in the buffer solution.

4.3.3. Thrashing results in solution

To investigate the optimized exposure ultrasound model, worms were assayed for thrashing after exposure to ultrasound. To perform the assay, an L4 age synchronized population of wildtype N2 and tau worms (*aex-3::tau*) were prepared. The “exposed” age synchronized population were transferred to polystyrene test tubes with 7 ml s-basal and exposed to ultrasound using a 4710 series ultrasonic homogenizer programmed to 1-MHz ultrasound for 3 seconds at 50% duty with a pulse frequency of 100 Hz. The “sham” age synchronized population were transferred to polystyrene test tubes with 7 ml of s-basal for 2-3 minutes to control for any effects from the buffer. Both populations, “sham” and “exposed” of each strain, were then transferred to standard NGM plates seeded with bacteria. Each age synched population was maintained by filtration. Twenty worms of each population were placed in 10 μ L of s-basal on an NGM only plate, and their thrashing was recorded. The thrashing results of each population are illustrated in Figure 64.

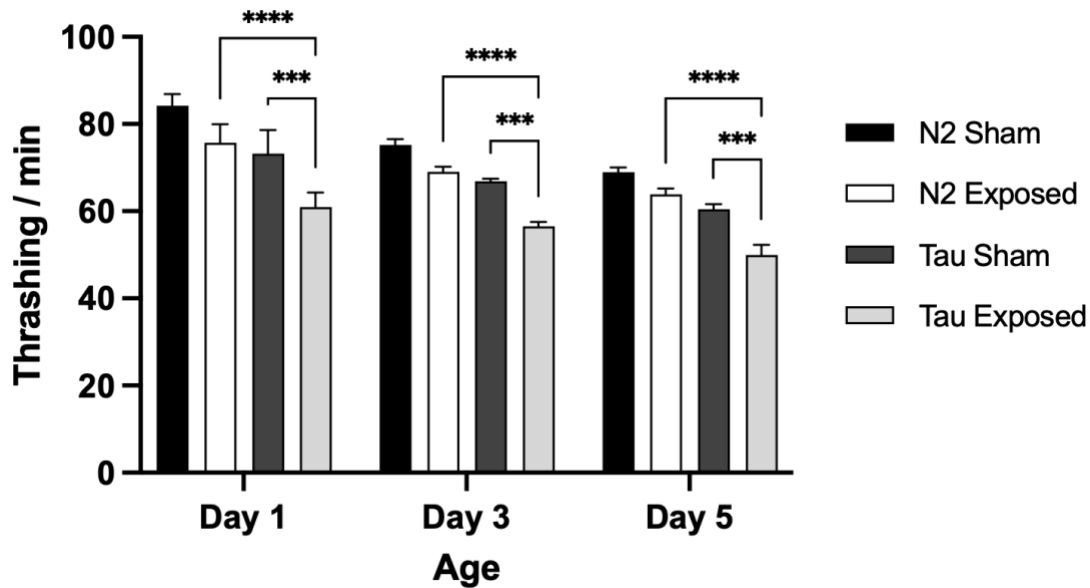


Figure 64: Quantified thrashing of N2 and *aex-3::tau* (Tau) with and without exposure to 3 seconds of ultrasound.

Three trials of 20 worms each were performed for each strain at each time point. The average thrashing from each group of 20 is reported for the individual value of that trial. Error bars are the SEM. A 2-way ANOVA was used to analyze the statistical significance of this result (* $P < 0.05$, ** $P < 0.01$, *** $P < 0.001$, **** $P < 0.0001$).

Figure 64 illustrates that there is a statistically significant difference between the N2 and tau strains exposed to ultrasound waves. Therefore, the presence of tau exacerbates the thrashing defects after ultrasound exposure, which is consistent with what is observed in mammalian models. Additionally, there is a statistically significant difference between the tau sham and tau strain exposed to ultrasound waves, which further suggests that tau exacerbates the lack of thrashing caused by ultrasound exposure. Furthermore, there is not a statistically significant difference between N2 sham and N2 worms exposed to ultrasound waves suggesting that ultrasound exposure alone is insufficient to induce a TBI like state in the wildtype worms. However, in the presence of tau, the ultrasound exposure is sufficient to observe a phenotype. Lastly, there is a statistically significant difference between N2 and tau (*aex-3::tau*) as expected and discussed in more detail in chapter 2.

4.4. Discussion of TBI ultrasound model

4.4.1. Physical fitness effects

Figure 61 illustrates that there is a significant difference between tau sham and tau strain exposed to ultrasound starting at day 7, which suggests that the ultrasound exposure effects, which simulate TBI, are exacerbated by the presence of tau. Additionally, there is a statistically significant difference between N2 sham and N2 worms exposed to ultrasound starting at day 10, which suggests that the ultrasound exposure effects are related or in addition to aging effects. Because the ultrasound effects took several days to present when a 2.5 cm gap was used between the ultrasound finger and the worms, the ultrasound exposure apparatus was modified to investigate if more intense exposure would lead to a more severe and/or earlier phenotype.

Figure 64 illustrates that there are statistically significant differences between tau sham and the tau worms exposed to ultrasound starting at day 1 and continuing through the lifespan of each population. Additionally, there is a significant difference between N2 exposed and tau worms exposed to ultrasound starting at day 1 and continuing throughout the lifespan. Therefore, the presence of tau seems to exacerbate the effect from ultrasound exposure. The effect is in addition to the expected aging effects which is also observed when one compares the older N2 populations to the younger N2 populations. The fitness evidence, taken holistically, suggests that the tau animal model expresses a specific lack of fitness phenotype observed in thrashing when exposed to ultrasound. The ultrasound model provides a method for one to investigate the role that tau plays in TBI as modeled by ultrasound exposure.

4.4.2. Model limitations

The model takes advantage of an ultrasonic finger as the source of ultrasound exposure to the worms. In both apparatuses, ultrasound exposure is not completely consistent because the

worms are not placed in the exact same region of the buffer. Therefore, the ultrasound intensity experienced by each worm will vary slightly as the intensity of the wave dissipates as it travels through the buffer. However, a more consistent exposure is present in the second apparatus in which the ultrasound finger is placed directly in the buffer solution. Additionally, commonly TBI in humans is observed in professional athletes who play sports that involve repeated head trauma, like American football. The model proposed here exposes the worms to one TBI event early in their lifespan and monitors the effect as the worms age. Therefore, another model could expose the worms to ultrasound every day or few days in their lifespan to better mimic the consistent exposure to head trauma experienced by athletes in high contact sports.

4.4.3. Future directions

One possible future direction is using the same exposure model, but instead of one exposure event, perform a series of TBI events throughout the lifespan of the worm. Therefore, one can better mimic the TBI as experienced by athletes. Furthermore, the model only investigated the physical fitness of the worms observed by thrashing. It would be interesting to investigate the neurological effects as well. For example, one can investigate neurological health by serotonin assay, cold tolerance, and GFP neural health assays as described in chapter 2. Additionally, it has been demonstrated that mechanical stress can induce detectable neurodegeneration¹⁴. The neurodegeneration was induced by mechanical stress through systematic exposure to mechanical stress by a Precellys Evolution homogenizer, which shakes biological samples violently usually to lyse the sample. The settings were optimized to induce trauma without completely lysing the worms. The mechanical stress lead to detectable loss of dopaminergic neurons as detected by loss of dopaminergic GFP in the *dat-1::GFP* strain¹⁴. Additionally, the neurodegeneration of dopaminergic, GABAergic, glutamatergic, serotonergic,

and cholinergic neurons induced by mechanical stress was further characterized by GFP retention of each tagged neuron measured by large-particle flow cytometry¹⁵. Dopaminergic neurons were the only class that showed significant neurodegeneration as measured by loss of GFP¹⁵. Therefore, one explanation for the fitness defects, as measured by decreased thrashing, induced by ultrasound exposure may be neurodegeneration of dopaminergic neurons. To investigate the role of dopaminergic neurons, the neural health after ultrasound exposure by measuring GFP of *dat-1::GFP* strain, which express GFP in dopaminergic neurons, can be explicitly studied using the fluorescent microscopy methods described in section 2.2.10. Additionally, the *aex-3::tau* worms can be treated with the mechanical stress model to investigate the role of tau in the pathology of the trauma as it has been suggested by recent literature¹. Further characterization of the model can uncover mechanistic information responsible for the lack of fitness observed in thrashing.

REFERENCES

REFERENCES

- (1) Edwards, G., 3rd; Zhao, J.; Dash, P. K.; Soto, C.; Moreno-Gonzalez, I. *J. Neurotrauma* **2020**, *37* (1), 80–92.
- (2) Control, U. S. D. of H. & H. S. C. F. D. (cdc); N. C. F. I. P. A.; US Department of Health & Human Services; Centers for Disease Control (CDC); National Center for Injury Prevention and Control *PsycEXTRA Dataset*. 2003. <https://doi.org/10.1037/e371602004-001>.
- (3) Masel, B. E.; DeWitt, D. S. *J. Neurotrauma* **2010**, *27* (8), 1529–1540.
- (4) Blennow, K.; Brody, D. L.; Kochanek, P. M.; Levin, H.; McKee, A.; Ribbers, G. M.; Yaffe, K.; Zetterberg, H.. *Nat Rev Dis Primers* **2016**, *2*, 16084.
- (5) Walker, K. R.; Tesco, G. *Front. Aging Neurosci.* **2013**, *5*, 29.
- (6) Blennow, K.; Hardy, J.; Zetterberg, H. *Neuron* **2012**, *76* (5), 886–899.
- (7) Edwards, G., 3rd; Moreno-Gonzalez, I.; Soto, C. *Biochem. Biophys. Res. Commun.* **2017**, *483* (4), 1137–1142.
- (8) Smith, D. H.; Uryu, K.; Saatman, K. E.; Trojanowski, J. Q.; McIntosh, T. K. *Neuromolecular Med.* **2003**, *4* (1-2), 59–72.
- (9) Pir, G. J.; Choudhary, B.; Mandelkow, E. *FASEB J.* **2017**, *31* (12), 5137–5148.
- (10) Kraemer, B. C.; Zhang, B.; Leverenz, J. B.; Thomas, J. H.; Trojanowski, J. Q.; Schellenberg, G. D. *Proc. Natl. Acad. Sci. U. S. A.* **2003**, *100* (17), 9980–9985.
- (11) Zulazmi, N. A.; Arulsamy, A.; Ali, I.; Zainal Abidin, S. A.; Othman, I.; Shaikh, M. F. *CNS Neurosci. Ther.* **2021**, *27* (4), 381–402.
- (12) Miansari, M.; Mehta, M. D.; Schilling, J. M.; Kurashina, Y.; Patel, H. H.; Friend, J.. *Sci. Rep.* **2019**, *9* (1), 12775.
- (13) Steele, L. M.; Kotsch, T. J.; Legge, C. A.; Smith, D. J. *Ultrasound Med. Biol.* **2021**, *47* (8), 2346–2359.
- (14) Egge, N.; Arneaud, S. L. B.; Fonseca, R. S.; Zuurbier, K. R.; McClendon, J.; Douglas, P. M. *Nat. Commun.* **2021**, *12* (1), 1484.
- (15) Solano Fonseca, R.; Metang, P.; Egge, N.; Liu, Y.; Zuurbier, K. R.; Sivaprakasam, K.; Shirazi, S.; Chuah, A.; Arneaud, S. L.; Konopka, G.; Qian, D.; Douglas, P. M. *Elife* **2021**, *10*.